TRIPLE EXCITATION EFFECTS IN THE FOCK-SPACE COUPLED CLUSTER METHOD

By

DAVID EDWARD BERNHOLDT

A DISSERTATION PRESENTED TO THE GRADUATE SCHOOL
OF THE UNIVERSITY OF FLORIDA IN PARTIAL FULFILLMENT
OF THE REQUIREMENTS FOR THE DEGREE OF
DOCTOR OF PHILOSOPHY

UNIVERSITY OF FLORIDA

1993

To Jan,
for so many reasons.

ACKNOWLEDGMENTS

Graduate school has been an educational experience in many ways, and a great many people have made important contributions to that education.

I would especially like to thank my advisor, Rod Bartlett, for the singular role he has played in my life. His research group members, especially John Stanton, have also shared knowledge and offered both help and challenges throughout my work with them. My colleagues, past and present, in the Quantum Theory Project have created a wonderful environment in which to learn and do research, and it has been my great pleasure to experience it. I would like to thank Drs. Vala and Weltner for numerous discussions and suggestions; I regret that I did not have time to examine more of their interesting molecules.

My research in this field began while I was an undergraduate at the University of Illinois, and I am deeply indebted to Cliff Dykstra and Shi-yi Liu for getting me started and for conveying to me their enthusiasm for the subject.

The daily existence of a graduate student often revolves around research, but there is much more to life. I thank my friends and family, who have tried to tell me this and who have shared other gifts with me over the years: humor, diversion, perspective, encouragement, sympathy, and love.

Finally, words cannot express my gratitude to Jan, who rode two different roller coasters at the same time and lived to tell the tale.

TABLE OF CONTENTS

ACKNOWLEDGMENTS iii

ABSTRACT vii

CHAPTERS

1 INTRODUCTION 1

2 THEORETICAL BACKGROUND 5

2.1 Overview 5

2.2 The Schrödinger Equation 5

2.3 Potential Energy Surfaces 6

2.4 Calculations on Potential Energy Surfaces 9

2.5 Vibronic Interactions 10

2.6 Basis Set Expansion 14

2.7 One-electron Approximations 15

2.8 The Correlation Problem 17

2.9 Occupation Number Representation 17

3 COUPLED CLUSTER METHODS 23

3.1 Introduction 23

3.2 Basic Equations 26

3.3 Reduction to Spin Orbital Equations 29

3.4 Numerical Solution of the Coupled Cluster Equations 33

3.5 The Coupled Cluster Effective Hamiltonian 33

3.6 Truncation of the Cluster Operator 38

4 FOCK SPACE COUPLED CLUSTER THEORY 42

4.1 Introduction 42

4.2 Structure of FSCC 43

4.3 Comparison with Single Reference CC Theory 50

4.4 Basic Equations 54

4.5 Reduction to Spin Orbital Equations 55

4.6 Approximations to the Full FSCCSDT Model 56

5 A CRITICAL ASSESSMENT OF FSCCSD AND THE THIRD-ORDER TRIPLES APPROXIMATIONS 64

5.1 Introduction 64

5.2 Effect of Changes in the Active Space 66

5.3 Ionization Potentials 71

5.4 Potential Energy Surfaces and Related Properties 79

5.5 Conclusions 87

6 THE STRUCTURE OF THE C_3^+ MOLECULE 90

6.1 Background 90

6.2 Computational Methods 91

6.3 The Heart of the Problem 93

6.4 Geometries of the Linear Stationary Points of C_5^+ 95

6.5 Relative Energies 97

6.6 Stability of the Stationary Point Structures 102

6.7 Implications for Other Carbon Clusters 105

6.8 Recapitulation 108

7 SUMMARY 109

APPENDIX

IMPLEMENTATION OF THE PERTURBATIVE TRIPLES MODELS 115

REFERENCES 125

BIOGRAPHICAL SKETCH 131

Abstract of Dissertation Presented to the Graduate School
of the University of Florida in Partial Fulfillment of the
Requirements for the Degree of Doctor of Philosophy

TRIPLE EXCITATION EFFECTS IN THE FOCK-SPACE COUPLED CLUSTER METHOD

By

DAVID EDWARD BERNHOLDT

May 1993

Chairman: Rodney J. Bartlett
Major Department: Chemistry

The Fock-space coupled cluster (FSCC) approach to the electron correlation problem offers several advantages over the more familiar single reference coupled cluster (CC) methods. It is capable of treating states with a multireference character, and it is capable of providing state-to-state energy differences for several states in a single calculation. As explained in this work, basic differences between the two theories result in higher-excited cluster operators being more important in FSCC methods than CC methods.

In order to improve the accuracy of FSCC calculations, this work involves the addition of triple excitation effects to the widely applied FSCC model restricted to single and double excitations (FSCCSD) for ionization potentials. Equations for the full model, including single, double, and triple excitations (FSCCSDT), are derived and various approximations are proposed as a compromise between the improvement in the

wavefunction and energy due to the inclusion of triples and the computational costs, which are significantly larger than for the FSCCSD model.

Two approximations to the full FSCCSDT model have been implemented and their performance is examined for a variety of molecules. Results are found to be generally good, providing results comparable to single reference coupled cluster methods with approximate inclusion of triple excitations.

Finally, both CC and FSCC methods are used to study the structures of several small carbon clusters, a class of molecules which has been shown to require high-quality theoretical methods and which can make use of both FSCC's multireference and direct energy difference capabilities. Detailed calculations show that the ground state of C_5^+ is a $^2\Sigma^+$, with $C_{\infty v}$ symmetry, but with low frequency bending vibrational modes. Additional calculations for other odd carbon cluster cations suggest that the "linear" structures of C_7^+ and C_9^+ observed experimentally may in fact be distorted from true linearity due to the Renner-Teller effect.

CHAPTER 1
INTRODUCTION

In recent years, advances in both experimental and theoretical chemistry have fueled an exciting synergy between the two fields [1]. Experimental innovations have allowed study of molecules in conditions similar to those commonly employed in theoretical calculations (low temperature, low density), producing data of increasing accuracy and specificity. Likewise, through increases in computational power and methodological sophistication, theoretical chemists have been able to tackle increasingly complex systems with high accuracy. Where experimental and theoretical data are directly comparable, critical evaluations of both approaches are possible. In other cases, the data are often complementary, allowing one or the other researcher to bring the problem into finer focus.

This has been especially apparent in research on atomic clusters, a field which has expanded rapidly in the past decade. Clusters are interesting for a variety of reasons. Metal clusters are used as models for the study of catalytic processes. Clusters of lighter atoms, particularly carbon, have been identified in circumstellar space and are expected also to be found in interstellar molecular clouds, where they may be important in the creation of new stars. They have also been found in combustion products on Earth. Clusters may have useful and unique physical properties, making them interesting from a materials viewpoint, and they are studied as models of how properties of bulk materials are approached by increasingly large collections of atoms.

Although the literature on clusters is expanding rapidly, the sought after understanding has not yet emerged. One reason for this is that clusters, even relatively small ones, are rather unlike "traditional" molecules which scientists have studied for centuries, and they often defy the "rules" and intuitions which researchers try to bring from traditional chemistry to cluster chemistry. Consequently, workers in the area are having to develop new ideas and new "rules" about the structure and properties of clusters.

An important component of creating this new understanding is having *reliable* data on the structure and properties of many clusters. Since there are few experiments which give direct, unambiguous structural data, theoretical approaches are particularly useful in this context. When the capabilities of experiment and theory do overlap, it is possible to compare results critically and perhaps improve both. To be truly useful, however, the theoretical methods employed must be accurate and reliable. The subject of this dissertation, the inclusion of triple excitation effects in the Fock-space coupled cluster (FSCC) method, was undertaken in response to exactly this need.

Coupled cluster (CC) and related many-body perturbation theory (MBPT) methods (see Chapter 3) have proven their ability to deliver extremely high-quality properties and energetics for a wide range of complex systems, and because of their *size extensivity* (proper scaling of the energy with the size of the system under study) [2,3], are preferred over configuration interaction (CI) methods for theoretical studies of clusters. Not every situation, however, is ideally suited to the use of traditional single reference CC methods. For example, close-lying electronic states may cause problems for even the most sophisticated CC methods, thus requiring a multireference description of the wavefunction

to obtain meaningful results. Ionization potentials (IPs) and electron affinities (EAs) are often obtained using experimental studies of clusters in photoionization and photoelectron spectroscopies. In order to provide comparable theoretical results for interpretation or confirmation of the spectra, separate calculations for the ground state and each excited state of interest are required when using familiar CC methods. It would be useful to have a method capable of giving IPs and EAs for several states of interest in a single calculation. Fock-space coupled cluster methods are one way to approach both of these problems.

Often referred to as Fock-space *multireference* coupled cluster theory, FSCC (see Chapter 4) can provide a multireference description of chosen electronic states of a molecule. Considered in another context, it can calculate the energies of several electron-detached or -attached states at the same time, thus simplifying the calculation of IPs and EAs. Because of formal differences between single reference CC and FSCC theories, however, a given truncation of the two methods does not necessarily give results of equivalent quality. For example, limiting both methods to single and double excitations, we find that an FSCCSD description of a particular state may leave out contributions which could be present in the CCSD description of the same state. Consequently, in order to improve the quality of the FSCC description, this work examines the inclusion of triple excitation effects in the FSCC method.

After setting the stage with a review of theory and terminology leading up to the correlation problem, the traditional coupled cluster equations are presented, emphasizing their use as an "input" to the FSCC method. Then, in some detail, equations for the FSCC

method are derived, focusing on the FSCCSDT model for IPs. The importance of triple excitations is examined, in comparison with single reference CCSD and CCSDT methods, and several approximations are proposed as a compromise between the computational cost of evaluating the complete triples contribution and quality required of the wavefunction and energies. Although this development was spurred by an interest in carbon clusters, FSCC methods, with or without triple excitations, are by no means limited to this application. In order to assess the performance of the FSCC methods, calculations are presented for a variety of molecules. Finally, Fock-space and single reference coupled cluster methods are used to study several carbon cluster cations.

CHAPTER 2
THEORETICAL BACKGROUND

2.1 Overview

Much of the theoretical chemistry literature assumes the reader is a practitioner in the field. This chapter is intended to provide a common ground for the concepts and notation used throughout this dissertation. It is by no means exhaustive, but should help non-specialists to understand the material that follows. References are given to the literature for more detailed treatments of various topics.

2.2 The Schrödinger Equation

We seek to solve the time-independent Schrödinger equation,

$$H|\Psi\rangle = E|\Psi\rangle \tag{2.1}$$

for a molecular system (one or more molecules of interest isolated from interaction with anything else). This equation tells us that a system in an eigenstate $|\Psi\rangle$ of the Hamiltonian operator H has an energy E. The usual nonrelativistic Hamiltonian can be divided into five different terms,

$$H = T_e + T_n + V_{en} + V_{ee} + V_{nn} \tag{2.2}$$

representing, respectively, the electronic and nuclear kinetic energies and the potentials due to interaction of electrons and nuclei, electrons with other electrons, and nuclei with

other nuclei. The individual terms, in Hartree atomic units, are defined as

$$T_e(r) = -\frac{1}{2}\sum_i \nabla_i^2$$

$$T_n(R) = -\sum_A \frac{1}{2M_A}\nabla_A^2$$

$$V_{en}(r,R) = -\sum_i \sum_A \frac{Z_A}{|r_i - R_A|} \tag{2.3}$$

$$V_{ee}(r) = \frac{1}{2}\sum_{i\neq j} \frac{1}{|r_i - r_j|}$$

$$V_{nn}(R) = \frac{1}{2}\sum_{A\neq B} \frac{Z_A Z_B}{|R_A - R_B|}$$

In these expressions, i and j refer to electrons, A and B refer to nuclei. R_A and r_i refer to the spatial coordinates of nucleus A and electron i, respectively, and Z_A and M_A are the charge and mass of nucleus A. The unsubscripted symbols r and R refer to the complete set of position vectors of the electrons and nuclei, respectively.

2.3 Potential Energy Surfaces

The terms of the full Hamiltonian, Eq. 2.2, can be grouped according to their dependence on the positions of the nuclei into a purely electronic component,

$$H_e = T_e + V_{ee}, \tag{2.4}$$

a purely nuclear term,

$$H_n = T_n, \tag{2.5}$$

and a potential which couples them,

$$V_{int}(r,R) = V_{en}(r,R) + V_{nn}(R). \tag{2.6}$$

If we choose one set of positions R as the origin, denoted by 0, we can expand the electron-nuclear interaction potential near this point in a Taylor series,

$$V_{int}(r,R) = V_{int}(r,0) + \sum_A \left(\frac{\partial V_{int}}{\partial R_A}\right)_0 R_A + \frac{1}{2}\sum_{A,B}\left(\frac{\partial^2 V_{int}}{\partial R_A \partial R_B}\right)_0 R_A R_B + \cdots. \tag{2.7}$$

The first term in the expansion can be thought of as the potential felt by the electrons due to a fixed set of nuclei, leading to the electronic Schrödinger equation,

$$(H_e(r) + V_{int}(r,0))|\Phi_k(r)\rangle = E'_k|\Phi_k(r)\rangle, \tag{2.8}$$

for a particular state $|\Phi_k(r)\rangle$ with energy E'_k.

In order to see how varying the nuclear positions effects these solutions, we must return to the full Schrödinger equation 2.1. By expanding the full wavefunction in terms of the solutions to the electronic wavefunction and a nuclear component,

$$|\Psi(r,R)\rangle = \sum_k |\Phi_k(r)\rangle \mathrm{X}_k(R), \tag{2.9}$$

and recognizing that the Hamiltonian of Eq. 2.8 is a subset of the full Hamiltonian, we obtain

$$\{H_e + V_{int,0} + H_n + W\}\sum_k |\Phi_k\rangle \mathrm{X}_k = E\sum_k |\Phi_k\rangle \mathrm{X}_k, \tag{2.10}$$

where $V_{int,0}$ denotes the leading term in the V_{int} expansion, and W denotes the remainder, $W(r,R) = V_{int}(r,R) - V_{int}(r,0)$, known as the *vibronic interaction*. $H_e + V_{int,0}$ is often

referred to as the *electrostatic* Hamiltonian, and is dependent on the nuclear coordinates only parametrically. Projecting on the left with an electronic eigenfunction, $\langle\Phi_m(r)|$, we obtain a coupled set of equations, (note that H_n is independent of the electronic coordinates r),

$$\left(E'_m + H_n\right)\mathrm{X}_m + \sum_k \langle\Phi_m|W|\Phi_k\rangle\mathrm{X}_k = E\mathrm{X}_m, \tag{2.11}$$

or using the more compact matrix element notation for W,

$$\left(E - E'_m - H_n\right)\mathrm{X}_m = \sum_{k\neq m} W_{mk}\mathrm{X}_k. \tag{2.12}$$

If there is no vibronic interaction between electronic states ($W_{mk} = 0$), then the equations decouple, giving

$$\left(H_n(R) + E'_m\right)\mathrm{X}_m(R) = E\mathrm{X}_m(R)\ \forall\, m, \tag{2.13}$$

which is the Schrödinger equation for the nuclei moving in the mean field of electronic state $|\Phi_m(r)\rangle$, and the solution to the full Schrödinger equation is simply $|\Psi(r,R)\rangle = |\Phi_m(r)\rangle\mathrm{X}_m(R)$. This is the origin of the idea of a *potential energy surface* (PES) as the set of nuclear configurations which satisfy Eq. 2.13 for a particular electronic state. Taking $W_{mk} = 0$ is known as the simple adiabatic or *Born-Oppenheimer* approximation [4,5].

In practice, although W_{mk} is not in general zero, the Born-Oppenheimer approximation is usually quite good because of the fact that the nuclei of a molecule are about 1836 times more massive than the electrons, so we can usually think of the nuclei moving slowly in the average field of the electrons, which are able to adapt almost instantaneously to the nuclear motions. This approximation is used in the majority of electronic

structure calculations to date, which simply evaluate the electronic wavefunction and energy, Eq. 2.8, at various points on the PES (nuclear configurations) and ignore the nuclear dynamics.

2.4 Calculations on Potential Energy Surfaces

The Born-Oppenheimer potential energy surface for a particular state of a molecule with N nuclei is (neglecting invariance to rigid translations and rotations of the entire nuclear framework) a $3N$-dimensional space which can be characterized according to its local shape. A *stationary point* is one at which the gradient of the energy with respect to nuclear displacements be zero. Stationary points may be minima, transition states, higher-order saddle points, or maxima. If the curvature (second derivative) at a stationary point is positive, the point is a *local minimum*, which is a locally stable geometric conformation for the state in question. If the curvature in one of the $3N$ directions is negative, with all others positive, the point is a *transition state*, which is a local maximum on a path connecting two local minima; transition states are very important in the theory of chemical reactions. If the stationary point has more than one direction of negative curvature, it is a saddle point (or local maximum), which is not chemically meaningful.

Stationary points on potential energy surfaces can be located using numerical optimization techniques, such as Newton-Raphson, quasi-Newton-Raphson, etc., but because individual calculations of the energy, gradient, and hessian (matrix of second derivatives of the energy), as required by the optimization method. are extremely expensive relative to evaluation of the optimization step, it is usually necessary to use chemical intuition

to choose regions of the PES on which to focus and sometimes to restrict the search to a subset of the full $3N$-dimensional space.

The hessian, which allows a stationary point to be characterized as a minimum, transition state, or saddle point, is also the primary input for evaluation of the vibrational frequencies at that structure (in the harmonic approximation). Since different molecules and different structures will generally have different vibrational spectra, it serves as a useful tool for the identification and characterization of unknown species.

If the electronic state of the molecule of interest is not known from other information, it may be necessary to consider potential energy surfaces for several states in order to locate the lowest energy global minimum of all the states, which is known as the *ground state* of the system.

2.5 Vibronic Interactions

Although the Born-Oppenheimer approximation and the idea of potential energy surfaces have served quantum chemistry well, there are certainly cases in which the W_{mk} matrix elements connecting different electronic states are significantly different from zero, and the Born-Oppenheimer picture is no longer adequate.

Consider the vibronic interaction term, W, truncated after the quadratic term, which is adequate for purposes of explanation. Making a linear transformation from cartesian coordinates R to symmetrized normal coordinates Q (obtained by diagonalizing the

hessian matrix), we have

$$W(r,Q) = \sum_{\alpha} \left(\frac{\partial V_{int}}{\partial Q_\alpha}\right)_0 Q_\alpha + \frac{1}{2}\sum_{\alpha,\beta} \left(\frac{\partial^2 V_{int}}{\partial Q_\alpha \partial Q_\beta}\right)_0 Q_\alpha Q_\beta. \tag{2.14}$$

Each normal coordinate, Q_α, belongs to an irreducible representation (irrep) Γ_α of the molecular point. Likewise, the electronic states $|\Phi_m\rangle$ belong to an irrep, Γ_m. Thus from group theory, we know that the *linear vibronic constant*,

$$F_{\Gamma_\alpha}^{(\Gamma_k \Gamma_m)} = \left\langle \Phi_k \left| \left(\frac{\partial V_{int}}{\partial Q_\alpha}\right)_0 \right| \Phi_m \right\rangle, \tag{2.15}$$

is nonzero if and only if $\Gamma_\alpha \in [\Gamma_k \times \Gamma_m]$. This is a general result for the interaction of any two states, but of particular importance is the case in which the two electronic states belong to the same irreducible representation. If the irrep is not degenerate, then $[\Gamma_k \times \Gamma_k] = \Gamma_k \times \Gamma_k = \Gamma_{A_1}$, so that the coupling is via totally symmetric motions, which by definition cannot change the symmetry of the molecule. If, on the other hand, the two electronic states (or components of states) belong to a degenerate irrep, the direct product results in non-totally symmetric representations, and thus the states are coupled by motions which break (lower) the symmetry of the molecular framework. This is the basis of the Jahn-Teller (JT) theorem [6], which says that for a nonlinear polyatomic molecule in an n-fold degenerate electronic state, the high symmetry point at which the n potential surfaces intersect cannot be a minimum on all n surfaces. In other words, there will always be at least one direction for which the energy is lowered when the degeneracy is lifted (by moving away from the high symmetry point). The tendency of a molecule in a degenerate state to lower its symmetry and thereby lift the degeneracy and lower its energy is known as the *Jahn-Teller effect.*

In the more general case, interaction to two near-lying states via a suitable nuclear motion causes the surfaces to repel each other. Looking at a slice of the two surfaces along the symmetry-breaking motion that couples the two states, the upper surface becomes more curved as the interaction increases, while the lower state is flattened. If the interaction is strong enough, the lower state may display a double minimum shape, with the original high symmetry point a transition state between the two minima. This is usually referred to as the *pseudo-Jahn-Teller effect* (PJTE) [7]. The magnitude of the PJT effect depends both on the separation of the two states and the magnitude of the linear vibronic constant.

The exclusion of linear molecules from the JT effect is also on the basis of symmetry arguments. The wavefunction of a linear molecule is either even or odd with respect to reflections containing the axis of the molecule or perpendicular to it, so of course the product of such functions will always be even. The nuclear motions that bend the molecule are odd in this respect, and so can never be contained in the direct product of the wavefunction representations — the linear vibronic constant $F_{\Gamma_a}^{(\Gamma_k \Gamma_k)}$ is zero for linear molecules.

For linear molecules, and other cases for which the linear vibronic constant is zero or negligibly small, the quadratic term of Eq. 2.14 comes into play. For linear molecules in degenerate states, the quadratic vibronic coupling leads to a condition similar to the JT effect, called the *Renner-Teller effect* (RTE) [8,9]. Lifting of the degeneracy can be easily visualized in this case. Consider a linear molecule oriented along the z axis, in a $^2\Pi$ state, so that one component of the π orbital, say π_x contains an electron. Bending motions

in the orthogonal directions x and y would normally be equivalent in a linear molecule, but if one component of the π is occupied, the electronic state of the bent structure will be different depending on whether the electron is now in an orbital in the plane of the molecule or perpendicular to it. Unlike the JT case, the Renner-Teller effect does not guarantee that lifting the degeneracy by bending will result in a lower energy. The two states will not be degenerate (except the linear geometry), but neither, one, or both may still be minima at the linear geometry, or the linear geometry may be a transition state between two equivalent bent minima depending on the magnitude of the interaction.

In the more general case, with states belonging to different irreps interacting, there is little to be gained from a symmetry analysis of the quadratic vibronic constant. There are usually many combinations of vibrational motions that can couple two electronic states for either degenerate or nondegenerate point groups, however these effects are usually relatively small.

Clearly vibronic coupling effects can cause major problems for computational methods based on the Born-Oppenheimer approximation, but if we are looking for minima on potential surfaces, it is clear that such points are usually *not* of interest — when the interactions are strong enough, they cause the symmetry of the molecule to be broken, thus moving it away from the degenerate or pseudo-degenerate point. As a result, it is often enough to *recognize* points on the PES at which strong vibronic interactions occur and then locate and follow the symmetry breaking to lower energies. Of course this approach will not always work, and even calculations *near* a (pseudo-) degenerate point can be quite taxing for the method, but it has been used in a number of studies

(see Bersuker's bibliography [10] for examples). In 1984, Lee *et al.* [11] demonstrated that analytically evaluated hessians could be used to compute bending frequencies for Renner-Teller molecules. In fact if due care is taken to stay on the correct PES during the calculation, hessians evaluated from finite differences of gradients, or even energies, can also give RT bending frequencies.

2.6 Basis Set Expansion

Several approaches may be taken to the solution of the electronic Schrödinger equation, but the most widely used and most generally applicable is expansion in a basis of Gaussian functions. These functions are usually (but not necessarily) chosen to mimic the *atomic orbital* (AO) description used in chemistry and are referred to by that name. A complete (infinite) basis would span all of space and thus allow an exact description of the wavefunction. In practice, however, computational resources place limits on the size of basis that may be employed, and it is necessary to compromise between the cost of the calculation and the accuracy required.

It is now possible to evaluate matrix elements of the Hamiltonian operator in terms of the AO basis set. For a set of functions $\{\chi_\mu\}$, we have, for example, the one- and two-electron integrals (or matrix elements) [12]

$$\begin{aligned} \langle \mu | h | \nu \rangle &= h_{\mu\nu} = \int \chi_\mu^*(\mathbf{x}_1) h \chi_\nu^*(\mathbf{x}_1) d\mathbf{x}_1 \\ \langle \mu\nu | \lambda\sigma \rangle &= \int \chi_\mu^*(\mathbf{x}_1)\chi_\nu^*(\mathbf{x}_2)\frac{1}{r_{12}}\chi_\lambda(\mathbf{x}_1)\chi_\sigma(\mathbf{x}_2) d\mathbf{x}_1 d\mathbf{x}_2 \end{aligned} \tag{2.16}$$

where

$$\mathbf{x}_i = \begin{cases} r_i\alpha(\omega_i), & \text{or} \\ r_i\beta(\omega_i) \end{cases} \tag{2.17}$$

is a combination of the position and spin of electron i, and $r_{12} = |r_1 - r_2|$. The left-hand sides of Eq. 2.16 are shown the bra-ket notation, originally due to Dirac [13], which is in common use and for the one-electron integral, a matrix element notation is also shown. Both the bra-ket and matrix element notations are used in the literature, and both will be used in this work.

2.7 One-electron Approximations

Given a basis of atomic orbitals, which are (very rough) approximations to the eigenstates of the atom, the first step in an electronic structure calculation is usually to find a set of one-electron functions for the molecule as a whole, called *molecular orbitals* (MOs). These orbitals correspond to the qualitative ideas about molecular orbitals often used by chemists.The most common prescription for calculating MOs is the Hartree-Fock (HF) Self-Consistent Field (SCF) procedure [12].

The result of an SCF calculation is a set of MOs $\{\phi_p\}$, which are represented as linear combinations of the AO basis functions,

$$\phi_p = \sum_{\mu} C_{\mu p}\chi_\mu \tag{2.18}$$

with the matrix C determined by the SCF procedure. Of these MOs, some will be *occupied* by electrons and some will be unoccupied, or *virtual* orbitals. The

antisymmetrized product of the occupied orbitals is the *Slater determinant* for that state.

Depending on the particular formulation (primarily the treatment of electrons with different spins) used in the HF procedure, it may be referred to as RHF, UHF, or ROHF, among other possibilities. The most straightforward is restricted Hartree-Fock (RHF), applicable only to closed shell molecules (where all electrons are paired), where the alpha and beta spin orbitals in each pair are restricted to have the same spatial function. The restricted open-shell Hartree-Fock (ROHF) formalism extends the RHF idea to open shell systems by requiring that all paired electrons have share the same spatial function, but allowing additional orbitals which may be occupied by single unpaired electrons. In the unrestricted Hartree-Fock (UHF) method (also known as DODS — different orbitals for different spins), the alpha and beta spin electrons have distinct spatial parts, allowing the possibility that they might be quite different.

Only when pairs of electrons have the same spatial component (RHF, ROHF) is it guaranteed that the HF wavefunction is an eigenfunction of the S^2 operator, satisfying $S^2|HF\rangle = s(s+1)|HF\rangle$. UHF wavefunctions may suffer from *spin contamination*, in which the wavefunction is an admixture of states of different S^2 values. Because the true wavefunction is always an eigenfunction of S^2, it is thus possible that a UHF wavefunction may be to some extent unphysical. Nevertheless, the UHF method has proven quite useful, particularly as the basis for formulating general (i.e. applicable to both closed and open shell systems) correlated methods.

2.8 The Correlation Problem

Although the SCF procedure provides a very useful qualitative description of molecules, it is generally inadequate for quantitative uses requiring high accuracy. The method considers each electron the average field of all others, which ignores the fact that the motion of each electron is instantaneously correlated with all others because of the Pauli Principle. For the higher accuracy required of most interesting applications, it is necessary to go beyond the one-electron approximation and treat correlation effects in the system.

The correlation problem is usually formulated in terms of the interaction between different configurations (occupations) of a set of one-electron functions. The molecular orbitals are usually used for this purpose because the idea of occupied and unoccupied orbitals is well defined and the derivation of equations for correlated methods are thus greatly simplified. The SCF determinant serves as a *reference* for the definition of the excited state configurations in which the correlated wavefunction is expanded.

2.9 Occupation Number Representation

The occupation number, or second quantized, formalism [14] is a convenient representation for the development of correlated methods because it represents in a compact way the changes in occupation of the various determinants. In this de-

scription and throughout this dissertation, the convention will be used that subscripts $i, j, \ldots, n$ refer to orbitals which are occupied in the reference determinant, $a, b, \ldots, f$ refer to virtual orbitals, and $p, q, \ldots, u$ refer to orbitals of either type.

Creation and annihilation operators are defined that act to create or destroy an electron in a particular one-electron function (MO). Thus the creation operator $a_p^\dagger$ would create an electron in orbital p, and the annihilation operator a_q would remove an electron from orbital q. The Pauli Principle is satisfied by the fact that $a_p^\dagger a_p^\dagger = a_q a_q = 0$, which is a result of the anticommutation relations among the creation and annihilation operators.

Strings of creation and annihilation operators act on the reference determinant, $|0\rangle$, to produce excited state determinants. For example, an electron can be promoted from an occupied orbital i to a virtual orbital a,

$$a_a^\dagger a_i |0\rangle = |\Phi_i^a\rangle = |_i^a\rangle \tag{2.19}$$

where the resulting excited state has been shown in two common notations. Similarly, higher excitations may be obtained

$$a_b^\dagger a_j a_a^\dagger a_i |0\rangle = |\Phi_{ij}^{ab}\rangle = |_{ij}^{ab}\rangle$$

$$a_c^\dagger a_k a_b^\dagger a_j a_a^\dagger a_i |0\rangle = |\Phi_{ijk}^{abc}\rangle = |_{ijk}^{abc}\rangle \tag{2.20}$$

$$\vdots$$

Operators such as the Hamiltonian are represented in the second quantized formalism by the matrix element of the operator in the basis of one-electron functions multiplied

by a string of creation and annihilation operators:

$$H = \sum_{p,q} h_{pq} a_p^\dagger a_q + \frac{1}{4} \sum_{p,q,r,s} \langle pq||rs\rangle a_p^\dagger a_q^\dagger a_s a_r \tag{2.21}$$

where we have used the antisymmetrized two-electron integral, $\langle pq||rs\rangle = \langle pq|rs\rangle - \langle pq|sr\rangle$.

Strings of creation and annihilation operators may be evaluated using Wick's theorem [15] and the concept of a normal order of operators. *Normal ordered* operator strings are those which have all $a_i^\dagger$ and all a_a to the right of the string, which can be accomplished using the anticommutation relations for second quantized operators. This is done to exploit the fact that $a_i^\dagger|0\rangle = a_a|0\rangle = 0$. The normal order of an operator string A is denoted *N[A]*, and has the property

$$\langle 0|N[A]|0\rangle = 0. \tag{2.22}$$

This result is obvious if all $a_i^\dagger$ and a_a operators are brought to the right, where they act on the reference giving zero immediately. If there are no $a_i^\dagger$ or a_a, then the operators act on the reference to create an excited state on the left hand side, which is orthogonal to the reference function on the right,

$$\left\langle 0|\Phi_{ij\cdots}^{ab\cdots}\right\rangle = 0. \tag{2.23}$$

Note too that in the absence of $a_i^\dagger$ or a_a, A=N[A].

Wick's theorem tells us that the *contraction* of a pair of operators is defined as

$$\begin{aligned} a_p^\dagger a_q &= N\left[a_p^\dagger a_q\right] + N\left[\overbrace{a_p^\dagger a_q}\right], \text{ or} \\ a_p a_q^\dagger &= N\left[a_p a_q^\dagger\right] + N\left[\overbrace{a_p a_q^\dagger}\right], \end{aligned} \tag{2.24}$$

with the following definitions according to whether p and q are occupied or virtual orbitals (they must be the same type since $\delta_{ai} = 0$)

$$\begin{aligned} N\left[\overbrace{a_i^\dagger a_j}\right] &= \delta_{ij} \\ N\left[\overbrace{a_i a_j^\dagger}\right] &= 0 \\ N\left[\overbrace{a_a^\dagger a_b}\right] &= 0 \\ N\left[\overbrace{a_a a_b^\dagger}\right] &= \delta_{ab} \end{aligned} \tag{2.25}$$

Longer strings of operators are evaluated by taking all possible single contractions, then all double contractions (two simultaneous contractions), up to full contractions, with the sign in each case determined by the permutations necessary to make pairs of contracted operators adjacent. As an example, consider the Hamiltonian, Eq. 2.21. The one-electron term is cast in normal ordered form by recognizing that

$$\begin{aligned} a_p^\dagger a_q &= N\left[a_p^\dagger a_q\right] + N\left[\overbrace{a_p^\dagger a_q}\right] \\ &= N\left[a_p^\dagger a_q\right] + \delta_{ij} \end{aligned} \tag{2.26}$$

so that

$$\sum_{p,q} h_{pq} a_p^\dagger a_q = \sum_{p,q} h_{pq} N\left[a_p^\dagger a_q\right] + \sum_i h_{ii}. \tag{2.27}$$

The two-electron term has a string of four operators, so all possible single and double contractions must be considered. There are four single contractions all of which can be

manipulated into the same form, and similarly for the two double contractions,

$$\frac{1}{4}\sum_{p,q,r,s}\langle pq||rs\rangle a_p^\dagger a_q^\dagger a_s a_r = \frac{1}{4}\sum_{p,q,r,s}\langle pq||rs\rangle N\left[a_p^\dagger a_q^\dagger a_s a_r\right] + \sum_{p,q,i}\langle pi||qi\rangle N\left[a_p^\dagger a_q\right] + \frac{1}{2}\sum_{i,j}\langle ij||ij\rangle. \tag{2.28}$$

When evaluating a product of several normal ordered operators, the same rules hold, but all contractions which are internal to any given operator have already been accounted for, so only those contractions connecting different normal ordered operators need be considered.

When developing correlated methods, it is convenient to employ the *normal ordered product* form, O_N, of a second quantized operator, O, defined by

$$O_N \equiv O - \langle 0|O|0\rangle. \tag{2.29}$$

This form has the property,

$$\langle 0|O_N|0\rangle = \langle 0|O - \langle 0|O|0\rangle|0\rangle = \langle 0|O|0\rangle - \langle 0|O|0\rangle = 0 \tag{2.30}$$

which allows one to focus on the correlation correction to the result rather than carrying the reference expectation value (a constant) through all of the equations. For example, consider the Hamiltonian. The normal ordered operator is the sum of Eqs. 2.27 and 2.28, or

$$N[H] = \sum_{p,q} h_{pq} N\left[a_p^\dagger a_q\right] + \sum_{p,q,i}\langle pi||qi\rangle N\left[a_p^\dagger a_q\right] + \frac{1}{4}\sum_{p,q,r,s}\langle pq||rs\rangle N\left[a_p^\dagger a_q^\dagger a_s a_r\right] + \sum_i h_{ii} + \frac{1}{2}\sum_{i,j}\langle ij||ij\rangle \tag{2.31}$$

and the expectation value is

$$\begin{aligned}\langle 0|H|0\rangle &= \left\langle 0\left|\sum_{p,q} h_{pq}a_p^\dagger a_q + \frac{1}{4}\sum\nolimits_{p,q,r,s}\langle pq||rs\rangle a_p^\dagger a_q^\dagger a_s a_r\right|0\right\rangle \\ &= \sum_i h_{ii} + \frac{1}{2}\sum_{i,j}\langle ij||ij\rangle.\end{aligned} \tag{2.32}$$

The normal ordered product form of the Hamiltonian is thus

$$\begin{aligned}H_N &= H - \langle 0|H|0\rangle \\ &= \sum_{p,q} h_{pq}N\left[a_p^\dagger a_q\right] + \sum\nolimits_{p,q,i}\langle pi||qi\rangle N\left[a_p^\dagger a_q\right] + \frac{1}{4}\sum\nolimits_{p,q,r,s}\langle pq||rs\rangle N\left[a_p^\dagger a_q^\dagger a_s a_r\right] \\ &= \sum_{p,q} f_{pq}N\left[a_p^\dagger a_q\right] + \frac{1}{4}\sum\nolimits_{p,q,r,s}\langle pq||rs\rangle N\left[a_p^\dagger a_q^\dagger a_s a_r\right]\end{aligned} \tag{2.33}$$

with the Fock operator,

$$f_N = \sum_{p,q} f_{pq}N\left[a_p^\dagger a_q\right] \equiv \sum_{p,q} h_{pq}N\left[a_p^\dagger a_q\right] + \sum_{p,q,i}\langle pi||qi\rangle N\left[a_p^\dagger a_q\right] \tag{2.34}$$

used in the final form. The normal ordered product Hamiltonian is also frequently written in terms of its one- and two-electron components,

$$H_N = f_N + W_N. \tag{2.35}$$

CHAPTER 3
COUPLED CLUSTER METHODS

3.1 Introduction

Two of the most common approaches currently in use for obtaining correlated energies and properties are configuration interaction (CI) and coupled cluster (CC) methods. Both methods use an expansion space of excited Slater determinants to represent the wavefunction; the difference between them originates with the particular form chosen for the expansion. In the CI case, a linear expansion is used,

$$|\Psi_{CI}\rangle = (1 + C)|0\rangle = (1 + C_1 + C_2 + \cdots)|0\rangle \tag{3.1}$$

where C_i generates all possible i-fold excitations from the reference determinant weighted by coefficients giving the importance of each determinant in the total CI wavefunction. In most cases, it is necessary for computational reasons, to truncate the expansion space somewhere short of including *all* possible excitations (up to n-fold for an n electron system). This results in a variationally determined wavefunction (and energy), but sacrifices the size extensivity property.

Size extensivity [2,3] is the requirement that the energy of a system scale properly with the number of electrons. It is most easily understood by considering an assembly of N identical non-interacting molecules. If each molecule, p, has an energy and reference function satisfying

$$H|0^{(p)}\rangle = E_0^{(p)}|0^{(p)}\rangle \tag{3.2}$$

(the one-electron functions of $|0^{(p)}\rangle$ are assumed to be localized on that molecule), then we can write the reference energy and wavefunction of the entire assembly as

$$E_0^{(total)} = \sum_{p=1}^{N} E_0^{(p)}$$
$$|0^{(total)}\rangle = \prod_{p=1}^{N} |0^{(p)}\rangle \tag{3.3}$$

Since the molecules are non-interacting, we expect the correlated energy and wavefunctions to be representable as similar sums and products, respectively. When a truncated CI expansion is applied to this system, however, this is not so. For an individual molecule, p, the coefficients $C_1^{(p)}, C_2^{(p)}, \ldots C_m^{(p)}$, with $m<n$, are determined by the Schrödinger equation,

$$H\left(1 + C_1^{(p)} + C_2^{(p)} + \cdots\right)|0^{(p)}\rangle = E_{CI}^{(p)}\left(1 + C_1^{(p)} + C_2^{(p)} + \cdots\right)|0^{(p)}\rangle \tag{3.4}$$

and give a product wavefunction which includes excitations up to Nm due to products of excitations on different molecules. If the assembly were treated as a whole, however, only up to m-fold excitations would appear in the wavefunction. Thus, they can never be equivalent. The energy of the assembly suffers similar problems. For example, a lattice of N non-interacting hydrogen molecules treated with CI restricted to double excitations (CID) has an energy which scales as $\sqrt{N}$ instead of N, resulting in an error of 12.3% for 10 molecules and 21.1% for 20 [16]. Calculations by Ahlrichs and coworkers at the CID level show that the difference between supermolecule (the two molecules separated by a very large distance calculated together) and the sum of individual molecular energies are $\sim$7 kcal mol^{-1} for BH_3 + BH_3 [17], and $\sim$15 kcal mol^{-1} for CH_3F + F^- [18].

The well known property of exponentials, $e^A e^B = e^{A+B}$ (where $[A,B]=0$), suggests an alternative solution to the problem. If the individual molecule wavefunctions are of the form

$$|\Psi^{(p)}\rangle = e^{T^{(p)}}|0^{(p)}\rangle \tag{3.5}$$

with $T^{(p)}$ being an expansion operator analogous to C, in Eq. 3.1, and satisfying

$$He^{T^{(p)}}|0^{(p)}\rangle = E^{(p)}e^{T^{(p)}}|0^{(p)}\rangle \tag{3.6}$$

then the product wavefunction is

$$\begin{aligned} |\Psi^{(total)}\rangle &= \prod_{p=1}^{N} e^{T^{(p)}}|0^{(p)}\rangle \\ &= e^{\left(\sum_{p=1}^{N} T^{(p)}\right)} \prod_{p=1}^{N} |0^{(p)}\rangle \\ &= e^{T^{(total)}}|0^{(total)}\rangle \end{aligned} \tag{3.7}$$

which is identical to the total wavefunction resulting from a calculation of the entire assembly. This is the form of the wavefunction employed in coupled cluster theory.

This simple physical picture demonstrates the need for the exponential wave operator, but it is the Brueckner-Goldstone linked diagram theorem [19–23], which CC methods satisfy [24], that guarantees size extensivity when this form is used. Thus when the system is composed of interacting fragments, the simple physical picture becomes clouded, but the size extensivity property is still guaranteed.

Having motivated the use of coupled cluster methods and the exponential wave operator, in the remainder of this chapter, we will derive the working equations of

coupled cluster theory and other results which will be needed for the Fock-space CC methods discussed in the next chapter.

3.2 Basic Equations

In order to expand the coupled cluster wavefunction in the space of Slater determinants, we define a set of *cluster operators* which are capable of representing the contributions to the wavefunction due to determinants of particular levels of excitation,

$$\begin{aligned} T_1 &= \sum_{i,a} t_i^a a_a^\dagger a_i \\ T_2 &= \sum_{\substack{i>j \\ a>b}} t_{ij}^{ab} a_a^\dagger a_b^\dagger a_i a_j \\ T_3 &= \sum_{\substack{i>j>k \\ a>b>c}} t_{ijk}^{abc} a_a^\dagger a_b^\dagger a_c^\dagger a_i a_j a_k \\ &\vdots \end{aligned} \tag{3.8}$$

where the *cluster amplitudes*, $t_{ijk\cdots}^{abc\cdots}$ are the scalar coefficients for each excited Slater determinant in the wavefunction. The cluster operators for each level of excitation are collected together into a single operator,

$$T = T_1 + T_2 + T_3 + \cdots \tag{3.9}$$

for convenience.

To obtain the multiplicatively separable coupled cluster wavefunction, the wave operator (which produces the correlated wavefunction from the reference) is exponential

in the cluster operators,

$$|\Psi_{cc}\rangle = \Omega_{cc}|0\rangle = e^T|0\rangle. \tag{3.10}$$

This wavefunction must satisfy the Schrödinger equation

$$He^T|0\rangle = E_{cc}e^T|0\rangle \tag{3.11}$$

where E_{cc} is the coupled cluster energy and H is the second quantized electrostatic Hamiltonian. In order to simplify later discussion, we change to the normal product form of H by subtracting $E_0 = \langle 0|H|0\rangle$ from both sides of Eq. 3.11,

$$\begin{aligned}(H - \langle 0|H|0\rangle)e^T|0\rangle &= (E_{cc} - E_0)e^T|0\rangle \\ H_N e^T|0\rangle &= E_{corr}e^T|0\rangle\end{aligned} \tag{3.12}$$

where the correlation contribution to the energy has been designated E_{corr}. Finally, we multiply both sides of Eq. 3.12 by e^{-T} to obtain

$$e^{-T}H_N e^T|0\rangle = E_{corr}|0\rangle \tag{3.13}$$

Notice that the operator $e^{-T}H_N e^T$ acts as an effective Hamiltonian operator, acting on the reference state to give the correlation energy; this quantity is often referred to as $\bar{H}_N$ in post-CC methods (i.e. those for which the derivation relies on having first solved for a CC energy and wavefunction).

The effective Hamiltonian can be simplified by the use of a Baker-Campbell-Hausdorff expansion

$$e^{-T}He^T = H + [H,T] + \frac{1}{2!}[[H,T],T] + \cdots \tag{3.14}$$

The commutators of strings of second quantized operators may be evaluated using the contraction theorem of Harris, Jeziorski and Monkhorst [25], with the result that the expansion terminates after the quadruply-nested commutator term because H (Eq. 2.21) contains only four operators. This result is often denoted

$$e^{-T} H e^{T} = \left(H e^{T} \right)_{c} \tag{3.15}$$

where the subscript c indicates that only so-called *connected* terms remain. The terminology arises from the diagrammatic formulation of the equations often used in CC theory: surviving terms are those in which their diagrammatic representation forms a connected figure, from which no component may be removed except by breaking lines. The algebraic analog is that the term cannot be separated into a product of distinct summations. *Disconnected* terms are those which can be separated into two components without breaking a line, or algebraically the term may be cast as the product of two distinct summations. Use of Eq. 3.15 greatly simplifies reduction of the operator form of the coupled cluster equations to a spin orbital form suitable for numerical work.

The equations which determine the CC energy and amplitudes are obtained from Eq. 3.13 by projecting from the left with the reference determinant and each class of excited determinants (single, double, triple, etc.). These projections provide equations which determine the energy, T_1, T_2, T_3, etc., respectively.

$$\langle 0 | \left(H_N e^{T} \right)_{c} | 0 \rangle = E_{corr} \tag{3.16}$$

$$\begin{aligned}
\left\langle \begin{matrix} a \\ i \end{matrix} \right| \left(He^T \right)_c \left| 0 \right\rangle &= 0 \\
\left\langle \begin{matrix} ab \\ ij \end{matrix} \right| \left(He^T \right)_c \left| 0 \right\rangle &= 0 \\
\left\langle \begin{matrix} abc \\ ijk \end{matrix} \right| \left(He^T \right)_c \left| 0 \right\rangle &= 0 \\
&\vdots
\end{aligned} \tag{3.17}$$

3.3 Reduction to Spin Orbital Equations

The operator expression for the energy, Eq. 3.16, can be expanded to

$$E_{corr} = \left\langle 0 \left| (f_N + W_N) \left(1 + T_1 + T_2 + \frac{1}{2!} T_1^2 + T_3 + T_1 T_2 + \frac{1}{3!} T_1^3 + \cdots \right) \right| 0 \right\rangle_c \tag{3.18}$$

by replacing H_N with its one- and two-body components (see Eq. 2.21) and expanding the exponential. Since the Hamiltonian is in normal product form, the lead term in the exponential expansion is $\langle 0|H_N|0\rangle = \langle 0|(H - \langle 0|H|0\rangle)|0\rangle = 0$. The remaining cluster operators act on the reference to give an excited determinant and a product of amplitudes. As a one-body operator, f_N can create at most a singly excited state acting to the left on the bra reference determinant, consequently nonzero contributions will result only from a singly excited state on the right. Similarly, the two-body W_N operator requires a doubly excited state on the right. Thus, the equation simplifies to

$$E_{corr} = \left\langle 0 \left| f_N T_1 + W_N \left(T_2 + \frac{1}{2!} T_1^2 \right) \right| 0 \right\rangle_c . \tag{3.19}$$

It should be observed that the CC energy includes contributions due only to T_1 and T_2 regardless of higher level cluster operators in T; higher clusters contribute only indirectly via their effects on T_1 and T_2.

Reduction of the amplitude equations (Eq. 3.17) to a more explicit operator form proceeds in a similar fashion. For example, the T_1 equation can be expanded to

$$0 = \left\langle \begin{matrix} a \\ i \end{matrix} \right| (f_N + W_N)\left(1 + T_1 + T_2 + \frac{1}{2!}T_1^2 + T_3 + T_1T_2 + \frac{1}{3!}T_1^3 + \cdots\right)\left|0\right\rangle_c \qquad (3.20)$$

A nontrivial equation is obtained when the combined action of H_N and the cluster expansion produces a single excitation $|{}_i^a\rangle$ on the right. The one-body operator f_N is capable of changing the excitation level by -1, 0, or +1, and W_N by -2, -1, 0, +1, or +2. The f_N +1 term and the W_N +2 term cannot form connected contractions with T, so they can only contribute to the T_1 and T_2 equations, respectively, via the "*1+*" term in the exponential expansion. Because of the nature of the Hamiltonian, mentioned above, it should be evident that the equation for a particular cluster amplitude T_m will involve contractions of f_N with products of cluster operators resulting in m and m+1 excitations, and W_N with cluster operator products yielding m-1 to m+2 excitations. Equations for

the first three cluster operators are thus

$$
\begin{aligned}
0 =& \left\langle \begin{matrix} a \\ i \end{matrix} \right| f_N \left(1 + \underline{T_1} + T_2 + \frac{1}{2!}\underline{T_1^2} \right) \\
& + W_N \left(\underline{T_1} + T_2 + \frac{1}{2!}\underline{T_1^2} + T_3 + \underline{T_1}T_2 + \frac{1}{3!}\underline{T_1^3} \right) \Big| 0 \Big\rangle_c \\
0 =& \left\langle \begin{matrix} ab \\ ij \end{matrix} \right| f_N \{ \underline{T_2} + T_3 + T_1\underline{T_2} \} + W_N \Big\{ 1 + T_1 + \underline{T_2} + \frac{1}{2!}T_1^2 + T_3 + T_1\underline{T_2} \\
& + \frac{1}{3!}T_1^3 + T_4 + T_1T_3 + \frac{1}{2!}\underline{T_2^2} + \frac{1}{2!}T_1^2\underline{T_2} + \frac{1}{4!}T_1^4 \Big\} \Big| 0 \Big\rangle_c \qquad (3.21) \\
0 =& \left\langle \begin{matrix} abc \\ ijk \end{matrix} \right| f_N \left\{ \underline{T_3} + T_4 + T_1\underline{T_3} + \frac{1}{2!}T_2^2 \right\} \\
& + W_N \Big\{ T_2 + \underline{T_3} + T_1T_2 + T_4 + T_1\underline{T_3} + \frac{1}{2!}T_2^2 + \frac{1}{2!}T_1^2T_2 \\
& + T_5 + T_1T_4 + \frac{1}{2!}T_2\underline{T_3} + \frac{1}{2!}T_1^2\underline{T_3} + \frac{1}{2!}T_1T_2^2 + \frac{1}{3!}T_1^3T_2 \Big\} \Big| 0 \Big\rangle_c
\end{aligned}
$$

where the operator determined by the equation has been underlined.

Conversion of the operator equations into the spin orbital equations useful for numerical work is done by considering in turn each of the operator products in the foregoing equations and using Wick's Theorem [15] to evaluate the possible contractions among the strings of second quantized operators contained in the Hamiltonian and cluster operators. This analysis can be carried out using a purely algebraic approach or a diagrammatic approach [26], but rather than adding greatly to the length and complexity of this overview we prefer to omit the detailed procedure here, and simply report the result.

Consider, for example, the first term of the CC energy as given by Eq. 3.19:

$$\begin{aligned}\langle 0|f_N T_1|0\rangle &= \sum_{p,q,i,a} f_{pq} t_i^a \left\langle 0 \middle| \left\{a_p^\dagger a_q\right\}\left\{a_a^\dagger a_i\right\} \middle| 0 \right\rangle \\ &= \sum_{p,q,i,a} f_{pq} t_i^a \delta_{pi}\delta_{qa}\langle 0|0\rangle \\ &= \sum_{i,a} f_{ia} t_i^a\end{aligned} \tag{3.22}$$

Similarly for the second term,

$$\begin{aligned}\left\langle 0 \middle| W_N \left(T_2 + \frac{1}{2}T_1^2\right) \middle| 0 \right\rangle &= \sum_{p,q,r,s,i,j,a,b} \frac{1}{4}\langle pq||rs\rangle \left(\frac{1}{4}t_{ij}^{ab} + \frac{1}{2}t_i^a t_j^b\right) \\ &\quad \times \left\langle 0 \middle| \left\{a_p^\dagger a_p^\dagger a_s a_r\right\}\left(\left\{a_a^\dagger a_b^\dagger a_i a_j\right\} + \left\{a_a^\dagger a_i\right\}\left\{a_b^\dagger a_j\right\}\right) \middle| 0 \right\rangle \\ &= \frac{1}{4}\sum_{p,q,r,s,i,j,a,b} \langle pq||rs\rangle \left(t_{ij}^{ab} + \frac{1}{2}t_i^a t_j^b\right)\delta_{pi}\delta_{qj}\delta_{sb}\delta_{ra}\langle 0|0\rangle \\ &= \frac{1}{4}\sum_{i,j,a,b} \langle ij||ab\rangle \left(t_{ij}^{ab} + \frac{1}{2}t_i^a t_j^b\right)\end{aligned} \tag{3.23}$$

which gives the spin orbital equations for the coupled cluster energy:

$$E_{corr} = \sum_{i,a} f_{ia} t_i^a + \frac{1}{4}\sum_{i,j,a,b} \langle ij||ab\rangle \left(t_{ij}^{ab} + \frac{1}{2}t_i^a t_j^b\right) \tag{3.24}$$

Spin orbital forms of the amplitude equations are obtained in the same way. Complete spin orbital equations for the CCSDTQ model, the most complete CC model implemented at the present time, may be found in the recent paper of Kucharski and Bartlett [27].

3.4 Numerical Solution of the Coupled Cluster Equations

The overall result, as can be seen in Eq. 3.21 is a set of coupled nonlinear equations for the amplitudes $t_{ijk\cdots}^{abc\cdots}$ based on the MO integrals f_{pq} and $\langle pq||rs\rangle$. These equations are usually solved by fixed-point iteration starting with a guess for t_{ij}^{ab} obtained from second-order perturbation theory, and it has been found that acceleration methods based on conjugate direction techniques [28–32] are very useful in obtaining faster convergence, and thus reducing the computational effort. Once the amplitudes are converged, Eq. 3.24 may be evaluated to obtain the CC energy. In many cases, the amplitudes and energy will be used, along with the MO integrals, as inputs to further calculations to determine the CC density matrix, gradients of the energy, or other results, for which it is often useful to work in terms of the CC effective Hamiltonian.

3.5 The Coupled Cluster Effective Hamiltonian

When the coupled cluster calculation is carried out as the first step in a Fock-space CC calculation, it is useful to form the elements of

$$\bar{H}_N = e^{-T} H_N e^T = \left(H_N e^T\right)_c \tag{3.25}$$

explicitly from the MO integrals and CC amplitudes because the FSCC equations can be expressed in a compact and computationally efficient form using $\bar{H}_N$. Note that this operator is non-Hermitian, so the bra-ket symmetry of the MO integrals (i.e. $\langle pq||rs\rangle = \langle rs||pq\rangle$) is not carried over to the elements of $\bar{H}_N$:$\langle pq|\bar{|}rs\rangle \neq \langle rs|\bar{|}pq\rangle$.

Because H_N contains at most four second quantized operators, $\bar{H}_N$ will include contractions of H_N with as many as four T clusters. Like H_N, the effective Hamiltonian is described as having one- and two-body components. In fact, while H_N terminates at two-body terms, $\bar{H}_N$ has up to n+2-body terms in an n electron system. Just as the Hamiltonian is often written in terms of f_N and W_N, the components of the effective Hamiltonian are usually denoted $\bar{f}_N$, $\bar{W}_N$, $\bar{I}\bar{I}_N, \ldots$

The $\bar{H}_N$ elements required for the Fock-space coupled cluster methods considered in the next chapter include all of the one- and two-body terms and a few of the three-body terms. They are obtained in the same manner as the spin orbital equations for the CC energy and amplitudes, above, and the results are shown below.

The first stage is to isolate the components of the expansion

$$\left(H_N e^T\right)_c = \left((f_N + W_N)\left(1 + T_1 + T_2 + \frac{1}{2!}T_1^2 + T_3 + T_1T_2 + \frac{1}{3!}T_1^3 + \cdots\right)\right)_c \tag{3.26}$$

from which contractions can form. At the operator level, the equations are closely related to the CC amplitude equations (Eq. 3.21), but with two important differences. First, $\bar{H}_N$ is defined based on *converged* cluster amplitudes, so Eq. 3.21 must be satisfied prior to forming the effective Hamiltonian elements. Secondly, like the Hamiltonian itself, the effective Hamiltonian can have -*n*, . . . , *0*, . . . , *n* excitation character for an *n*–body component. So while $\left\langle {}^{abc\cdots}_{ijk\cdots}\middle|\bar{H}_N\middle|0\right\rangle = 0$ is identical to the CC amplitude equations given above, the effective Hamiltonian itself contains numerous terms besides those required

to satisfy the equation. Thus the one-body component is

$$\bar{f}_N = \Big(f_N \Big\{ 1 + T_1 + T_2 + \frac{1}{2!} T_1^2 \Big\} + W_N \Big\{ T_1 + T_2 + \frac{1}{2!} T_1^2 + T_3 + T_1 T_2 + \frac{1}{3!} T_1^3 \Big\} \Big)_c \tag{3.27}$$

and the two- and three-body components of $\bar{H}_N$, are

$$\bar{W}_N = \Big(f_N \{ T_2 + T_3 + T_1 T_2 \} + W_N \Big\{ 1 + T_1 + T_2 + \frac{1}{2!} T_1^2 + T_3 + T_1 T_2 + \frac{1}{3!} T_1^3 + T_4 + T_1 T_3 + \frac{1}{2!} T_2^2 + \frac{1}{2!} T_1^2 T_2 + \frac{1}{4!} T_1^4 \Big\} \Big)_c \tag{3.28}$$

and

$$\bar{III}_N = \Big(f_N \Big\{ T_3 + T_4 + T_1 T_3 + \frac{1}{2!} T_2^2 \Big\} + W_N \Big\{ T_2 + T_3 + T_1 T_2 + T_4 + T_1 T_3 + \frac{1}{2!} T_2^2 + \frac{1}{3} T_1^2 T_2 + T_5 + T_1 T_4 + \frac{1}{2!} T_2 T_3 + \frac{1}{2!} T_1^2 T_3 + \frac{1}{2!} T_1 T_2^2 + \frac{1}{3!} T_1^3 T_2 \Big\} \Big)_c \tag{3.29}$$

Reduction to spin orbital form follows the same procedure used for the CC equations. In general, the n-body component of the effective Hamiltonian will have $(n+1)^2$ different terms according to the distinct labelings of the indices as occupied or virtual orbitals. The one corresponding to the n–fold excitation will, of course, be zero and for higher n, an increasing number of other terms will be zero. For example in $\bar{III}_N$ it is impossible to form terms with -3, -2, or -1 excitation character, as well as half of the possible 0 excitation terms (the all occupied and all virtual labelings). Thus while the number and complexity of higher-body effective Hamiltonian terms does increase, it is not as

explosive as that seen in many-body perturbation theory (MBPT) [26]. The spin orbital equations for $\bar{H}_N$ are give in Tables 3.1–3.3.

Table 3.1. One-body coupled cluster effective Hamiltonian elements in spin orbital form. Excitation level of operator is given in the first column. See text for explanation of notation.

-1	$\bar{f}_{ai} =$	$f_{ia} + \langle im\|\|ae\rangle t_m^e$
0	$\bar{f}_{ij} =$	$f_{ij} + f_{if}t_j^f - \langle im\|\|je\rangle t_m^e + \frac{1}{2}\langle im\|\|fe\rangle t_{jm}^{fe} + \langle im\|\|fe\rangle t_j^f t_m^e$
0	$\bar{f}_{ab} =$	$f_{ab} - f_{mb}t_m^a + \langle am\|\|be\rangle t_m^e - \frac{1}{2}\langle nm\|\|be\rangle t_{nm}^{ae} - \langle nm\|\|be\rangle t_n^a t_m^e$
+1	$\bar{f}_{ia} =$	$f_{ai} - f_{mi}t_m^a + f_{ae}t_i^e + f_{me}t_{im}^{ae} - f_{me}t_i^e t_m^a - \langle ma\|\|ie\rangle t_m^e$
		$-\frac{1}{2}\langle nm\|\|ie\rangle t_{nm}^{ae} - \langle nm\|\|ie\rangle t_n^a t_m^e + \frac{1}{2}\langle am\|\|fe\rangle t_{im}^{fe} + \langle am\|\|fe\rangle t_i^f t_m^e$
		$+\frac{1}{4}\langle mn\|\|ef\rangle t_{imn}^{aef} + \langle mn\|\|ef\rangle t_{im}^{ae} t_n^f - \frac{1}{2}\langle mn\|\|ef\rangle t_i^e t_{mn}^{af}$
		$-\frac{1}{2}\langle mn\|\|ef\rangle t_m^a t_{in}^{ef} - \langle mn\|\|ef\rangle t_i^e t_m^a t_n^f$

Table 3.2. Two-body coupled cluster effective Hamiltonian elements in spin orbital form. Excitation level of operator is given in the first column. See text for explanation of notation.

-2	$\langle ij\|\bar{\|}ab\rangle =$	$\langle ij\|\|ab\rangle$
-1	$\langle ij\|\bar{\|}ka\rangle =$	$\langle ij\|\|ka\rangle + \langle ij\|\|ea\rangle t_k^e$
-1	$\langle ai\|\bar{\|}bc\rangle =$	$\langle ai\|\|bc\rangle - \langle mi\|\|bc\rangle t_m^a$
0	$\langle ij\|\bar{\|}kl\rangle =$	$\langle ij\|\|kl\rangle + (-)^p P(kl)\langle ij\|\|ke\rangle t_l^e + \frac{1}{2}\langle ij\|\|ef\rangle t_{kl}^{ef}$
		$+(-)^p P(kl)\langle ij\|\|ef\rangle t_k^e t_l^f$
0	$\langle ab\|\bar{\|}cd\rangle =$	$\langle ab\|\|cd\rangle - (-)^p P(ab)\langle am\|\|cd\rangle t_m^b + \frac{1}{2}\langle mn\|\|cd\rangle t_{mn}^{ab}$
		$+(-)^p P(ab)\langle mn\|\|cd\rangle t_m^a t_n^b$
0	$\langle ia\|\bar{\|}jb\rangle =$	$\langle ia\|\|jb\rangle - \langle im\|\|jb\rangle t_m^a + \langle ia\|\|eb\rangle t_j^r - \langle im\|\|eb\rangle t_{jm}^{ea} - \langle im\|\|eb\rangle t_j^e t_m^a$

Table 3.2. (Continued) Two-body coupled cluster effective Hamiltonian elements in spin orbital form. Excitation level of operator is given in the first column. See text for explanation of notation.

$$
\begin{aligned}
+1 \quad \langle ia|\bar{|}jk\rangle = \; & \langle ia||jk\rangle + f_{ie}t^{ea}_{jk} - \langle im||jk\rangle t^{a}_{m} + (-)^{p}P(jk)\langle ia||je\rangle t^{e}_{k} \\
& + (-)^{p}P(jk)\langle im||je\rangle t^{ea}_{mk} - (-)^{p}P(jk)\langle im||je\rangle t^{e}_{k}t^{a}_{m} \\
& + (-)^{p}P(jk)\langle ia||ef\rangle t^{e}_{j}t^{f}_{k} + \tfrac{1}{2}\langle ia||ef\rangle t^{ef}_{jk} + \tfrac{1}{2}\langle mi||ef\rangle t^{efa}_{mjk} \\
& + \langle mi||ef\rangle t^{e}_{m}t^{fa}_{jk} - \tfrac{1}{2}\langle im||fe\rangle t^{fe}_{jk}t^{a}_{m} \\
& - (-)^{p}P(jk)\langle im||fe\rangle t^{fa}_{jm}t^{e}_{k} - (-)^{p}P(jk)\langle im||fe\rangle t^{f}_{j}t^{e}_{k}t^{a}_{m} \\
+1 \quad \langle ab\bar{|}|ci\rangle = \; & \langle ab||ci\rangle - f_{mc}t^{ab}_{mi} + \langle ab||ce\rangle t^{e}_{i} - (-)^{p}P(ab)\langle am||ci\rangle t^{b}_{m} \\
& + \tfrac{1}{2}\langle mn||ci\rangle t^{ab}_{mn} + (-)^{p}P(ab)\langle mn||ci\rangle t^{a}_{m}t^{b}_{n} \\
& + (-)^{p}P(ab)\langle am||ce\rangle t^{eb}_{mi} - (-)^{p}P(ab)\langle am||ce\rangle t^{e}_{i}t^{b}_{m} \\
& - \tfrac{1}{2}\langle mn||ec\rangle t^{eab}_{mni} - \langle mn||ec\rangle t^{e}_{m}t^{ab}_{ni} + (-)^{p}P(ab)\langle nm||ce\rangle t^{a}_{n}t^{e}_{i}t^{b}_{m} \\
& + \tfrac{1}{2}\langle nm||ce\rangle t^{ab}_{nm}t^{e}_{i} + (-)^{p}P(ab)\langle nm||ce\rangle t^{a}_{n}t^{e}_{i}t^{b}_{m} \\
+2 \quad \langle ab\bar{|}|ij\rangle = \; & \langle ab||ij\rangle - (-)^{p}P(ij)f_{mj}t^{ab}_{im} + (-)^{p}P(ab)f_{be}t^{ae}_{ij} \\
& + f_{me}t^{abe}_{ijm} - (-)^{p}P(ij)f_{me}t^{ab}_{im}t^{e}_{j} - (-)^{p}P(ab)f_{me}t^{ae}_{ij}t^{b}_{m} \\
& - (-)^{p}P(ab)\langle mb||ij\rangle t^{a}_{m} + (-)^{p}P(ij)\langle ab||ej\rangle t^{e}_{i} + \tfrac{1}{2}\langle mn||ij\rangle t^{ab}_{mn} \\
& + \tfrac{1}{2}\langle ab||ef\rangle t^{ef}_{ij} - (-)^{p}P(ij)\langle mb||ie\rangle t^{ae}_{mj} + (-)^{p}P(ab)\langle mn||ij\rangle t^{a}_{m}t^{b}_{n} \\
& + (-)^{p}P(ij)\langle ab||ef\rangle t^{e}_{i}t^{f}_{j} - (-)^{p}P(ij)\langle mb||ie\rangle t^{a}_{m}t^{b}_{j} \\
& - \tfrac{1}{2}(-)^{p}P(ij)\langle nm||je\rangle t^{abe}_{inm} + \tfrac{1}{2}(-)^{p}P(ab)\langle bm||fe\rangle t^{afe}_{ijm} \\
& - (-)^{p}P(ij)\langle mn||ei\rangle t^{e}_{m}t^{ab}_{nj} + (-)^{p}P(ab)\langle ma||ef\rangle t^{e}_{m}t^{fb}_{ij} \\
& - (-)^{p}P(ij)(ab)\langle nm||ie\rangle t^{a}_{n}t^{eb}_{mj} + (-)^{p}P(ij)(ab)\langle am||fe\rangle t^{f}_{i}t^{eb}_{mj} \\
& + \tfrac{1}{2}(-)^{p}P(ij)\langle mn||ej\rangle t^{e}_{i}t^{ab}_{mn} - \tfrac{1}{2}(-)^{p}P(ab)\langle mb||ef\rangle t^{a}_{m}t^{ef}_{ij} \\
& + (-)^{p}P(ij)(ab)\langle mn||ej\rangle t^{e}_{i}t^{a}_{m}t^{b}_{n} - (-)^{p}P(ij)(ab)\langle mb||ef\rangle t^{e}_{i}t^{a}_{m}t^{f}_{j} \\
& + \tfrac{1}{4}\langle mn||ef\rangle t^{abef}_{ijmn} + \langle mn||ef\rangle t^{abe}_{ijm}t^{f}_{n} - \tfrac{1}{2}(-)^{p}P(ij)\langle mn||ef\rangle t^{e}_{i}t^{afb}_{mnj} \\
& - \tfrac{1}{2}(-)^{p}P(ab)\langle mn||ef\rangle t^{a}_{m}t^{efb}_{inj} + (-)^{p}P(ij)\langle mn||ef\rangle t^{ae}_{im}t^{fb}_{nj} \\
& + \tfrac{1}{4}\langle mn||ef\rangle t^{ef}_{ij}t^{ab}_{mn} - \tfrac{1}{2}(-)^{p}P(ab)\langle mn||ef\rangle t^{ae}_{ij}t^{bf}_{mn}
\end{aligned}
$$

Table 3.2. (Continued) Two-body coupled cluster effective Hamiltonian elements in spin orbital form. Excitation level of operator is given in the first column. See text for explanation of notation.

$$
\begin{aligned}
&-\tfrac{1}{2}(-)^p P(ij)\langle mn||ef\rangle t_{im}^{ab} t_{jn}^{ef} - (-)^p P(ij)(ab)\langle mn||ef\rangle t_i^e t_m^a t_{nj}^{fb} \\
&+\tfrac{1}{2}(-)^p P(ij)\langle mn||ef\rangle t_i^e t_j^f t_{nm}^{ab} + \tfrac{1}{2}(-)^p P(ab)\langle mn||ef\rangle t_m^a t_n^b t_{ij}^{ef} \\
&-(-)^p P(ij)\langle nm||fe\rangle t_n^f t_i^e t_{mj}^{ab} - (-)^p P(ab)\langle nm||fe\rangle t_n^f t_m^a t_{ij}^{eb} \\
&+(-)^p P(ij)\langle mn||ef\rangle t_i^e t_m^a t_j^f t_n^b
\end{aligned}
$$

The summation convention (all repeated indices are summed) has been used to save space and simplify presentation of these formulae. The permutation symbols, $(-)^p P()$, are used in the same fashion as Lee *et al.* [33] and Kucharski and Bartlett [27]. A permutation of two indices, e.g. $(-)^p P(ij)$, denotes two terms. One is the identity permutation, with signature p=+1, while the second is the term with indices i and j interchanged. A permutation of three indices, e.g. $(-)^p P(ijk)$, represents six terms with signature p=+1 for cyclic permutations and p=-1 for acyclic permutations. The symbol $(-)^p P(i/jk)$ indicates that permutations $i \leftrightarrow j$ and $i \leftrightarrow k$ should be taken, but not $j \leftrightarrow k$; the signature is the same as for a binary permutation. Finally, a composite symbol, such as $(-)^p P(i/jk, ab)$, indicates that the direct product of the two sets of permutations (i/jk and ab) should be taken.

3.6 Truncation of the Cluster Operator

It is worth noting that we have made no approximations in deriving the equations given above, and the energy, wavefunction, and effective Hamiltonian thus determined would be exact (for the chosen atomic orbital basis). Unfortunately, the number of

Table 3.3. Three-body coupled cluster effective Hamiltonian elements needed for Fock-space (1,0), (0,1), and (1,1) sectors in spin orbital form. (The full $I\bar{I}I_N$ includes an element at excitation levels +2, and +3 in addition to those shown here.) Excitation level of operator is given in the first column. See text for explanation of notation.

0	$\langle aij\bar{\|}\|klc\rangle =$	$\langle ij\|\|ec\rangle t^{ae}_{kl}$
0	$\langle abi\bar{\|}\|jcd\rangle =$	$-\langle mi\|\|cd\rangle t^{ab}_{jm}$
+1	$\langle ija\bar{\|}\|klm\rangle =$	$(-)^p P(ml/k)\langle ji\|\|ek\rangle t^{ae}_{ml} + \frac{1}{2}\langle ji\|\|ef\rangle t^{cab}_{imn}$
		$+(-)^p P(k/lm)\langle ji\|\|ef\rangle t^{ae}_{ml} t^{f}_{k}$
+1	$\langle abc\bar{\|}\|dei\rangle =$	$-(-)^p P(b/ac)\langle mb\|\|de\rangle t^{ca}_{im} + \frac{1}{2}\langle mn\|\|de\rangle t^{cab}_{imn}$
		$+(-)^p P(b/ac)\langle mn\|\|de\rangle t^{ca}_{im} t^{b}_{n}$
+1	$\langle iab\bar{\|}\|jck\rangle =$	$-\langle mi\|\|ec\rangle t^{abe}_{jkm} + (-)^p P(jk)\langle mi\|\|ec\rangle t^{ab}_{jm} t^{e}_{k}$
		$+(-)^p P(ab)\langle mi\|\|ec\rangle t^{ae}_{jk} t^{b}_{m} - (-)^p P(jk)\langle mi\|\|jc\rangle t^{ab}_{km}$
		$+(-)^p P(ab)\langle ia\|\|ec\rangle t^{be}_{kj}$
+2	$\langle iab\bar{\|}\|jkl\rangle =$	$(-)^p P(jk/l)\langle im\|\|jk\rangle t^{ab}_{ml} + (-)^p P(j/kl, ab)\langle ia\|\|je\rangle t^{eb}_{kl}$
		$-(-)^p P(k/jl, ab)\langle mi\|\|ke\rangle t^{a}_{m} t^{eb}_{jl} - (-)^p P(jkl)\langle im\|\|ek\rangle t^{e}_{j} t^{ab}_{ml}$
		$+(-)^p P(jk/l, ab)\langle im\|\|fe\rangle t^{af}_{kj} t^{eb}_{ml} - \frac{1}{2}(-)^p P(jk/l)\langle im\|\|ef\rangle t^{ef}_{kl} t^{ab}_{ml}$
		$+(-)^p P(j/kl, ab)\langle ia\|\|ef\rangle t^{e}_{j} t^{fb}_{kl} + f_{ie} t^{eab}_{jkl}$
		$+(-)^p P(j/kl)\langle im\|\|je\rangle t^{eab}_{mkl} + \frac{1}{2}(-)^p P(ab)\langle ia\|\|ef\rangle t^{efb}_{jkl}$
		$+(-)^p P(j/kl)\langle im\|\|fe\rangle t^{f}_{j} t^{eab}_{mkl} - \frac{1}{2}(-)^p P(ab)\langle im\|\|ef\rangle t^{aef}_{kjl} t^{b}_{m}$
		$+(-)^p P(jk/l, ab)\langle im\|\|fe\rangle t^{af}_{kj} t^{eb}_{ml} - \frac{1}{2}(-)^p P(jk/l)\langle im\|\|ef\rangle t^{ef}_{kl} t^{ab}_{ml}$
		$-(-)^p P(k/jl, ab)\langle mi\|\|ef\rangle t^{e}_{k} t^{a}_{m} t^{fb}_{jl} - (-)^p P(jkl)\langle im\|\|fe\rangle t^{f}_{j} t^{e}_{k} t^{ab}_{ml}$
		$+\frac{1}{2}\langle mi\|\|ef\rangle t^{efab}_{mjkl} + \langle mi\|\|ef\rangle t^{e}_{m} t^{fab}_{jkl}$

amplitudes to be determined is *O(N!)* for N AO basis functions. This rapidly becomes too expensive to compute using current and forseeable computer facilities, so it is necessary to make approximations. The obvious choice is to limit the cluster operators included in T to lower levels of excitation because the number of amplitudes grows by a factor

of $n(N\text{-}n)$ for each additional excitation. Because of the exponential nature of the CC wave operator, some higher excitation effects are incorporated by products of lower-level excitations (i.e. T_1T_2 is a triple excitation). In fact in most cases, such products dominate the wavefunction at a given level of excitation [34].

The single excitations alone cannot have any contribution to the energy, so the first reasonable approximation is $T=T_2$, known as the CCD (coupled cluster-doubles) model. With the doubles present, the singles can also contribute, so $T=T_1+T_2$, the CCSD model, would be next on the hierarchy. Increasingly sophisticated methods are obtained by adding the next level cluster operator: CCSDT, CCSDTQ, . . .

To obtain approximate versions of the equations given in this chapter, simply consider all cluster operators not present in the desired model to be zero and eliminate them from the equation. For example, CCSD equations would have $T_3=T_4=T_5=0$, and all terms involving these operators would be eliminated. Observe, however, that products of T_1 and T_2 giving overall triple, quadruple, and higher excitations *would* still appear. This is a consequence of the exponential expansion and is the reason why a given truncation of coupled cluster theory recovers more of the correlation energy than the same truncation of operator manifold in the linear CI expansion (Eq. 3.1).

In practice, the CCSD model has proven widely applicable, and the more expensive CCSDT model, and approximations which involve perturbative inclusion of the triple excitation effects, provide higher accuracy and have been shown capable of handling some problems that would otherwise require multireference techniques [34]. The CCSDT model, or perturbative approximations, are currently the practical limit for the majority

of interesting systems. Further, the computer code used in this work does not presently include the full CCSDT model, so calculation of $\bar{H}_N$ is limited to the CCSD level.

CHAPTER 4
FOCK SPACE COUPLED CLUSTER THEORY

4.1 Introduction

In the preceding chapter, the CC equations were derived in a spin orbital framework. This approach allows the use of wide range of reference functions (RHF, UHF, ROHF, QRHF, etc.) thus allowing application to both closed and open shell systems with relative ease. For open shell molecules, these spin orbital based CC methods may be characterized as eigenfunctions of the S^2 operator in a projected sense, $\langle 0|S^2|\Psi_{cc}\rangle = s(s+1)$, for ROHF and QRHF references, or not at all, for UHF references. Although they have been very successful [34], failure to be a *rigorous* eigenfunction, $S^2|\Psi_{cc}\rangle = s(s+1)|\Psi_{cc}\rangle$, makes this approach less desirable to some workers in the field. The Fock space coupled cluster method grew out of a search for an approach to open shell systems which would be a rigorous eigenfunction of S^2 and be capable of handling the multiple reference determinants needed to represent many open shell states.

There are two primary approaches to the treatment of multireference systems. The Hilbert space approach, also referred to as state-specific, or valance-universal, treats a manifold of states with a constant number of electrons, and each Hilbert space CC calculation focuses on a particular state. The Fock space (FS) approach treats states with different numbers of electrons (mathematically, a Fock space is a sum of Hilbert spaces with different numbers of electrons), simultaneously calculating several different states.

The FSCC method is, at present, the more developed of the two, and offers the useful feature, mentioned in Chapter 1, that it can provide data for more than one state in a single calculation.

In this chapter, we will develop the FSCC equations in more detail, obtaining spin orbital equations for IPs at the FSCCSDT level. The FSCC approach will be compared with the familiar, and (reasonably) well understood single reference CC approach to point up the inequivalence between FSCC and CC calculations at the same level of truncation and note the increased importance of higher excitations (triples in particular) in the FSCC approach. Finally, a number of approximations to the full inclusion of triple excitations are proposed in order to include some triple excitation effects but reduce the computational effort required.

4.2 Structure of FSCC

A multireference description of a correlated wavefunction means that the determinantal expansion is partitioned into two components. The *model* space includes the determinants desired as references, and the *complementary* space, which is orthogonal to the model space, contains excited determinants resulting from each of the model space functions. The same division holds trivially for single reference CC, with the one reference determinant being the model space and all excited determinants being in the complementary space. These two spaces may be represented by projection operators, P, and Q, for the model and complementary spaces respectively, defined from the functions

they include:

$$P = \sum_p |\phi_p\rangle\langle\phi_p|$$
$$Q = \sum_q |\phi_q\rangle\langle\phi_q| = 1 - P \tag{4.1}$$

which are orthogonal

$$PQ = QP = 0 \tag{4.2}$$

and idempotent

$$PP = P,\ QQ = Q. \tag{4.3}$$

For convenience, we choose a single determinant one-electron reference function, $|0\rangle$, to provide an unambiguous identification of occupied and virtual orbitals. The idea of a particle-hole rank, denoted (m,n), is used to indicate the states related to $|0\rangle$ by the addition of m electrons (*particles* in the otherwise empty virtual orbitals) and the removal of n electrons (*holes* in the occupied orbitals). Thus singly ionized states are in the (0,1) sector, electron-attached states are in the (1,0) sector, and the (1,1) sector includes states obtained by exciting a single electron from $|0\rangle$. Higher particle-hole ranks give multiply ionized or multiply attached states, excitations involving more than one electron, and combinations such as "shake-ups" (combination of detachment of an electron and excitation of another). The idea of the model space and its orthogonal complement can also be specialized to a particular particle-hole rank, giving projection operators $P^{(m,n)}$ and $Q^{(m,n)}$, respectively.

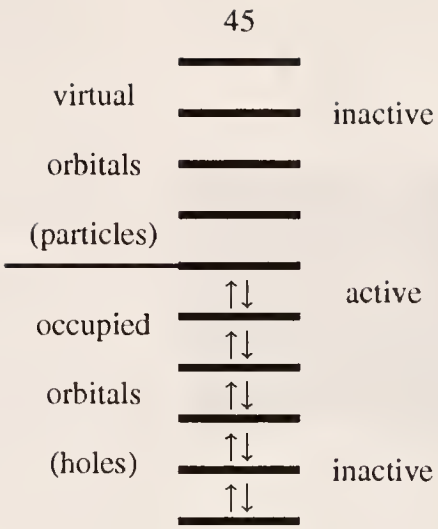

Figure 4.1. Division of orbital space into active and inactive groups.

In order to define the model space, the orbital space of the reference determinant, $|0\rangle$, is divided into two classes. *Active* orbitals are those which change occupation in the various model functions, while *inactive* orbitals maintain the same occupancy. Since the reference function has already been divided into virtual and occupied orbitals, the result is a four different categories of orbitals: active occupied, active virtual, inactive occupied, and inactive virtual. These divisions are shown in Figure 4.1. Once the active orbitals are chosen, the model space for each particle-hole rank is determined — all appropriate occupations of the active space are included. For example in Figure 4.1, the (0,1) sector (one electron removed) model space includes six determinants and the (1,0) sector has four because there are four ways to add a single electron to the active virtual space; there are 12 spin-conserving single excitations within the active space, hence 12 model functions in the (1,1) sector. It should be noted that this scheme provides for exactly one model function, $|0\rangle$, in the (0,0) sector, and the calculation in this sector is exactly the single reference CC method discussed in the preceding chapter.

Model spaces can be divided into two types, complete or incomplete [35]. A *complete* model space is one that contains all possible occupations of the active orbitals, while in an *incomplete* model space (IMS), some occupations of the active orbitals belong to the Q space. The pure ionization and pure electron addition sectors, (0,n) and (m,0) sectors are always complete, but any mixed sector is, in general, incomplete. For example, the (1,1) sector has all single excitations within the model space in P, but places all double, triple, and higher excitations into the Q space. The (1,1) sector is, however, part of a special class of IMS known as the *quasi-complete* model space [35,36]. In this case, the active orbitals are divided into disjoint sets, each with a fixed number of electrons. If each of these subsets is complete within itself, the entire model space is quasi-complete.

The FSCC wavefunction for a state is obtained from a wave operator, Ω, operating on a linear combination of model space functions:

$$|\Psi_{\mathrm{FSCC}}\rangle = \Omega|\Psi_k\rangle. \tag{4.4}$$

where

$$|\Psi_k\rangle = \sum_i C_{ki}|\phi_i\rangle. \tag{4.5}$$

The wave operator used in FSCC is an exponential of cluster operators, just as in the single reference theory, but with a normal product used to avoid contractions within the cluster operators itself (this is not necessary in the single reference formalism since it is impossible for those cluster operators to contract among themselves),

$$\Omega = \left\{e^S\right\}. \tag{4.6}$$

The cluster operator itself, however, has a somewhat different structure from the single reference case:

$$S = S^{(m,n)} = \sum_{\substack{k=0\ldots m \\ l=0\ldots n}} T^{(k,l)}, \tag{4.7}$$

where (m,n) is the highest sector relevant to the problem, and the $T^{(k,l)}$ for a given sector includes single, double, and higher excitation cluster operators for that sector:

$$T^{(k,l)} = T_1^{(k,l)} + T_2^{(k,l)} + T_3^{(k,l)} + \cdots \tag{4.8}$$

Such a wave operator is *valance-universal* because it applies to all sectors from (0,0) to (m,n). As mentioned above, the (0,0) sector is a CC calculation with $|0\rangle$ as the reference, so $T^{(0,0)}$ is nothing more than the familiar CC cluster operator described in the previous chapter. Cluster operators for other sectors are different from the (0,0) ones because they apply to spaces with different numbers of electrons, or at least electrons in different places than in $|0\rangle$ (i.e. active virtuals may contain electrons and active occupieds may receive electrons). In the (0,1) sector, for example, one of the virtual orbital labels on a cluster amplitude becomes an active occupied, corresponding to the fact that in this sector, an electron has been removed from that group, making it possible for the empty orbital to receive an electron. The differences by sector in the cluster operators is depicted in graphical form by Rittby and Bartlett [37] for a number of sectors, and some implications of these differences are discussed in Section 4.3, below.

To derive the FSCC equations themselves, we begin from the Schrödinger equation for the FSCC wavefunction,

$$H\Omega|\Psi_k\rangle = E_k\Omega|\Psi_k\rangle. \tag{4.9}$$

This equation can be rewritten in terms of the model space functions by defining a matrix ϵ' having the E_i as eigenvalues and C as eigenvectors, and using the model space projector, P, to effectively encompass the entire model space,

$$H\Omega P = \Omega\epsilon' P. \tag{4.10}$$

Using the fact that the (0,0) sector cluster operator commutes with the others [38], we can decouple the (0,0) sector calculation from the rest of the FSCC calculation. First, we extract $T^{(0,0)}$ from the wave operator,

$$\Omega = e^{T^{(0,0)}}\tilde{\Omega} = e^{T^{(0,0)}}\left\{e^{\tilde{S}^{(m,n)}}\right\}, \tag{4.11}$$

where

$$\tilde{S}^{(m,n)} = \sum_{\substack{k=0\ldots m,l=0\ldots n \\ k+l\neq 0}} T^{(k,l)}, \tag{4.12}$$

and multiply both sides of the Schrödinger equation by $\exp\left(-T^{(0,0)}\right)$ to obtain

$$e^{-T^{(0,0)}}H_N e^{T^{(0,0)}}\tilde{\Omega}P = \tilde{\Omega}\epsilon' P \tag{4.13}$$

Recalling that the coupled cluster effective Hamiltonian, derived in the preceding chapter, is

$$\begin{aligned}\bar{H}_N &= e^{-T^{(0,0)}}He^{T^{(0,0)}} - \langle 0|\bar{H}|0\rangle \\ &= e^{-T^{(0,0)}}He^{T^{(0,0)}} - E_{cc,|0\rangle}\end{aligned} \tag{4.14}$$

where $E_{cc,|0\rangle}$ is the CC energy of the reference function $|0\rangle$, and defining a new matrix, $\epsilon = \epsilon' - E_{cc,|0\rangle}$, which, when diagonalized, represents energy *differences* between $E_{cc,|0\rangle}$ and the final state, we can write the FSCC Schrödinger equation in the simplified form:

$$\bar{H}_N\tilde{\Omega}P = \tilde{\Omega}\epsilon P. \tag{4.15}$$

Projecting Eq. 4.15 on the left with $P\tilde{\Omega}^{-1}$, we can isolate ϵ as the FSCC *effective Hamiltonian,*

$$PH_{N,\text{eff}}P \equiv P\tilde{\Omega}^{-1}\bar{H}_N\tilde{\Omega}P = P\epsilon P, \tag{4.16}$$

which, upon diagonalization, gives the state-to-state energy differences we seek. Note that this result could have been obtained by requiring intermediate normalization, $P\tilde{\Omega}P = 1$, but Mukherjee [39] has shown that for the general case of an incomplete model space, intermediate normalization is incompatible with size extensivity. Although this will not cause problems for the (0,1) sector, our ultimate focus, we prefer to derive generally applicable equations as far as possible. To determine the cluster operators, we project Eq. 4.15 on the left with the complementary space determinants, giving

$$Q\bar{H}_N\tilde{\Omega}P - Q\tilde{\Omega}PH_{N,\text{eff}}P = 0, \tag{4.17}$$

which is often referred to as the Bloch equation. Mukherjee and coworkers have shown that for complete and quasi-complete model spaces, $H_{N,\text{eff}}$ in Eq. 4.17 is connected and the energies obtained by diagonalizing it are size extensive [39–44].

Haque and Mukherjee [38,45] have also shown that there is a *subsystem embedding condition* (SEC) in the FSCC equations which allows Eq. 4.17 to be solved separately for each sector in a hierarchical fashion. As already observed, the (0,0) sector reference problem decouples from the rest of the Fock-space problem. The (1,0) and (0,1) sectors can be solved with only the (0,0) results — they do not depend on any higher sectors. Given the (0,0), (1,0), and (0,1) sector amplitudes and $H_{N,\text{eff}}$, the (2,0), (1,1), and (0,2)

sectors can be solved — once again, no information from higher sectors is required. In this fashion, the solution of the desired (m,n) sector is built up from lower sectors, rather than requiring the solution to a set of coupled equations for all sectors. The SEC is also very useful in the development of computer programs for FSCC because the implementation of a new sector should not require any changes to the lower sectors.

4.3 Comparison with Single Reference CC Theory

Before going on to derive the more specific equations for Fock-space methods, it is worth taking a look at how the FSCC approach differs from the more familiar single reference formulation.

As has been noted, the Fock space coupled cluster amplitudes differ from (0,0) sector amplitudes in that they involve excitations between the occupied or virtual orbitals and orbitals of the same type in the active space. In the reference function, $|0\rangle$, such amplitudes would be zero because active occupied orbitals would be fully occupied, so no excitation could deposit an electron there, and active virtuals would be completely unoccupied, providing no electron to excite to another virtual. In the model space, however, there will be determinants with holes in the active occupied space and particles in the active virtual space, so such amplitudes may be nonzero. This fact changes the character of FSCC single, double, etc., excitation amplitudes from their familiar (0,0) sector interpretations and means that a given truncation of FSCC will not provide the same results for a given state as the same truncation of the (0,0) sector equations applied to the model space function.

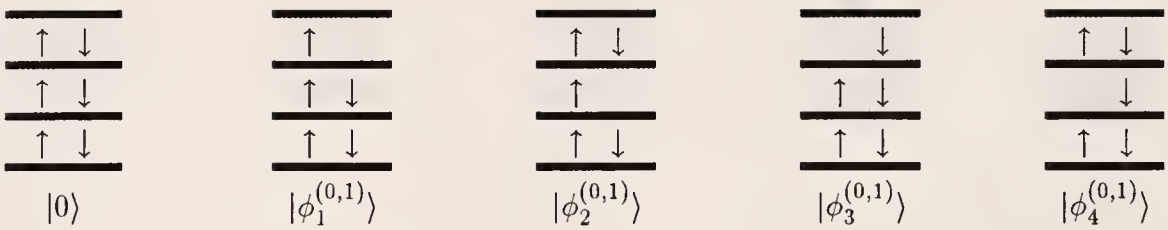

Figure 4.2. Prototypical reference functions and model space determinants. Active orbitals are shaded.

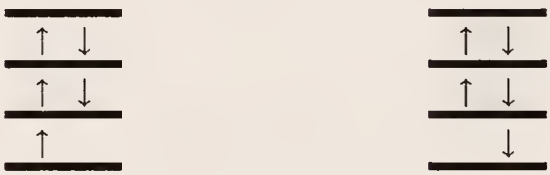

Figure 4.3. Determinants appearing both in the single excitation space of CCSD calculations on the four model functions and in the FSCCSD singles space.

To make this idea more concrete, consider a FSCCSD IP calculation compared to CCSD calculations based on the individual determinants in the model space. Using an RHF reference function with three occupied orbitals and one virtual orbital, if the two highest occupied orbitals are made active, we have four determinants in the model space, as shown in Figure 4.2.

A CCSD calculation on any of the model space functions has seven determinants in the single excitation space, and the union of the four single excitation spaces contains 20 distinct determinants. FSCCSD, on the other hand, restricts single excitations to be from an inactive occupied orbital to an active occupied, which allows only four amplitudes and yields two distinct determinants, shown in Figure 4.3. The remaining 18

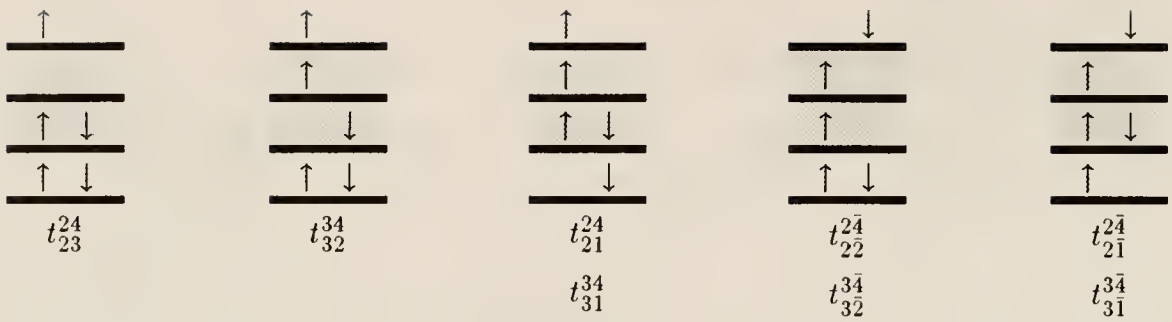

Figure 4.4. Examples of determinants arising from spectator double excitations in FSCC, corresponding to single excitations in the CC model. Shown are all determinants generated from the $|\phi_1^{(0,1)}\rangle$ model function with the relevant amplitudes from $T_2^{(0,1)}$ indicated below each one. Orbitals are numbered from lowest energy (bottom) to highest (top); beta spin electrons are indicated by a bar over the orbital index.

CCSD determinants are generated in the Fock space calculation by a class of excitations referred to as *spectator* doubles. FS double amplitudes include one excitation from an occupied orbital to an active occupied. There is no restriction on the initial orbital, so it may be active as well — in fact it may be the *same* as the final orbital. This null excitation, which is necessary to distinguish between excitations connecting different model functions to the same final determinant [46,45], makes spectator doubles effectively single excitations in the usual coupled cluster sense. Figure 4.4 shows the spectator doubles arising from model function $|\phi_1^{(0,1)}\rangle$, along with the corresponding amplitudes.

When considered at truncation to only double excitations (CCD and FSCCD), the Fock space approach is going to include some (but not all) effects of single excitations — a potential advantage. When higher cluster operators are included, however, FSCC is at an unequivocal disadvantage. Compare, for the same model problem, the double excitations obtained from the CC and FSCC approaches. FSCCSD generates 22 "true"

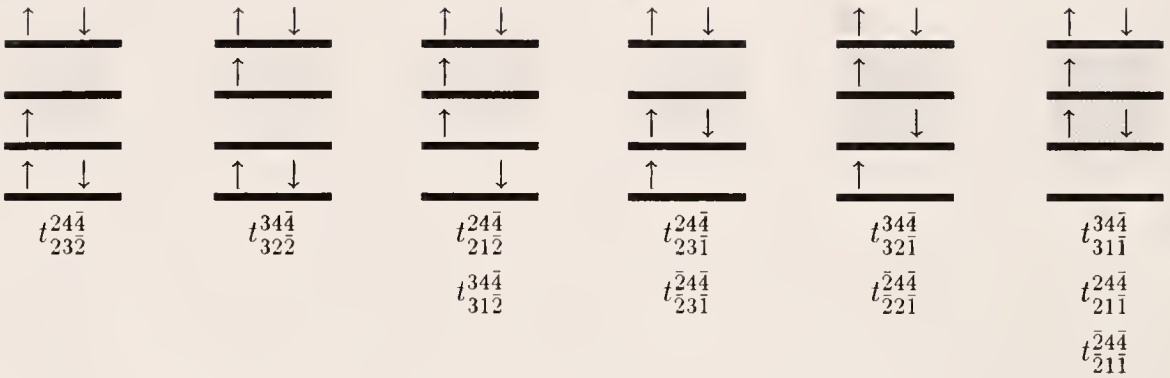

Figure 4.5. Examples of determinants arising from spectator triple excitations in FSCC, corresponding to double excitations in the CC model. Shown are all determinants generated from the $|\phi_1^{(0,1)}\rangle$ model function with the relevant amplitudes from $T_3^{(0,1)}$ indicated below each one. Orbitals are numbered from lowest energy (bottom) to highest (top); beta spin electrons are indicated by a bar over the orbital index.

doubly excited determinants, while CCSD calculations on the individual model functions yield 18 additional determinants. The "extra" CCSD determinants are created in FSCC by spectator triple excitations, a few of which are displayed in Figure 4.5.

From these examples, it should be evident that for a FSCC IP calculation to match the expansion space of a single reference CC of a given truncation on one of the model functions, the FSCC calculation must include spectator contributions from the next higher cluster operator. The same would be true of EA calculations, and in higher sectors, more indices of a given amplitude terminate in the active space (p=m+n for the (m,n) sector), so it would be necessary to include spectators from the p^{th} higher cluster operator to obtain an expansion space equivalent to that of the single reference CC.

4.4 Basic Equations

From this point, we will focus on the (0,1) sector, which describes one-electron ionizations with respect to the reference state and are of particular interest in this work.

From Eq. 4.17, the detailed operator equations which determine each cluster operator are easily determined by expanding the exponential wave operator, as in the previous chapter. Note that in FSCC, products of cluster operators in the exponential expansion contribute to other sectors, making the (0,1) equations a good deal simpler than their CC counterparts.

$$P^{(0,1)}\bar{H}_{N,\mathrm{eff}}P^{(0,1)} = P^{(0,1)}\Big\{\bar{f}_N\Big(1+T_1^{(0,1)}+T_2^{(0,1)}\Big) + \bar{W}_N\Big(T_2^{(0,1)}+T_3^{(0,1)}\Big) + I\bar{I}I_N T_3^{(0,1)}\Big\}_c P^{(0,1)} \tag{4.18}$$

$$0 = Q_1^{(0,1)}\Big\{\bar{f}_N\Big(1+T_1^{(0,1)}+T_2^{(0,1)}\Big) + \bar{W}_N\Big(T_2^{(0,1)}+T_3^{(0,1)}\Big) + I\bar{I}I_N T_3^{(0,1)} - T_1^{(0,1)}\bar{H}_{N,\mathrm{eff}}^{(0,1)}\Big\}_c P^{(0,1)} \tag{4.19}$$

$$0 = Q_2^{(0,1)}\Big\{\bar{f}_N\Big(T_2^{(0,1)}+T_3^{(0,1)}\Big) + \bar{W}_N\Big(1+T_1^{(0,1)}+T_2^{(0,1)}+T_3^{(0,1)}\Big) + I\bar{I}I_N\Big(T_2^{(0,1)}+T_3^{(0,1)}\Big) - T_2^{(0,1)}\bar{H}_{N,\mathrm{eff}}^{(0,1)}\Big\}_c P^{(0,1)} \tag{4.20}$$

$$0 = Q_3^{(0,1)}\Big\{\bar{f}_N T_3^{(0,1)} + \bar{W}_N\Big(T_2^{(0,1)} + T_3^{(0,1)}\Big) + I\bar{I}I_N\Big(1 + T_1^{(0,1)} + T_2^{(0,1)} + T_3^{(0,1)}\Big) - T_3^{(0,1)}\bar{H}_{N,\mathrm{eff}}^{(0,1)}\Big\}_c P^{(0,1)} \tag{4.21}$$

4.5 Reduction to Spin Orbital Equations

Equations 4.18–4.21 are transformed to spin orbital form following the same procedures used in the previous chapter for the CC amplitude equations and $\bar{H}_N$. The resulting equations for the FSCCSDT method for ionization potentials are given in Eq. 4.22–4.25, below. The notation is the same as that used in the previous chapter with a few additions. The Fock-space cluster amplitudes are called τ to avoid any possibility of confusion with the (0,0) sector amplitudes, t. A single dot on an orbital index, $\dot{m}$, indicates restriction to *inactive* orbitals, and a double dot, $\ddot{m}$, indicates restriction to *active* orbitals (this choice of notation is meant to remind readers familiar with the diagrammatic notation of the "circled arrow" used to denote inactive lines, and the double arrow for active lines).

$$\big(H_{N,\mathrm{eff}}\big)_{\ddot{i}\ddot{k}} = \bar{f}_{\ddot{i}\ddot{k}} - \bar{f}_{\dot{m}\ddot{k}}\tau_{\dot{m}}^{\ddot{l}} + \bar{f}_{me}\tau_{\dot{k}\dot{m}}^{\ddot{i}\ddot{e}} - \frac{1}{2}\Big\langle mn\bar{||}\ddot{k}e\Big\rangle\tau_{mn}^{\ddot{i}\ddot{e}} + \frac{1}{4}\big\langle mn\bar{||}ef\big\rangle\tau_{\dot{k}mn}^{\ddot{i}\ddot{e}f} \tag{4.22}$$

$$0 = \bar{f}_{\ddot{i}\dot{k}} - \bar{f}_{\dot{m}\dot{k}}\tau_{\dot{m}}^{\ddot{l}} + \bar{f}_{me}\tau_{\dot{k}\dot{m}}^{\ddot{i}\ddot{e}} - \frac{1}{2}\Big\langle mn\bar{||}\dot{k}e\Big\rangle\tau_{mn}^{\ddot{i}\ddot{e}} + \frac{1}{4}\big\langle mn\bar{||}ef\big\rangle\tau_{\dot{k}mn}^{\ddot{i}\ddot{e}f} + \tau_{\dot{k}}^{\ddot{m}}\big(H_{N,\mathrm{eff}}\big)_{\ddot{l}\ddot{m}} \tag{4.23}$$

$$0 = \left\langle \ddot{l}a|\bar{|}ki \right\rangle + \bar{f}_{ae}\tau_{ki}^{\ddot{l}a} - (-1)^p P(ki)\bar{f}_{mi}\tau_{km}^{\ddot{l}a} - \langle \dot{m}a|\bar{|}ki\rangle\tau_{\dot{m}}^{\ddot{l}}$$

$$+ \frac{1}{2}(-1)^p P(ki)\langle mn|\bar{|}ki\rangle\tau_{mn}^{\ddot{l}a} - \langle ma|\bar{|}ke\rangle\tau_{mi}^{\ddot{l}e} - \frac{1}{2}\langle man|\bar{|}kie\rangle\tau_{mn}^{\ddot{l}e}$$

$$+ \bar{f}_{me}\tau_{kim}^{\ddot{l}ae} + \frac{1}{2}(-1)^p P(ki)\langle mn|\bar{|}ke\rangle\tau_{mni}^{\ddot{l}ea} + \frac{1}{2}\langle ma|\bar{|}ef\rangle\tau_{kmi}^{\ddot{l}ea} + \tau_{ki}^{\ddot{m}a}\left(H_{N,\text{eff}}\right)_{\ddot{l}\ddot{m}} \tag{4.24}$$

$$0 = \left\langle \ddot{l}ab|\bar{|}kij \right\rangle - (-)^p P(k/ij)\langle mb|\bar{|}ij\rangle\tau_{km}^{\ddot{l}a} + (-)^p P(ki/j)\langle ab|\bar{|}ej\rangle\tau_{ki}^{\ddot{l}e}$$

$$+ \frac{1}{2}(-)^p P(ab)\langle man|\bar{|}kij\rangle\tau_{mn}^{\ddot{l}b} - (-)^p P(ki/j)\langle mib|\bar{|}kie\rangle\tau_{mj}^{\ddot{l}e} - \langle \dot{m}ab|\bar{|}kij\rangle\tau_{\dot{m}}^{\ddot{l}}$$

$$+ (-)^p P(ab)\bar{f}_{be}\tau_{kij}^{\ddot{l}ae} - (-)^p P(ki/j)\bar{f}_{mj}\tau_{kim}^{\ddot{l}ab} + (-)^p P(ki/j)\langle mn|\bar{|}ki\rangle\tau_{mnj}^{\ddot{l}ab}$$

$$- (-)^p P(k/ij,ab)\langle ma|\bar{|}ke\rangle\tau_{mij}^{\ddot{l}eb} + \tau_{kij}^{\ddot{m}ab}\left(H_{N,\text{eff}}\right)_{\ddot{l}\ddot{m}} \tag{4.25}$$

4.6 Approximations to the Full FSCCSDT Model

In the single reference CC world, the full CCSDT model has seen limited use for a number of reasons

- Complexity of the method — the triples equations have many more terms than single and double excitations, thus requiring substantially more effort to code them into a computer program.
- Primary and secondary memory (i.e. physical memory and disk space) requirements for storage and manipulation of the cluster amplitudes, which are significantly more

numerous than the double excitation amplitudes — a factor of $n(N\text{-}n)$ in the language of section 3.6.

- Time constraints, since many more amplitudes must be determined, the time required increases in a similar fashion.

As a result, a number of approximations to the full CCSDT method have been proposed and have proven quite effective at incorporating important effects of triple excitations while at the same time minimizing the above concerns [33,47–52]. These concerns might also be raised with respect to the full FSCCSDT method, so in the same spirit, we propose several approximations of FSCCSDT as a compromise between the cost and performance of the full model.

There are two different approaches to approximating FSCC triples which may be considered. One, in analogy to the approximate triples treatments of single reference CC, involves truncations and perturbative approximations to the triples equations. The second method is to restrict the triples amplitudes which are evaluated to something less than the full set. This approach, which has not been employed in CC theory, is suggested by the earlier observation that spectator triples must be included to, in some sense, duplicate the expansion space of a single reference CCSD calculation. The two approaches are not exactly orthogonal, but can be considered, by and large, independently.

In single reference CC theory, there are no self–evident subsets of the triples amplitudes, so this approach has not been tried (or at least not reported in the literature). In FSCC, however, there are two obvious subsets which might be considered. The smallest set would be the spectator amplitudes, as suggested by the discussion in the

previous section. A larger set would be to include all active-active amplitudes. This set, which includes the spectators, allows excitations from any active orbital into any other (spectators involve an active orbital scattering into itself, and the full set of triples allows scattering from inactive orbitals to occupied orbitals as well as active to active).

As we saw in the previous section, it is necessary to introduce spectator triples in the Fock space approach in order to match the expansion space of a CCSD treatment of each of the model functions in turn. On the other hand, since FSCC describes all states of interest with a single set of amplitudes (with diagonalization of the effective Hamiltonian distinguishing among individual states), it can be argued that it is impossible for it to be equivalent to a separate CC calculation for each model function, and the differences in the expansion space between the two approaches should not be a concern. Indeed, a number of calculations in the literature [53,54,43,55, for example] support the idea that FSCCSD is well-balanced and the results obtained are numerically on a par with other methods. The CCSD method has been widely applied, and its behavior is reasonably well understood — certainly there is far more experience with CCSD than with any FSCC method — and this, more than any special quality of CCSD underlies the desire for a FSCC method that can mimic it. Only a critical examination of the proposed spectator and active-active approximations for a wide range of systems can determine if they will improve the results over FSCCSD or destroy the balance of the FSCC method.

The second approach to reducing the cost of a FSCCSDT calculation is to approximate or ignore the most expensive terms to evaluate. In this sense, the simplest possible approximation would be to evaluate the triple excitation contribution perturbatively from

converged FSCCSD amplitudes. The single reference analog to this approach is the CCSD+T(CCSD) method, in which the triple excitation contribution is correct through fourth order — the first order at which it appears.

For the FSCC perturbation expansion, we follow the choice of Pal, Rittby, and Bartlett [56] which was also implicit in the work of Haque and Kaldor [57], of counting orders in terms of H, the reference state Hamiltonian. Alternatives, such as using $\bar{H}$ would lead to inconsistencies between the (0,0) sector definitions and those of higher sectors. For example, $\bar{f}$ and $\bar{W}$ are first order in H, while the higher components, $I\bar{I}I, \ldots$ are at least second order. Counting orders in $\bar{H}$ would place all of these terms on the same level, making a perturbation expansion of Eq. 4.21 useless.

Although in both CC and FSCC the triple excitation amplitudes first appear in second order of perturbation theory, in the CC formalism excitations beyond singles and doubles contribute only indirectly to the energy via their contributions to the singles and doubles amplitudes, and thus triples first appear in the energy in *fourth* order. In FSCC, all clusters contribute directly to $H_{N,\mathrm{eff}}$ and thus the energy, so the triples first manifest themselves in *third* order. Inclusion of the third order triples effects based on converged FSCCSD amplitudes was first proposed by Haque and Kaldor [57], and called CCSD+T. Later, Pal, Rittby, and Bartlett [56] discuss the third order model using the name MRCCSD+T(3) and propose several other approximations. The MRCCSD+T*(3) model attempts to include some higher order terms by replacing the f and W required in T(3) with their counterparts from the effective Hamiltonian, $\bar{f}$ and $\bar{W}$. The nature of this method, which will be referred to as *FSCCSD+T(3)* in this work, can be seen from the spin orbital

FSCCSDT equations given above. The terms which contribute to the $T_3^{(0,1)}$ amplitudes in second order are those on the first row of Eq. 4.25, with appropriate restrictions on the $\bar{H}_N$ elements: the $\bar{W}_N$ elements of the second and third terms are simply the bare two-electron integrals in first order, and only two terms of $\langle lab|\bar{|}kij\rangle$ appear at this level (the first two terms of $\langle iab|\bar{|}jkl\rangle$ in Table 3.3). The second order triples amplitudes in turn contribute to $H_{N,\text{eff}}$ (and thus the energy) in third order thought the final term of $H_{N,\text{eff}}$ in Eq. 4.22.

The extension of this approach to higher orders of perturbation theory is obvious. A fourth-order method, *FSCCSD+T(4)*, would be obtained by the following steps:

1. Second-order $T_3^{(0,1)}$ amplitudes, as evaluated above, give third-order contributions when inserted in the $T_1^{(0,1)}$ and $T_2^{(0,1)}$ amplitude equations. This correction to the $T_1^{(0,1)}$ and $T_2^{(0,1)}$ amplitudes can be directly contracted into $H_{N,\text{eff}}$, giving a fourth order correction to the energy.
2. The third-order $T_3^{(0,1)}$ must be evaluated. This requires the fourth, fifth and sixth terms from Eq. 4.25, and additional terms from $\langle lab|\bar{|}kij\rangle$ (terms 3–10 of $\langle iab|\bar{|}jkl\rangle$ in Table 3.3). Note that even if the (0,0) reference calculation does not include triple excitations, approximate $T_3^{(0,0)}$ amplitudes can be formed at second order in perturbation theory, and therefore must be included in the general case. Computational experiments will be required to determine the effect of approximate $T_3^{(0,0)}$ in $\bar{H}_N$.

Of course such a perturbation expansion could go on for a very long time, but in practice, better results are likely to be obtained (based on SRCC experience) by iterating an approximate triples equation as part of the FSCCSD calculation. The

simplest approximation for which this makes any sense is T(4), described in the preceding paragraph — it is the first perturbative method for which $T_3^{(0,1)} \rightarrow T_2^{(0,1)}$ and $T_3^{(0,1)} \rightarrow T_1^{(0,1)}$ contributions occur. The procedure is simple: In each iteration of the FSCC calculation, after the single and double excitation amplitudes have been evaluated, the T(4) procedure is used to calculate the contribution of triples excitations to $H_{N,\text{eff}}$ and the singles and doubles amplitudes. Instead of this being the end of the calculation, the new $T_1^{(0,1)}$ and $T_2^{(0,1)}$ amplitudes, and $H_{N,\text{eff}}$ are fed back into the next cycle of iteration. Note that there are no $T_3^{(0,1)} \rightarrow T_3^{(0,1)}$ contributions in this method, so the triple excitation amplitudes do not need to be kept from one iteration to the next, and also avoids the most expensive part of the $T_3^{(0,1)}$ equation to evaluate. This approach is the same as that taken by Urban *et al.* [48] in approximating single reference CCSDT. In the hopes of maintaining some consistency in nomenclature between SRCC and Fock-space approaches, this method should be called FSCCSDT-1.

In the single reference case, the idea has been extended in a series of additional iterative approximations, CCSDT-2 [48,50], CCSDT–3 [48,50], and CCSDT-4 [51], which include more and more of the terms due to triples, but continuing to exclude $T_3^{(0,0)} \rightarrow T_3^{(0,0)}$, thus avoiding the most expensive terms both computationally and for storage space. In the FSCC case, the $T_3^{(0,1)}$ equation has a simpler structure, and only $T_3^{(0,1)} \rightarrow T_3^{(0,1)}$ terms remain after the FSCCSDT-1 approximation.

Over the years, experience with various SRCC approximate triples methods has led to refinements in several of them. One of the main observations is that including selected higher order terms in a perturbative or iterative method can pro-

duce better results. For example, Watts, Gauss, and Bartlett [58] have recently introduced the CCSD[T] method, which is a modification of CCSD+T(CCSD), the simplest SRCC perturbative triples method. They differ in the inclusion of a fifth-order term and in the requirement that non-Hartree-Fock (i.e. QRHF or ROHF) references be treated properly. This requires that terms involving off-diagonal f elements be considered since they are zero for a Hartree-Fock reference, but nonzero in the non-HF case. Transforming the reference functions to semicanonical orbitals [59] has the effect of diagonalizing the occupied-occupied and virtual-virtual blocks of the Fock matrix, so that terms involving f_{ij} or f_{ab} can be avoided. This leaves occupied-virtual Fock matrix elements, f_{ai} to be accounted for, which involves shifting these terms down one order of perturbation theory, from first to zeroth order.

In the Fock-space coupled cluster framework, however, the situation is somewhat different. The transformation to semicanonical orbitals diagonalizes blocks of f, not $\bar{f}_N$. Even with such a transformation, the leading terms in $\bar{f}_{ij}$ and $\bar{f}_{ab}$ are first order in the non-HF case. This would result in $\bar{F}T_3^{(0,1)} \rightarrow T_3^{(0,1)}$ contributions, one of the most expensive terms in FSCCSDT, beginning with the third-order amplitudes (FSCCSD+T(4)). Thus as far as *approximations* to FSCCSDT go, such a requirement would be reasonable only for the most basic third-order method, FSCCSD+T(3). This would add the $FT_3^{(0,0)}$ term of $\langle lab||kij\rangle$ (see Table 3.3) and the $FT_2^{(0,0)}$ terms of $\langle mb||ij\rangle$ and $\langle ab||ej\rangle$ (see Table 3.2), and would require evaluation of the $\bar{F}T_3^{(0,1)} \rightarrow T_2^{(0,1)} \rightarrow H_{N,\mathrm{eff}}^{(0,1)}$ term of Eq. 4.24 since $\bar{f}_{me}$ is now zeroth order.

There is one further matter regarding approximation to the FSCCSDT equations. Mattie [60] has proven that for the (0,1) sector of Fock-space, the values of the roots obtained by diagonalizing $H_{N,\text{eff}}$ are independent of the active space used for the calculation. In other words, if two orbitals, a and b are taken as active, the resulting ionization potentials would be identical to those obtained from separate calculations with either a or b alone active. This is a very useful result because it means that we do not have to worry about choosing the "right" active space for a given calculation in order to get good results. However the proof of this invariance rests on the FSCC amplitudes and $H_{N,\text{eff}}$ satisfying the Fock-space Bloch equation 4.17. None of the approximate FSCCSDT methods described above satisfy Eq. 4.17, so the invariance is lost. It remains to be seen how large this effect will be, or if there is an alternative route to the invariance condition that will work with approximate solutions.

As a start towards understanding the FSCC triple excitation correction as well as we now understand the single reference triples correction, the remainder of this work will focus on the third-order triples approximations, FSCCSD+T(3) and FSCCSD+T*(3). The implementation of these methods for both closed and open-shell reference functions is described in some detail in the Appendix, including the final, spin-integrated equations from which the computer code was written. In the following chapters, these methods are applied to a variety of molecules in order to assess their performance.

CHAPTER 5
A CRITICAL ASSESSMENT OF FSCCSD AND THE THIRD-ORDER TRIPLES APPROXIMATIONS

5.1 Introduction

Before applying a new theoretical method to otherwise unknown molecular systems, it is important to get a feel for its behavior — strengths, weaknesses, and overall quality — by comparing the results obtained with new method to other theoretical and experimental data for similar types of problems. This "calibration" of a method is a continuous and dynamic process — each time the method is used for a new problem, more information about its performance is gained, thus modifying the assessment of its accuracy and applicability.

Choosing the appropriate standard of comparison for a new method is in most cases not a simple matter. Experimental results are an obvious choice, but there some potential problems. Experimental corresponding to readily computed results are not always available or may not be known accurately. For example, FSCC most readily provides vertical ionization potentials, but only adiabatic may be available from experiment. For potential energy surfaces — geometries, relative energies, and the like — there is usually very limited experimental data. Structures may be known for minima on the PES, but experiments which can probe transition states are quite new, and have not yet produced a sizeable body of data on different systems. The vibrational spectra of a given species

may be only partially known, and in many experiments, assignment of spectral lines to particular species can be a very hard problem. It is also possible for a calculation to obtain the right (experimental) answer but for the wrong reasons — a fortuitous cancellation of errors. If such problems are given due attention, experimental results can be a very useful measure the performance of a theoretical method, but it is worth considering other standards as well.

Comparison of a new method with experimental results often introduces more variables than one would like. For example, the choice of basis set may not be adequate to obtain high-quality theoretical results. Full CI provides the exact answer for a given basis set and Hamiltonian, and therefore offers an excellent standard of comparison for new methods. Unfortunately, FCI calculations are very expensive, so the results available for comparison are somewhat limited. Another option is to compare with methods that, from a well-defined theoretical standpoint, are better than the method in question. An example of this would be comparing methods which approximates triple excitation effects to the full triples model such as CCSD(T) vs. CCSDT, or FSCCSD+T(3) vs. FSCCSDT. In this work, however, as is often the case, the approximate method has been implemented before the full method because of the additional complexity of the full model, forcing such comparisons to wait until the more complete method is implemented. A final alternative is comparison of the new method with one for which the behavior is relatively well understood, but which cannot be clearly designated as a "better" method. Although these comparisons are the least definite, they are, of necessity, the most common in the calibration of any new method.

This chapter is a beginning at the calibration of the FSCCSD+T(3) and FSCCSD+T*(3), models. The molecules chosen for these calculations are drawn largely from applications of the FSCCSD method already in the literature, and in this work extended to include triple excitation contributions. The intent is to get an overview of the performance of the new methods for a variety of systems, most of which have also been the subject of single reference CC calculations, thus providing a useful point of comparison.

5.2 Effect of Changes in the Active Space

The triples approximations, as was noted in the previous chapter, do *not* have the same invariance with respect to the choice of active space as occurs for complete methods. In order to simplify later comparisons, we first examine the effect of the change in active space on the third-order triples models. The "error bars" obtained in this section may then be kept in mind later on, where a single choice of active space will be used in comparisons of the new FSCC methods with other results.

Because $H_{N,\mathrm{eff}}$ is block diagonal due to molecular symmetry, the active space within a particular symmetry block can be changed without affecting the others. If, in a series of calculations, the active space for a particular irrep remains unchanged, the IPs of that symmetry will not change. This is the case regardless of changes to the active space in other irreps. Conversely, changing the active space within a given irrep will result in slightly different IPs.

In order to assess the magnitude of this effect, calculations have been carried out on a number of molecules using different active spaces. The molecules, listed in Table 5.1, include a number for which the IPs themselves are studied below, and several additional systems with fairly low symmetry actual or computational symmetry. The idea behind these additional molecules was to see if having more occupied orbitals in each irrep (and therefore a larger set of possible active spaces) would result in larger variations in the calculated IPs. FSCCSD+triples calculations were carried out on each molecule using a DZP basis at the DZP/SCF optimized geometry for a set of active spaces consisting of

1. the largest active space for which the underlying FSCCSD could be converged (referred to as the "reference" active space),
2. single orbital active spaces for each of the orbitals in the reference active space, and
3. a series of active spaces obtained by starting with the lowest IP and successively adding the next highest IP.

This choice provides a slightly larger set of data on the variation of lower IPs, but those are usually the roots of greatest interest anyway. Analysis of these calculations involved first reducing the data to obtain a set of unique active spaces within each symmetry block, then computing for each IP, the mean, range, and mean difference from the available data. The mean was chosen as the reference point because there is no theoretical basis for preferring one active space over another as the "correct" one, except perhaps for having *all* occupied orbitals active, which proved impossible to converge in most cases. Table 5.1 presents the largest range and mean difference observed among the various IPs

Table 5.1. Effect of changes in active space in the T(3) and T*(3) models. for a variety of molecules. Ranges and mean differences of IPs are given in mH.

Molecule	Point group[a]	Active orbitals[b]	n[c]	FSCCSD+T(3) Range[d]	FSCCSD+T(3) Mean Diff.[e]	FSCCSD+T*(3) Range[d]	FSCCSD+T*(3) Mean Diff.[e]
C_3H_6[f]	C_s	3	3	0.023	0.010	0.023	0.010
CH_2[g]	C_{2v}	3	3	0.078	0.035	0.065	0.029
CH_2NH[g]	C_s	4	4	0.744	0.220	0.545	0.165
CH_2PH[g]	C_s	4	2/4	0.103	0.052	0.074	0.028
CH_3Cl[f]	C_s (C_{3v})	4	4	0.008	0.004	0.006	0.003
CH_3CN[f]	C_s (C_{3v})	4	4	0.354	0.133	0.284	0.107
CH_3NC[f]	C_s (C_{3v})	4	4	0.044	0.022	0.044	0.022
CH_3NH_2[f]	C_s	4	4	0.226	0.083	0.175	0.066
H_2CO[g]	C_{2v}	2	2	1.118	0.559	0.931	0.466
$HOCl$[f]	C_s	3	2	1.844	0.921	1.581	0.790
HOF[f]	C_s	3	2	3.467	1.734	2.757	1.379
N_2[g]	D_{2h} ($D_{\infty h}$)	3	3	1.297	0.576	0.861	0.383

[a] Computational point group (full point group).

[b] Largest active space used in the irrep containing the root showing the largest variation.

[c] Number of different active spaces sampled for the root showing the largest variation. Same for T(3)/T*(3) unless two values are given.

[d] Largest range (difference between largest and smallest values) for a single root. (in mH).

[e] Mean difference ($\frac{1}{n}\sum_{i=1}^{n}\left|\mathrm{IP}_i - \overline{\mathrm{IP}}\right|$) for the root showing the largest variation (in mH).

[f] Calculated with a DZP basis at the DZP/SCF optimized geometry.

[g] Calculated using the geometry and basis used in the ionization potential calculations in the next section.

for each molecule, along with an indication of the number of distinct active spaces in which that IP was computed.

The largest variation is observed for HOF, with HOCl, N_2, and H_2CO close behind. For a number of other species, however, the variation is quite small. Interestingly, the largest variations are seen among molecules with higher symmetry and smaller active spaces rather than large ones. This obviously suggests that the number of occupied orbitals is not the most important determinant of the variation, however examination of the FSCCSD and reference CCSD results provided no clues to distinguish molecules like HOF or H_2CO from ones with a small variation, such as CH_3Cl.

Comparison of the T(3) and T*(3) results shows that the range and mean difference for T*(3), which includes some higher-order terms, are at least as good as, and generally better than, those for T(3). Although there are a few cases where going to the T*(3) approximation changes which of the IPs has the largest variation, generally it is the same ionization for both.

In order to verify that the variation is not due to an inadequacy of the DZP basis sets used for most results in Table 5.1, a second set of calculations was carried out on HOF using Dunning's correlation consistent PVQZ basis [61], which is $5s4p3d2f1g$ on O and F, and $4s3p2d1f$ on H for a total of 125 basis functions (using spherical harmonic functions), compared to $4s2p1d$ and $2s1p$ for the DZP basis, totalling 37 basis functions (using cartesian functions). Table 5.2 presents the mean ionization potential and its variation with active space for the lowest five IPs of HOF calculated using both basis sets. There are changes in the range of variation from one basis to the other — some roots have a larger range with the PVQZ basis, others have a smaller range. In general, however, the they are roughly the same, suggesting that the variation is largely independent of the basis set.

Table 5.2. Effect of changes in the active space on the calculated ionization potentials (in mH) of HOF for two basis sets.

Sym.	n	DZP basis			PVQZ basis		
		Mean IP	Range	Mean Diff.	Mean IP	Range	Mean Diff.
			FSCCSD+T(3)				
a′	3	545.7	1.158	0.608	559.0	1.176	0.480
a′	3	672.8	3.186	1.064	686.0	3.529	1.281
a′	2	775.7	3.467	1.734	765.3	3.714	1.856
a″	2	466.5	0.171	0.085	482.0	0.118	0.059
a″	2	657.6	0.138	0.069	674.2	0.093	0.047
			FSCCSD+T*(3)				
a′	3	538.0	1.391	0.547	550.5	1.076	0.431
a′	3	665.9	2.465	0.853	678.1	2.872	1.033
a′	2	749.8	2.757	1.379	758.4	3.080	1.540
a″	2	459.7	0.073	0.037	474.3	0.033	0.017
a″	2	646.9	0.044	0.022	662.5	0.012	0.006

Given the data above, a reasonable estimate of the error bars due to changes in the active space is ±2 mH for both methods. (It must be pointed out that there are certainly to be systems with larger variations, but more experience will be required to understand the origin of the large variations and therefore be able to identify the worst offenders.) These correspond to about ±0.05 eV or ±1.3 kcal mol^{-1}. Although this may seem like a fairly large uncertainty, particularly for comparing energies at different points on a potential energy surface, there are several important factors worth noting. First, this is a conservative estimate for entirely unknown molecules. Many of the molecules in Table 5.1 are more than an order of magnitude better. Also, the table presents only

the *largest* variation — many others were significantly smaller. Secondly, it must be remembered that for molecules with symmetry, many of the IPs exhibit no variation because there is only one possible choice of active space in that symmetry. Finally, it is a fairly simple matter, and not computationally expensive, to obtain a feel for the variation of any molecule of interest. Only one (0,0) sector calculation is required to try out several FSCC active spaces, and the FSCC calculations themselves are very inexpensive compared to the (0,0) reference.

As a result, while the uncertainties associated changing the active space in T(3) and T*(3) calculations for the general case might be considered large for some applications much tighter limits may often be obtained with minimal effort. For the remainder of this chapter, the active spaces used will correspond directly to those results which are reported. Uncertainties due to the active space will be introduced into discussions as appropriate.

5.3 Ionization Potentials

Although it can be used in many other ways, the "natural" result of a (0,1) sector FSCC calculation is the energy of the vertical ionization process — extracting an electron from a molecule without allowing the geometry to relax to that of the resulting ion. Calculation of ionization potentials is, thus far, the predominant application of the FSCCSD method and such calculations will provide the bulk of the data for characterization of the approximate triples methods. These results will be compared with SRCC calculations, experimental results, and a benchmark full CI calculation for the methylene molecule by Bauschlicher and Taylor [62].

Table 5.3. Vertical ionization potentials of $^1A_1$ and $^3B_1$ CH_2 (in eV) calculated with a DZP basis.

Method	$^1A_1 \rightarrow$			$^3B_1 \rightarrow$	
	1^2A_1	2^2A_1	$^2B_2$	$^2A_1$	$^2B_1$
FSCCSD	10.21	22.54	14.92	10.14	11.30
FSCCSD+T(3)	10.32	22.74	15.00	10.26	11.43
FSCCSD+T*(3)	10.28	22.68	14.96	10.23	11.39
Full CI	10.26	22.14	14.85	10.16	11.31
QRHF-CCSD	10.20	22.25	14.84	10.14	11.30
QRHF-CCSD[T]	10.25	22.28	14.85	10.16	11.31
QRHF-CCSDT-1	10.25	22.28	14.85		
QRHF-CCSDT	10.25	22.15	14.85		

Note: Geometry, basis set, and full CI results taken from Bauschlicher and Taylor [62]. QRHF-CC results for $^1A_1$ ionizations from Watts, Gauss, and Bartlett [58]. $^3B_1$ calculations used a UHF-CCSD reference function.

Table 5.3 presents FSCC calculations on ionization potentials of methylene in comparison with both the full CI data from Bauschlicher and Taylor, and several QRHF-CC calculations. At the FSCCSD level, four of the five calculated IPs are within 0.1 eV of the full CI number, with the $^1A_1 \rightarrow 2^2A_1$ result 0.4 eV off. The effect of the T(3) correction to FSCCSD is to move all of the results away from full CI, but four of the roots are still within 0.1 eV, while the $^1A_1 \rightarrow 2^2A_1$ number has changed to 0.6 eV away from full CI. Introducing some higher order effects via the T*(3) model shifts all of the results back toward full CI, but not as close as the FSCCSD result. These differences from full CI cannot result from uncertainties due to the choice of active space, which from Table 5.1 are about 0.001 eV (0.04 mH) for this particular molecule. By contrast,

the single reference QRHF-CC calculations start out with all five ionizations within 0.11 eV of full CI, and the inclusion of triple excitations at various levels improves the results to match full CI within 0.01 eV. This behavior suggests that the single reference CCSD provides a good approximation to the various states in question, and that triple excitations are relatively unimportant, which would seem to conflict with the FSCC results.

It is important to recall, however, that there is a fundamental difference between FSCC and SRCC with respect to the nature of their excitation operators. As discussed in the previous chapter, spectator triple excitations must be added to the FSCCSD method to achieve an expansion space that is in some sense equivalent to that of the SRCC. But even then, the FSCC amplitudes are restricted by the necessity to represent several ionized states simultaneously. Thus, we should not expect the FSCCSD to produce results identical to a single reference CCSD, nor should we expect triple excitation corrections to behave in the same way. The differences between FSCC and SRCC shown in Table 5.3 and others, below, should be interpreted as a manifestation of these differences.

These differences between single reference and Fock-space methods can also be seen in the other calculations presented here (Tables 5.4–5.9). The sign of the FSCC triples correction is frequently opposite that of the SRCC triples corrections, and their magnitudes do not appear to be related — a large SRCC triples contribution does not necessarily imply a large FSCC triples correction, and vice versa. The size of the SRCC and FSCC triples contributions are rather different as well. The largest SRCC effect is about 0.2 eV, while the FSCCSD+T(3) correction is as large as 0.8 eV, and 0.5 eV for T*(3). All this is further support for the idea that the nature of the excitation operator hierarchy is

Table 5.4. Vertical ionization potentials of CH_2NH (in eV) calculated at the experimental geometry with a DZP basis.

Basis/Method	Orbital			
	5a′	1a″	4a′	3a′
FSCCSD	10.34	12.29	15.08	17.19
FSCCSD+T(3)	10.71	12.35	15.30	17.46
FSCCSD+T*(3)	10.55	12.29	15.20	17.34
QRHF-CCSD	10.40	12.14	15.17	17.32
QRHF-CCSDT-1	10.43	12.28	15.11	17.14
Experiment [63]	10.52	12.43	15.13	17.04
Experiment [64]	10.70	12.48	15.11	17.07
Experiment [65]	10.56	12.44	15.00	17.00

Notes: Geometries, basis sets, and QRHF-CC results taken from [66].

Table 5.5. Vertical ionization potentials of CH_2PH (in eV) calculated at the experimental geometry with a DZP basis.

Basis/Method	Orbital			
	1a″	5a′	4a′	3a′
FSCCSD	10.08	10.28	13.17	15.14
FSCCSD+T(3)	10.01	10.33	13.25	15.41
FSCCSD+T*(3)	9.98	10.28	13.25	15.27
QRHF-CCSD	9.90	10.22	13.15	15.15
QRHF-CCSDT-1	10.05	10.24	13.15	
Experiment [67]	10.30	10.70	13.20	15.00

Notes: Geometries, basis sets, and QRHF-CC results taken from [66].

different in single reference and Fock-space coupled cluster methods.

Table 5.6. Vertical ionization potentials for $^3\Sigma_g^-$ O_2 (in eV) at the experimental geometry.

Method	Basis	O_2^+ Final State			
		$^2\Pi_g$	$^4\Sigma_g^-$	$^4\Pi_u$	$^4\Sigma_u^-$
FSCCSD	DZP	11.76	17.75	16.40	24.16
FSCCSD+T(3)	DZP	12.13	17.99	16.30	24.98
FSCCSD+T*(3)	DZP	12.08	17.87	16.29	24.66
UHF-CCSD	DZP	12.13	17.80	16.15	24.64
UHF-CCSD(T)	DZP	11.95	17.77	16.26	24.40
FSCCSD	PVQZ++	12.37	18.34	16.94	24.74
FSCCSD+T(3)	PVQZ++	12.82	18.48	16.74	25.43
FSCCSD+T*(3)	PVQZ++	12.57	18.34	16.71	25.11
UHF-CCSD(T)	PVQZ++	12.39	18.26	16.76	24.82
Expt. (Adiabatic)		12.07	18.17	16.11	24.58
Expt. (Vertical)		12.35	18.33	16.85	24.66

Notes: Geometry taken from Herzberg [68]. Basis sets, SRCC, and experimental result taken from [69].

Examining the various tables, we see that the SRCC triples correction usually improves agreement with experiment, while the FSCC triples corrections appear to shift the calculated result away from the experimental one as often as towards it. It is also worth noting that the T*(3) correction is generally smaller than T(3) and gives better agreement with experimental results. Overall, FSCCSD and FSCCSD+T*(3) seem to do about the same in comparison with experiment, with an average absolute difference from the experimental results of roughly 0.2 eV. The single reference CCSD results have an average absolute difference of closer to 0.3 eV, which is improved to 0.2 eV

Table 5.7. Vertical ionization potentials of H_2CO (in eV) evaluated at the experimental geometry with a [5*s*3*p*1*d*/2*s*1*p*] basis.

Method	Orbital of ionized electron		
	$2b_2$	$1b_1$	$5a_1$
FSCCSD	10.51	14.36	15.75
FSCCSD+T(3)	10.96	14.49	16.30
FSCCSD+T*(3)	10.77	14.40	16.06
QRHF-CCSD	10.59	14.19	15.77
QRHF-CCSD[T]	10.63	14.37	15.83
QRHF-CCSDT-1b	10.63	14.39	15.83
QRHF-CCSDT-3	10.58	14.31	15.76
Experiment [70]	10.88	14.38	16.00

Notes: Geometry taken from Herzberg [68]. The basis set consisted of Dunning's (9*s*5*p*)→[5*s*3*p*] set on C and O, and his (4*s*)→[2*s*] set with exponents scaled by 1.44 on H [71], with polarization functions exponents of 0.654 (C), 1.211 (O), and 0.7 (H) [72].

by the addition of triple excitation effects. Thus, it would appear that FSCCSD and FSCCSD+T*(3) perform about as well as single reference CCSD(T) in comparison with experiment, but the single reference calculations (so far) have an edge in the predictability.

In order to give proper weight to the performance of these methods relative to experiment, we must consider the potential problems inherent in experimental data, as mentioned in the Introduction. Most of these problems are displayed by one or more of the experimental results in this chapter.

The natural result of a FSCC calculation is a vertical ionization potential, while experiment may provide vertical, adiabatic, or both. Adiabatic IPs are not directly comparable with calculated vertical ionization potentials, since they depend on the change

Table 5.8. Vertical ionization potentials of N_2 (in eV) at R=2.0693 au with a [5*s*4*p*1*d*] basis.

Method	Orbital of ionized electron		
	$3\sigma_g$	$1\pi_u$	$2\sigma_u$
FSCCSD	15.44	17.14	18.64
FSCCSD+T(3)	15.58	16.86	19.04
FSCCSD+T*(3)	15.44	16.88	18.81
QRHF-CCSD	15.39	16.69	18.71
QRHF-CCSDT-1	15.36	16.87	18.57
Experiment	15.60	16.98	18.78

Notes: Geometry, basis, and QRHF-CC and experimental results taken from Rittby and Bartlett [73].

Table 5.9. Vertical ionization potentials of ketene and diazomethane (in eV) calculated at experimental geometries calculated with a DZP basis.

Method	Ketene		Diazomethane	
	$2b_1$	$2b_2$	$2b_1$	$2b_2$
FSCCSD	9.40	14.25	8.60	13.79
FSCCSD+T(3)	9.39	14.49	8.52	13.85
FSCCSD+T*(3)	9.35	14.38	8.47	13.77
QRHF-CCSD	9.29	14.31	8.43	13.78
QRHF-CCSD(T)	9.38	14.24	8.54	13.73
Experiment	9.64 (a)	13.84 (a)	9.00 (a)	14.13 (v)

Notes: Geometries, basis sets, and experimental results taken from Rittby, Pal, and Bartlett [55]. Experimental IPs are *adiabatic* or *vertical*, as indicated in the table.

in geometry from the neutral to the ion. If the ion and neutral geometries are very similar, the vertical and adiabatic IPs will also be nearly the same, but in general, the adiabatic

IP is only a lower bound for the vertical one. In cases where the experimental value is adiabatic or unspecified, a larger difference from the computed vertical IP must be expected.

A second problem with experimental results is that, as with theoretical methods, different experimental techniques can give somewhat different results. This is illustrated in Table 5.4, which lists three sets of experimental data for methyleneamine, differing among themselves by as much as 0.2 eV.

A third complication of using experimental data is that details of the calculation other than the correlation method become important, particularly the basis set. Most of the calculations presented here use a DZP or slightly better quality basis set. While very useful for comparing one theoretical method to another, these basis sets may not be adequate, however, to obtain good results compared to experiment. Table 5.6 shows the ionization potentials of O_2 as calculated using both DZP (32 functions) and an augmented PVQZ basis (126 functions) in order to demonstrate the effect of basis set on both the FSCC and SRCC IPs. It is clear that the PVQZ++ basis provides a much better comparison with the experimental results than the DZP basis, for both FSCC and SRCC calculations. The change in FSCC results due to increasing the basis set is about 0.5–0.6 eV, and for the SRCC 0.4–0.5 eV. Although there is no experimental comparison, a similar basis set effect can also be seen in the HOF results in Table 5.2, where the change from a DZP to a PVQZ basis changes the IPs by 0.2–0.4 eV. It would seem, then, that correlated calculations with DZP-quality basis sets should not be expected to reproduce experimental results too well.

Given that the basis sets used here are generally too small, coupled with the other problems of the experimental data themselves, it would seem that an error of 0.2 eV for these calculations is not unreasonable, and is not necessarily an indication of intrinsic problems with the method. Indeed, the fact that the SRCC results show a similar margin of error with respect to experiment is a good sign for FSCC. It would seem that the biggest difference in this regard between the single reference and Fock-space results is the relative lack of consistency of the FSCC triples corrections, which can probably be better understood with more calculations.

5.4 Potential Energy Surfaces and Related Properties

Another use of FSCC methods is for the study of potential energy surfaces, especially with the ability to look at several surfaces in the same calculation. The basic result of the FSCC calculation is still an energy difference, but when added to the absolute energy of the (0,0) sector reference, it provides an absolute energy for the state of interest. In the (0,1) sector case, the state of interest has one electron removed relative to the reference (0,0) state. While this may seem a round about way of calculating the PES of a molecule, it has practical advantages in many cases. For calculations on molecules with low-lying electronic states or symmetry breaking phenomena, direct calculation of the PES by traditional single reference methods frequently suffers from convergence and other problems due to the proximity of other states to the one of interest. On the other hand, the same molecule with another electron is often well-behaved at the same geometries. This the same as the ionization process, but from the opposite point of

view — in this case, we want to talk about the final state, while in IPs, it is traditional to look at it from the point of view of the initial state.

This application of FSCC methods is a very recent development, and there are only a few such applications in the literature. Moreover, because they deal with symmetry breaking problems, there is little conclusive experimental evidence to allow concrete conclusions to be drawn about the performance theoretical methods. Comparisons are possible with single reference calculations, though as we shall see, the comparison of high-level SRCC calculations with Fock-space results does not always lead to an unambiguous determination of which approach is more reliable. Nevertheless, FSCC is very well suited to such applications and will undoubtedly see increasing use in the study of potential energy surfaces (beginning with the next chapter of this work), so it is worth trying to get a feel for its performance.

Engelbrecht and Liu, in a 1983 paper [74], used multiconfiguration self-consistent field (MCSCF) plus CI calculations to characterize the $^3A_2$ state of CO_2. This state, which is bent (C_{2v} symmetry), has the SCF occupation

$$(\text{core})3a_1^2 2b_2^2 4a_1^2 3b_2^2 5a_1^2 1b_1^2 1a_2 4b_2^2 6a_1$$

and interacts strongly with the configuration

$$(\text{core})3a_1^2 2b_2^2 4a_1^2 3b_2^2 5a_1^2 1b_1 1a_2^2 4b_2^2 6a_1$$

because both the a_2 and b_1 orbitals transform as a'' in C_s symmetry. As a result, SCF calculations can obtain a lower energy by going to a C_s structure.

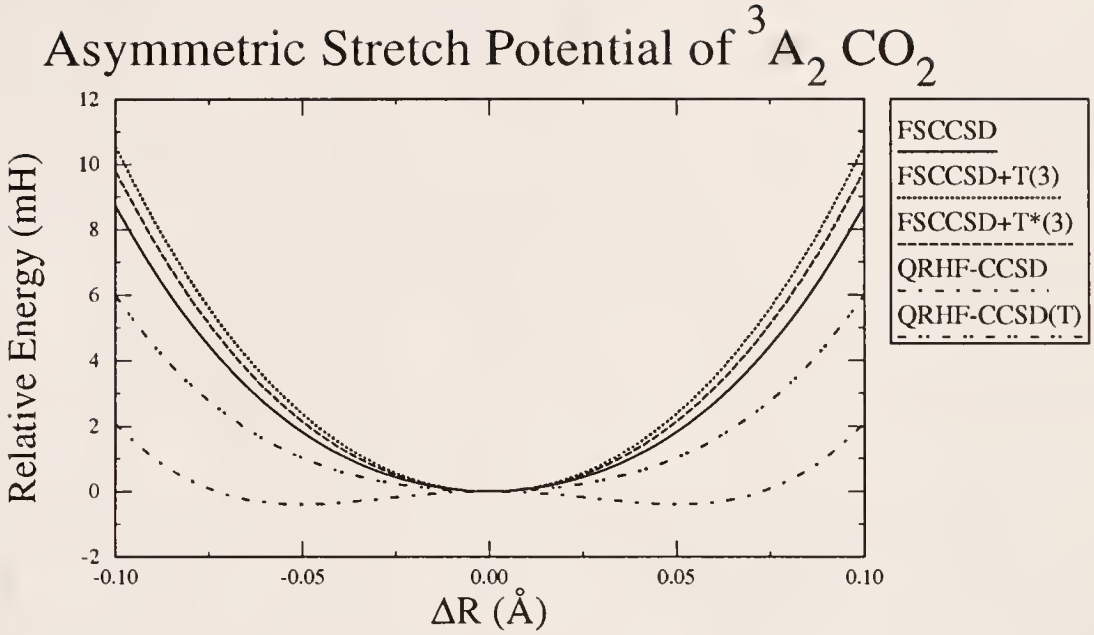

Figure 5.1. Potential curves for the asymmetric stretch mode ($\Delta R = \frac{1}{2}(R_1 - R_2)$) of $^3A_2$ CO_2 at various levels of theory. The C_{2v} structure is the DZP/FOCIB geometry of Engelbrecht and Liu [74].

With suitable methods, such interactions can be treated properly, and reasonable potential energy surfaces obtained, but this requires the ability to describe inherently multireference states. Most such methods are not many-body in nature, and of course we prefer a size extensive approach if possible (Chapter 3).

It has been observed that QRHF-based coupled cluster methods are capable of handling many multireference problems when sufficient triple excitation effects are incorporated [34]. In Figure 5.1, we see two QRHF-CC potential curves for the asymmetric stretch of CO_2, which were calculated from closed-shell CO_2^{2-} SCF orbitals. The QRHF-CCSD curve has a double minimum shape, while the QRHF-CCSD(T) method

gives a stable C_{2v} structure. This is consistent with the MCSCF+CI calculations of Engelbrecht and Liu and their conclusion that the equilibrium structure of this state is C_{2v}.

The results of three sets of Fock-space coupled cluster calculations using $^2A_1$ CO_2^- as the (0,0) reference are also displayed in Figure 5.1. FSCCSD gets the proper shape of the PES even without triple excitation effects, and the inclusion of triples makes small adjustments to the shape of the surface. (Note that, as in the IP calculations, the FSCCSD+T*(3) results lie between FSCCSD and FSCCSD+T(3).) This behavior is what we might expect from a method that is designed in a multireference framework.

Another symmetry-breaking problem to which a number of single and multireference approaches have been applied is the nitrate radical, NO_3. Different experiments have been interpreted in terms of either a totally symmetry D_{3h} equilibrium geometry, or a lower symmetry C_{2v} structure with one N-O bond length different from the other two. However, as Kawaguchi and coworkers [75] comment, no one has advanced a model which explains all of the available spectroscopic data.

In the most recent theoretical examination of the problem, Stanton, Gauss, and Bartlett [76] located three stationary points on the NO_3 surface using the QRHF-CCSD method. The D_{3h} structure was determined to be a local minimum, and two C_{2v} structures were found. They are characterized by the relationship between the unique N-O bond distance and the other two: one long/two short (1L2S) or one two long/one short (2L1S). The 1L2S structure was also found to be a local minimum, and the 2L1S a transition state 192 cm^{-1}

Table 5.10. Calculated relative energies (in kcal mol^{-1}) of C_{2v} and D_{3h} NO_3 structures.

Method	DZP basis		PVTZ basis	
	1L2S-D_{3h}	2L1S-D_{3h}	1L2S-D_{3h}	2L1S-D_{3h}
FSCCSD	2.50	1.05	2.94	1.05
FSCCSD+T(3)	3.03	1.64	3.72	1.73
FSCCSD+T*(3)	2.74	1.35	3.36	1.41
QRHF-CCSD	-2.59	-2.04	-2.96	
QRHF-CCSD(T)	0.34		0.57	
QRHF-CCSDT-3	0.21			

Notes: Geometries, optimized at the DZP/QRHF-CCSD level, taken from [76]. The C_{2v} geometries are characterized by one of the NO bonds being longer (1L2S) or shorter (2L1S) than the other two. QRHF-CC relative energies taken from [77].

higher in energy than the 1L2S state; both C_{2v} structures being lower in energy than the totally symmetry structure. Their conclusion is that the molecule has a C_{2v} equilibrium geometry, but probably has an extremely low barrier to pseudorotation, which would give spectra with characteristic of a D_{3h} system.

In a later paper focusing on different orbital choices for single reference treatments of symmetry breaking problems, Stanton *et al.* [77] calculated relative energies of the D_{3h} and C_{2v} minima using more sophisticated methods than in their first paper. Their QRHF-CC results are shown in Table 5.10 along with FSCC results using the same basis sets and geometries. Using both DZP and PVTZ basis sets, QRHF-CCSD calculations favor the C_{2v} minimum by about 3 kcal mol^{-1}. As soon as triples corrections are introduced, either using the noniterative CCSD(T) approximation or the iterative CCSDT-3 model, the energies shift in favor of the totally symmetric structure, but by only 0.5 kcal mol^{-1}.

FSCC, on the other hand, predicts the D_{3h} structure to be lower for all three methods shown, but by roughly 3 kcal mol^{-1}.

Given previous experience with QRHF-CC methods applied to problems of this sort, we should have greater confidence in the QRHF-CCSD(T) and T-3 results than in results without triple excitations, but with the available data, it is impossible to tell whether the single reference numbers including triple excitations or the FSCC results are more reliable. As Stanton *et al.* [77] observe, "An extremely sophisticated (and expensive) calculation would be required to firmly establish the nature of the D_{3h} stationary point."

C_3^+ is another molecule for which both experimental and theoretical studies have produced differing opinions on the nature of the ground state. Coulomb explosion data can be interpreted in terms of either a floppy linear molecule or a bent structure, depending on the vibrational temperature of the sample [78,79]. On the theoretical side, the consensus is that the ground state is a bent $^2B_2$ with the linear $^2\Sigma_u^+$ higher in energy [80]. The energy difference between these two states is still not a settled issue. This is important because if the barrier is small enough, the molecule may be quasilinear — although the true ground state is bent, a large amplitude bending motion could bring the molecule through the linear structure.

Tables 5.11 and 5.12 present the results of FSCC optimizations, vibrational frequency calculations, and relative energies in comparison with single reference CC results from Watts, Stanton, Gauss, and Bartlett [80] which include full CCSDT calculations. All three Fock-space methods give essentially the same geometry for both structures, comparing most closely with the single reference CCSD results. For the vibrational frequencies of the

Table 5.11. Optimized geometries and vibrational frequencies of $^2B_2$ C_3^+, using a DZP basis.

Method	R (Å)	θ (°)	ω_1 (a_1) (cm^{-1})	ω_2 (a_1) (cm^{-1})	ω_3 (b_2) (cm^{-1})
FSCCSD	1.328	71.6	1685	583	1269
FSCCSD+T(3)	1.336	70.2	1643	614	1221
FSCCSD+T*(3)	1.335	70.5	1651	603	1225
CCSD	1.337	68.3	1668	687	1215
CCSD(T)	1.350	68.3	1601	515	1074
CCSDT-1	1.350	69.0	1558	569	1078
CCSDT-2	1.347	69.0	1612	595	1213
CCSDT	1.350	68.0	1601	638	1021

Notes: Basis set and SRCC results taken from Watts, *et al.* [80].

Table 5.12. Optimized geometries, and vibrational frequencies of $^2\Sigma_u^+$ C_3^+, and energy relative to $^2B_2$ C_3^+, using a DZP basis.

Method	R (Å)	$\omega(\pi_u)$ (cm^{-1})	$\omega(\sigma_g)$ (cm^{-1})	$\omega(\sigma_u)$ (cm^{-1})	E($^2\Sigma_u^+$ - $^2B_2$) (kcal mol^{-1})
FSCCSD	1.312	88	1227	492*i*	7.1
FSCCSD+T(3)	1.315	71*i*	1203	1911	10.9
FSCCSD+T*(3)	1.316	532	1205	1462	8.6
CCSD	1.314			2500*i*	13.2
CCSD(T)	1.327			1431*i*	2.9
CCSDT-1	1.339			1135	-1.7
CCSDT-2	1.329			1595	2.2
CCSDT	1.327			451*i*	4.9

Notes: Basis set and SRCC results taken from Watts, *et al.* [80].

$^2B_2$ state, the FSCC results are also basically the same, and correspond most closely with

the CCSDT-2 approximate iterative triples model among the single reference calculations. On the basis of several calculations with a larger basis set, Watts and coworkers suggest that the true harmonic frequencies should lie in the ranges 1590–1629, 592–638, and 1094–1173 cm^{-1}, and compared to these, the FSCC ω_1 and ω_3 are slightly high.

The asymmetric stretching frequency (σ_u) of the $^2\Sigma_u^+$ state (Table 5.12) is a more complex problem. An imaginary frequency in this mode indicates that the $D_{\infty h}$ structure is a transition state, and a lower energy can be obtained by changing the bond lengths asymmetrically. For both single reference and Fock-space methods, the calculated frequency varies widely. Also, the bending mode (π_u) changes dramatically with the choice of FSCC method. Such large changes due to different correlation methods are usually an indication that important aspects of the problem are not being taken into account, and a more detailed examination, using both single reference and Fock-space methods would be in order.

Table 5.12 also presents the energy differences between the linear and bent structures. Note that the single reference CCSDT-1 method places the linear structure lower in energy than the bent one. Watts *et al.* attributed this to an apparent tendency for the iterative nature of the CCSDT-1 method to overemphasize problems in the closely-related CCSD(T) model in difficult cases, thus producing poorer results than the perturbative CCSD(T) method.

Their CCSDT ΔE of 4.9 kcal mol^{-1} is in reasonable accord with CISDTQ calculations of Grev, Alberts, and Schaefer [81,82] indicating a 4.1 kcal mol^{-1} difference. Taylor *et al.* [83] used multireference CI methods to obtain a separation of 1.68 kcal mol^{-1} with

a DZP basis set, and claim that this should be very close to the full CI limit. These authors also show that multireference effects are important for both the bent and linear structures. Despite the multireference character of the FSCC approach, all three methods presented here give a significantly larger energy gap than Taylor's calculations. The problem with the relative energies of the two states may be due, at least in part, to the apparent problems in properly describing the $^2\Sigma_u^+$ state. It would seem, on this minimal evidence, that where single reference methods including triple excitations have problems, Fock-space methods do as well.

5.5 Conclusions

A variety of results has been presented using the Fock-space coupled cluster methods FSCCSD, FSCCSD+T(3), and FSCCSD+T*(3), for both ionization potential problems at fixed geometries, and in cases where the potential surfaces must be explored.

Overall, the performance of the FSCC methods is good. FSCCSD results usually compare well with single reference CCSD(T) calculations. The FSCC triples corrections seem initially to be less predictable, than the triples correction in single reference methods. The Fock-space triple excitations have a different nature than their SRCC counterparts, and it will require more experience with these methods to understand them and discern the system they follow.

Including some higher-order contributions in the T*(3) method seems to have a "dampening" effect compared to the basic T(3) model, which causes the T*(3) results to compare better with experimental results or other calculations. This is probably similar

to the single reference coupled cluster case, where the simplest perturbative inclusion of triples, CCSD+T(CCSD) was found to be significantly improved by the inclusion of certain higher order terms, resulting in the CCSD(T) model. For the present, the FSCCSD+T*(3) method seems to be preferable to the purely third-order FSCCSD+T(3). In the long run, it is probably worthwhile to investigate more systematic ways of incorporating higher-order terms in the FSCC triples contribution, as discussed in the previous chapter.

Numerically, effects of changing the active space in the FSCCSD+triples methods have been demonstrated to introduce uncertainties as large as ±2 mH in calculated energies (IPs or state energies), however most of the molecules examined have much lower uncertainties. On the whole, both FSCCSD and FSCCSD+T*(3) seem to do about as well compared to experiment as SRCC methods including perturbative triples, and better than CCSD. For very accurate comparison with experiment for both FSCC and single reference methods, however, a large basis is required.

For energy differences on potential energy surfaces, where the requirements are tighter than on IPs, Fock-space results do not seem to compare as well with single reference methods as for IPs. Although the signs of relative energies evaluated using FSCC seem to match higher-quality single reference calculations, the Fock-space energy gaps are noticeably larger than in the SRCC case. The cases examined are hard problems, both experimentally and theoretically, and it is not clear that either approach can be claimed to be better. Consequently, great care must be taken with such results, and more study would be most useful.

The FSCC methods all seem to do quite well in determining local properties of potential surfaces — geometries, vibrational frequencies, etc. In most of these cases, there does not appear to be a substantial difference among the three FSCC methods examined, except for linear C_3^+, for which both single reference methods including triple excitations and Fock-space methods seem to have problems.

In addition to the quality of results of a new method, one should also consider its ease of use and cost in comparison with competitive methods. By this measure, FSCC methods have a decided advantage over the single reference approaches. An FSCC calculation, even including triple excitation effects, amounts to a small fraction of the cost of the (0,0) sector CCSD reference calculation. In contrast, each of the IP calculations required separate SRCC calculations for the neutral, and for each ion state, and at least one of those on an open-shell molecule, for which the SRCC is about four times more expensive than a closed shell calculation. In most cases, the reference CCSD calculation used in the Fock-space approach is a closed shell, and all of the IPs can be computed in a single calculation. For potential energy surfaces, the ability to explore several surfaces at once is also a distinct advantage over single reference methods.

CHAPTER 6
THE STRUCTURE OF THE C_5^+ MOLECULE

6.1 Background

Although there is relatively little experimental data on C_3^+, discussed in the preceding chapter, there is even less known about C_5^+. The experiments which have observed C_5^+ have done so with a mass spectrometer in reactivity [84], fragmentation [85–87], or mobility [88] studies. The essential conclusion of these papers (with respect to C_5^+) is that there is a single isomer (multiple isomers show up starting with C_7^+) and that its reactivity and mobility are similar to those of its neighbors, C_4^+ and C_6^+, and the whole set of clusters from C_2^+ to C_6^+ are commonly labeled as "linear" molecules [84,88]. (C_3^+, which theoretical results agree is actually bent, fits the trends for "linear" clusters in the experimental data as well as C_5^+ does, suggesting that the "linear" label cannot be interpreted rigorously.)

Recently, matrix-isolated infrared spectroscopy experiments, using isotopically mixed graphite, produced an IR band that could be attributed to a planar pentagonal (D_{5h} symmetry) C_5^+ molecule [89]. The neutral C_5 cluster has been well established, both theoretically and experimentally, to have a linear ground state [90], with cyclic structures much higher in energy. In this situation, it would seem unlikely that the cation would be so different from the neutral that a cyclic cation

would be observable, but the existence of isoenergetic linear and cyclic structures of neutral C_4, which is now generally accepted [90,91], was once also thought unlikely.

A series of SCF and MBPT(2) calculations [92] established that D_{5h} C_5^+ could not be responsible for the observed band, and a reanalysis of the experimental data led to assignment of the band to a $C_3 \cdot H_2O$ adduct, in agreement with a later assignment by Ortman *et al.* [93]. The low-level calculations pointed toward a linear ground state for C_5^+, but there were major problems with spin contamination of the UHF-based calculations, stability of the SCF solution, symmetry breaking, and failure to converge calculations on some states. In this chapter we attempt to understand the source of the troubles with lower-level calculations and to establish the true ground state structure of C_5^+ using high-quality many-body methods.

6.2 Computational Methods

The majority of the calculations in this work used a DZP basis set comprised of Dunning's (9s5p)/[4s2p] double-zeta set [71] and a polarization function (α=0.654) as optimized by Redmon, Purvis, and Bartlett [72]. All six cartesian *d* components were retained, giving a total of 80 contracted basis functions. At selected points on the various potential energy surfaces, a larger PVTZ basis [61] was used to compute the energy. This is a (10*s*5*p*2*d*1*f*)/[4*s*3*p*2*d*1*f*] generally-contracted basis, which was used with spherical harmonic polarization components (5*d* and 7*f*), for a total of 150 contracted basis functions.

Both single reference QRHF-based and Fock-space coupled cluster methods have been used and in both types of calculations, triple excitation effects have been considered, mostly through perturbative corrections: QRHF-CCSD(T), FSCCSD+T(3), and FSCCSD+T*(3). Both QRHF-CC and FSCC calculations used the closed shell neutral C_5 molecule as a reference. The reasons for using both SRCC and Fock-space approaches are both historical and practical. When work on this project was first begun, no efficient FSCC program was available and QRHF-based approaches were the best choice to deal with the problems observed in the UHF calculations mentioned earlier. When the newly-completed ACES II FSCCSD code was applied to this molecule, the nature of the problems became apparent, and it was clear that understanding the C_5^+ molecule was a problem well-suited to this method because of its closely-spaced, strongly interacting electronic states.

In some calculations, the carbon 1*s* orbitals and the corresponding virtual orbitals (five occupied and five virtual for the DZP basis with cartesian angular momentum functions, five occupied and four virtual for the spherical harmonic PVTZ basis) were not correlated in order to reduce the computational cost. The effect of dropping these orbitals on the relative energies is negligible.

Geometry optimizations have been carried out using QRHF-CCSD and all three Fock-space methods. Analytic gradient techniques were used with the QRHF-CCSD calculations, but gradients have not been formulated for FSCC yet, so optimizations were performed via numerical differentiation of FSCC energies. Similarly, vibrational frequencies were evaluated from the numerical second derivatives of the FSCC energy,

or by numerical differentiation of the QRHF-CCSD analytic gradients. All optimizations and frequency calculations used the DZP basis set.

6.3 The Heart of the Problem

In neutral C_5, the highest occupied orbital in the Hartree-Fock approximation is of π_g symmetry, and the next highest are σ_u^+ and σ_g^-. Using Koopmans' theorem ionization potentials, the two $^2\Sigma$ states of C_5^+ obtained by removing electrons from either of the σ orbitals should be more than 60 kcal mol^{-1} above the $^2\Pi$. Unfortunately, for molecules not well-described at the SCF level, as the original calculations suggested for C_5^+, Koopmans' approximation is not very useful.

QRHF-CCSD optimization of the $^2\Pi_g$ state went well, but there were problems with the Σ states: The $^2\Sigma_u^+$ state optimized to a stationary point, but only after significant computational effort because large T_1 and T_2 amplitudes made the calculations very hard to converge, and the $^2\Sigma_g^-$ state could not be converged at all. In addition, attempts to calculate the vibrational frequencies of the $^2\Sigma_u^+$ state, to see if it is in fact a local minimum, produced unphysical results for the σ_u modes. Such problems are characteristic of a symmetry breaking or state interaction problem — the large cluster amplitudes indicating that other determinants mix strongly with the SCF reference determinant, and the unphysical vibrational frequencies a reflection of a discontinuity in the PES, often caused by individual calculations in the finite difference frequency evaluation that may have converged to a low-lying excited state relative to the one of interest.

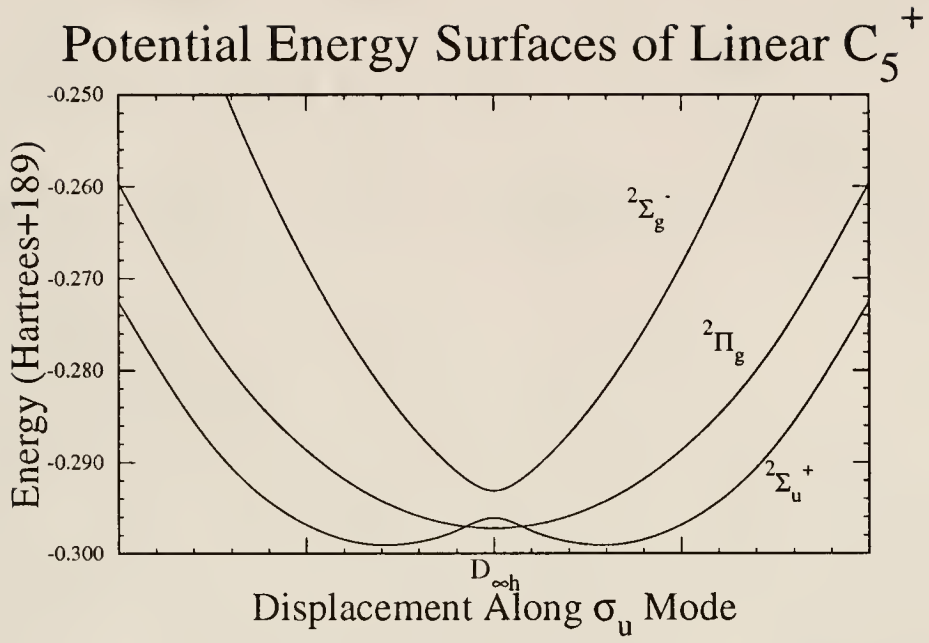

Figure 6.1. DZP/FSCCSD potential curves for three states of C_5^+, centered on the DZP/QRHF-CCSD $^2\Sigma_u^+$ stationary point.

A FSCCSD calculation at the $^2\Sigma_u^+$ geometry revealed that all three states were within about 2.2 kcal mol^{-1} rather than the 60 kcal mol^{-1} separation predicted by Koopmans' theorem. The proximity of the two Σ states, which couple by an asymmetric stretching (σ_u) motion produces a pseudo-Jahn-Teller effect (PJTE), giving the $^2\Sigma_u^+$ PES a minimum at a $C_{\infty v}$ structure, breaking the perpendicular symmetry plane and the center of inversion. This is shown in Figure 6.1, which displays the energy of the three states for motion along the σ_u mode leading to the minimum energy for the $^2\Sigma_u^+$ state. Such a system is ideally suited for the application of FSCC (0,1) methods since not only do the states require a multireference description, but the neutral C_5 molecule provides a well-behaved, closed shell (0,0) sector reference function.

Table 6.1. Optimized geometries of linear stationary points of C_5^+ (in Å).

State/Method	$C_1 - C_2 - C_3 - C_4 - C_5$			
$^2\Pi_g$ C_5^+	R_{12} (=R_{45})	R_{23} (=R_{34})		
QRHF-CCSD	1.351	1.299		
FSCCSD	1.350	1.300		
FSCCSD+T(3)	1.352	1.301		
FSCCSD+T*(3)	1.353	1.301		
$^2\Sigma^+$ C_5^+	R_{12}	R_{23}	R_{34}	R_{45}
QRHF-CCSD	1.245	1.347	1.265	1.344
FSCCSD	1.237	1.350	1.258	1.348
FSCCSD+T(3)	1.254	1.327	1.274	1.330
FSCCSD+T*(3)	1.248	1.339	1.265	1.339
$^2\Sigma_u^+$ C_5^+	R_{12} (=R_{45})	R_{23} (=R_{34})		
QRHF-CCSD	1.288	1.299		
FSCCSD	1.291	1.299		
FSCCSD+T(3)	1.295	1.299		
FSCCSD+T*(3)	1.294	1.299		
C_5[a)]	R_{12} (=R_{45})	R_{23} (=R_{34})		
105 CGTO/CEPA-1	1.289	1.283		
	$H - C_1 - C_2 - C_3 - C_4 - C_5$			
HC_5^+[b)]	R_{12}	R_{23}	R_{34}	R_{45}
111 CGTO/CEPA-1	1.227	1.335	1.254	1.336

a) From Botschwina and Sebald [94].

b) From Botschwina [95]; R_{H1}=1.076 Å.

6.4 Geometries of the Linear Stationary Points of C_5^+

Once the origin of the convergence and other problems with the QRHF-CC calculations was recognized, the situation was greatly improved. The $^2\Sigma_g^-$ state could

immediately be eliminated from consideration as a possible ground state of the system, and symmetry lowering by the $^2\Sigma_u^+$ state due to the PJTE interaction also increases its separation from the $^2\Pi_g$ state, which should reduce second-order vibronic coupling between the two states.

Table 6.1 presents the final optimized geometries of the two $D_{\infty h}$ and one $C_{\infty v}$ linear stationary points using both QRHF-CC and FSCC methods. For comparison, the geometries of neutral C_5, as optimized by Botschwina and Sebald [94], and the closely related system, HC_5^+, as optimized by Botschwina [95]. The three Fock-space approaches and QRHF-CCSD all agree on the structures of these stationary points, with differences among methods similar to those seen for C_3^+ in the previous chapter, and certainly no larger than would be expected for different correlation methods.

The $^2\Sigma_u^+$ structure is very similar to the neutral C_5 geometry, having nearly equal bond lengths with the inner one slightly longer. The $^2\Pi_g$ state has longer outer bonds, and a more pronounced difference between inner and outer bond distances. The $C_{\infty v}$ $^2\Sigma^+$ structure is essentially a shift of atoms 2 and 4 towards 1 and 3, respectively, from the $^2\Sigma_u^+$ structure, resulting in a molecule with alternating bond lengths but essentially the same overall length (at the FSCCSD+T*(3) level, it lengthens by 0.1 Å, but for the others the difference is insignificant). Interestingly, the $^2\Sigma^+$ structure is also very similar to that of HC_5^+, suggesting the possibility that the two species might have other common characteristics.

Table 6.2. Relative energies (in kcal mol^{-1}) of linear C_5^+ stationary points.

Method	Structure[a)]	Energy Relative to $^2\Sigma^+$	
		$^2\Pi_g$	$^2\Sigma_u^+$
DZP/QRHF-CCSD	QRHF-CCSD	11.9	29.9
DZP/QRHF-CCSD[T]	QRHF-CCSD	6.1	3.9
DZP/FS CCSD	FS CCSD	0.6	6.7
DZP/FS CCSD+T(3)	FS CCSD+T(3)	-13.9	2.0
DZP/FS CCSD+T*(3)	FS CCSD+T*(3)	-9.1	3.9
PVTZ/QRHF-CCSD	QRHF-CCSD	13.4	30.1
PVTZ/QRHF-CCSD[T]	QRHF-CCSD	8.6	3.8
PVTZ/FS CCSD	FS CCSD	3.1	6.9
PVTZ/FS CCSD+T(3)	FS CCSD+T(3)	-11.7	5.1
PVTZ/FS CCSD+T*(3)	FS CCSD+T*(3)	-6.9	6.8

[a)] All structures were optimized using the DZP basis.

6.5 Relative Energies

Although the single reference and Fock-space methods agree on the geometries of these species, they do not agree so well on relative energies. As shown in Table 6.2, QRHF-CC methods and FSCCSD predict the $^2\Sigma^+$ structure to be more stable by varying amounts, while FSCC methods including triples predict the $^2\Pi_g$ state to be more stable. The variations in the FSCC triples results due to choice of active space are on the order of 0.2 kcal mol^{-1} for this molecule, so they cannot have an appreciable effect on these results. There are two important trends in the relative energies, one related to the FSCC triples methods, and the other due to the basis.

The effect of increasing the basis set from DZP to PVTZ is a very uniform change of approximately 2.5 kcal mol^{-1} in the relative energy, however the direction of the change is opposite for the two groups of methods: For the QRHF-CC and FSCCSD methods, the gap between the $^2\Pi_g$ and $^2\Sigma^+$ states widens, while for the FSCCSD+T(3) and FSCCSD+T*(3) methods, the gap is reduced. These changes match what would be expected if the change in basis stabilized the $^2\Sigma^+$ state while leaving the $^2\Pi_g$ state essentially unchanged for all methods. Such an effect could result if the $^2\Sigma^+$ state has a relatively diffuse character which for which the change to a PVTZ basis brings significant improvement, while the $^2\Pi_g$ state does not gain any special advantage from the larger basis.

The second important trend in is the marked difference in the relative energies between the QRHF-CC and FSCCSD methods on one hand and FSCCSD+T(3) and FSCCSD+T*(3) on the other. For both basis sets, there is change of 10–15 kcal mol^{-1} in the relative energies, and the order of the states is reversed.

Looking at the actual energies of the states, rather than relative energies, reveals that the FSCC third-order triples contribution is positive for the Σ states and negative for the Π state, and large enough to change the order of the states. Comparison with the raw data from the previous chapter and for some other linear carbon clusters, discussed below, reveals an interesting fact: In almost every case, for nonlinear molecules, the T(3) and T*(3) corrections to FSCCSD have a positive sign, regardless of the symmetry of the state. For linear molecules, however, the pattern is that Σ states have a positive triples contribution, while Π states have a negative contribution. This means that, for the

IP calculations on linear molecules, triples nearly always increase the IP of Σ states and decrease that of Π states. For cases in which the relative energy is of interest, the results will of course depend on the relative order of states at the FSCCSD level. In addition, nonlinear structures of C_5^+ calculated in the course of this work (structures with no more than about 30° deviation from linearity in any one angle), the same pattern is obtained for states which correlate to the linear Σ or Π states, regardless of their actual symmetry. For example, in C_{2v} symmetry, the first two states of B_1 symmetry correlate to the $^2\Pi_g$ and $^2\Sigma_u^+$ linear states respectively, and the triple excitation effect on these states is predicted by which state they correlate to in the linear molecule.

Such a pattern is not inherent in the FSCCSD+T(3) or FSCCSD+T*(3) equations, which while taking into account the symmetry of the molecule, in no way depend on it. Computationally, the presence of counter-examples among the various linear molecules surveyed (one Π state of O_2^+ and one of C_9^+) confirms that it is not built into the equations. Also, the positive/negative pattern could not be established for nondegenerate/degenerate states molecules in degenerate point groups other than the linear ones. It would seem that some characteristic of the electronic structure of these linear molecules causes the behavior, probably exaggerated by the low level of approximation of the FSCC triples contribution. The higher order terms included in the T*(3) model reduce the difference in energies by about 5 kcal mol^{-1} compared to the FSCCSD+T(3) result, so improving the treatment of FSCC triples would probably produce a more reasonable answer.

Table 6.3. Relative energies (in kcal mol^{-1}) of $D_{\infty h}$ C_5^+ stationary points for several QRHF-CC triples approximations; FSCC values are also given for reference.

Method[a)]	Relative Energy	
	$^2\Pi_g$	$^2\Sigma_u^+$
QRHF-CCSD	-18.4	0.0
QRHF-CCSD[T]	2.2	0.0
QRHF-CCSDT-1b	6.5	0.0
QRHF-CCSDT-3	1.7	0.0
FSCCSD	-6.1	0.0
FSCCSD+T(3)	-15.9	0.0
FSCCSD+T*(3)	-13.0	0.0

[a)] QRHF-CC calculations performed at the QRHF-CCSD optimized geometry, FSCC calculations at the optimized geometry for that method. All calculations used a DZP basis.

The question that must now be answered is which method(s) provide the most reliable relative energies. The results for C_3^+, for both QRHF-CC and FSCC approaches, as shown in Table 5.12, do not provide a clear answer, but some useful comparisons can be drawn. In the single reference CC case, there is for both molecules, a significant change in the relative energy upon inclusion of the perturbative triples correction. This is consistent with results for SRCC method applied to other systems that would normally be considered multireference in nature — the CCSD result is quite misleading, but even the lowest order addition of triple excitations gives a reasonable result. Going to the next higher-level inclusion of the triple excitation effects, CCSDT-1, the results appear somewhat worse compared with other triples methods. This is also the case in C_5^+, as shown in a comparison of energies at the two $D_{\infty h}$ stationary points in Table 6.3. In

their paper on C_3^+, Watts *et al.* [80] attributed this behavior to the large fourth-order contribution of the CCSD[T] method being exaggerated by iteration in the CCSDT-1 method. At still higher levels, the triple excitation effect stabilizes for both C_3^+ and C_5^+.

The FSCC results have also been shown in Table 6.3 with the same zero of relative energy as for the QRHF-CC data in order to simplify comparison. As for C_3^+, the FSCCSD result is not in line with the QRHF-CC numbers including triple excitation effects. For C_5^+, the difference is made more pronounced by the fact that it changes the order of the two states. The inclusion of third-order triples effects in FSCCSD, which has already been shown to strongly favor the Π state over the Σ, gives relative energies similar to the QRHF-CCSD single reference results. The same pattern is seen in the C_3^+ relative energies of Table 5.12.

Experience with QRHF-CC methods for problems of this sort suggests that, when triples excitation effects are included, the results are quite good, and in this case we have been able to demonstrate a "convergence" in the relative energies with increasingly sophisticated triples approximations. FSCC, on the other hand, does not show any convergence, and it appears that the Σ–Π splitting may be artificially exaggerated for linear molecules by the third-order triples approximations. All this serves to make the FSCC relative energies less believable than the QRHF-CCSD[T] ones. By combining the trends for DZP/QRHF-CC calculations in Table 6.3 with the data in Table 6.2, the PVTZ/QRHF-CCSD[T] relative energies, which place the $^2\Pi_g$ state about 9 kcal mol^{-1} higher than the $^2\Sigma^+$ state should be good predictor of results from higher-level correlation treatments, with an accuracy of ±4 kcal mol^{-1}. Larger basis sets would be expected to

preferentially stabilize the $^2\Sigma^+$ state, because of its more diffuse nature, until the space is saturated. However this would serve to *increase* the gap between the states, so there is little likelihood that simply enlarging the basis would produce a qualitative change in the order of the states.

6.6 Stability of the Stationary Point Structures

To this point, nothing has been said about whether or not these structures are actually local minima or some other type of stationary point. This is, of course, an important question because if these structures are not stable, further searching will be required to locate true local minima. This is especially true for the $^2\Pi_g$ state, which, since it is degenerate, is susceptible to the Renner-Teller effect (RTE).

In this section, harmonic frequencies are presented based on QRHF-CCSD, FSCCSD, FSCCSD+T(3), and FSCCSD+T*(3) calculations. All of these methods have problems in these circumstances, which will be discussed as appropriate. However it should be stated up front that QRHF-CCSD[T] or higher level single reference results would be most desirable, but their computational cost at the present time is prohibitive for such an application. The conclusions drawn here have been checked by point-wise exploration of the surfaces away from linear geometries.

Table 6.4 shows the harmonic frequencies computed for the $^2\Pi_g$ structure. All four methods agree on the σ stretching frequencies, however the bending modes are more complicated. Both QRHF-CCSD and FSCCSD showed some lifting of the degeneracy of the π modes, as might be expected from the RTE. The FSCCSD+T(3) and FSCCSD+T*(3)

Table 6.4. Harmonic vibrational frequencies of $^2\Pi_g$ C_5^+ (in cm^{-1}) using various theoretical methods.

Mode	QRHF-CCSD		FSCCSD		FSCCSD+T(3)	FSCCSD+T*(3)
π	$137i$	187	$93i$	$90i$	29	$43i$
π	$88i$	116	21	24	55	55
π	242	490	494	495	496	494
σ_g	760		761		757	757
σ_u	1262		1306		1292	1288
σ_g	1828		1895		1885	1880
σ_u	1884		1904		2121	2023

methods did not produce exactly degenerate modes, but the differences were quite small. The primary conclusion from these data and from additional calculations carried out at nonlinear structures is that the PES for bending from this state is extremely flat. The FSCC data required using numerical differentiation techniques on the energy. The usual procedure is to perturb the positions of the nuclei by 5 mBohr to obtain the necessary points. In this case, in order to get even the smallest measurable change in energy, the step size for the bending frequencies had to be increased by an order of magnitude. But with such a large step, the anharmonicity of the surface causes problems. As a consequence, the FSCC π frequencies, with the possible exception of the 495 cm^{-1} mode, should not be given any credence. The QRHF-CCSD frequencies were evaluated from numerical differentiation of analytic gradients, and so should be numerically more reliable, but the lack of triple excitation effects, in view of their crucial importance for a reasonable representation of the system, make the QRHF-CCSD bending frequencies equally questionable.

Table 6.5. Harmonic vibrational frequencies of $^2\Sigma^+$ C_5^+ (in cm^{-1}) using various theoretical methods.

Mode	QRHF-CCSD	FSCCSD	FSCCSD+T(3)	FSCCSD+T*(3)
π	148i	161	122i	94i
π	113	273	75	94
π	381	478	414	411
σ	771	778	790	783
σ	1452	1453	1498	1474
σ	2100	2142	2054	2093
σ	2237	2291	2238	2261

For $^2\Sigma^+$ C_5^+, the vibrational frequencies shown in Table 6.5 are somewhat better than those for the $^2\Pi_g$ state. Once again, the stretching frequencies are in accord for all four methods. For the π modes, the surface is fairly flat compared to most molecules (but less so than for the $^2\Pi_g$ state), so numerically, the FSCC results have a sizeable margin of error. However for the same reasons cited above, the QRHF-CCSD results should not be entirely trusted, leaving FSCCSD as the best choice. As a check for the nature of a possible nonlinear minimum, the FSCCSD+T*(3) minimum was located. This is a $^2A'$ state, which has one terminal carbon bent away from the linear axis by about 10°. At the DZP/FSCCSD+T*(3) level, this geometry is about 4 kcal mol^{-1} more stable than the linear $^2\Sigma^+$ state. The small energy difference attests to the anharmonicity of the surface in this region.

Thus vibrational frequency calculations indicate that both states are probably linear, but floppy — particularly the $^2\Pi_g$ state. Even if, with higher-level correlated methods, it is found that there are in fact nonlinear minima, there is no evidence to suggest that

the ordering of the states will change. Due to the very large anharmonicities of bending modes on both surfaces, the computed π frequencies should not be considered reliable. However the stretching frequencies should be good, and may be useful in experimental studies of this molecule.

6.7 Implications for Other Carbon Clusters

The numerous complexities encountered for C_5^+ prompt questions about what the situation might be for other odd-numbered cationic carbon clusters. In a sense, the "problems" of C_5^+ stem from the fact that it has so many states close in both energy and geometry, in such a way that they can interact strongly. Using the Fock-space coupled cluster approach, it is relatively easy to explore the structure of other clusters and see how their electronic structure compared to that of C_5^+.

For these calculations, the 6–31G*/SCF optimized geometries of the neutral clusters of Raghavachari and Binkley [96] were used, since they provide a consistent set of structures though C_9. DZP/FSCCSD calculations were performed at these geometries to obtain the vertical energy differences between the low-lying states. The results of these calculations are shown in Table 6.6.

There are two importance effects to note in this data. First, the relative energy of the two Σ states (highlighted in the table) decreases from C_3^+ to a crossover point at C_7^+, where they are essentially degenerate, then in C_9^+ the gap begins to widen again, but with the *gerade* symmetry state lower. The second effect is that of the lowest Π state, which alternates between *gerade* and *ungerade*, and drops from 18 kcal mol^{-1} *above* the

Table 6.6. Relative energies of low-lying electronic states of carbon cations (in kcal mol^{-1}).

Molecule	State and relative energy			
C_3^+	$^2\Sigma_u^+$	$^2\Sigma_g^-$	$^2\Pi_g$	
	0	18.77	36.44	
C_5^+	$^2\Sigma_u^+$	$^2\Sigma_g^-$	$^2\Pi_u$	$^2\Pi_g$
	0	1.71	2.67	69.88
C_7^+	$^2\Pi_g$	$^2\Sigma_u^+$	$^2\Sigma_g^-$	$^2\Pi_u$
	0	11.91	11.93	57.29
C_9^+	$^2\Pi_u$	$^2\Sigma_g^-$	$^2\Sigma_u^+$	$^2\Pi_g$
	0	20.83	20.95	50.47

Σ states to 21 kcal mol^{-1} *below* them. These two effects combine in C_5^+ with that the result that three states are (at this geometry) all within 3 kcal mol^{-1}.

Based on these data, the pseudo-Jahn-Teller interaction of the two Σ states would peak for C_7^+, where they are essentially degenerate, then decrease as the cluster lengthens and the states separate again. As the cluster lengthens, we would also expect the energy lowering from the $D_{\infty h}$ symmetry to the $C_{\infty v}$ minimum to decrease, since small changes in bond length would have a lesser effect on the energy of the overall system. At the same time, gap between the Π state and the Σs widens, making it unlikely that even the distorted $C_{\infty v}$ Σ state would be competitive for the ground state. Finally, the $^2\Pi$ state is subject to the Renner-Teller effect, which would likely (but not necessarily) result in a nonlinear ground state.

Calculations at the optimized $^2\Sigma_u^+$ structure of C_3^+, given in the previous chapter, and at various C_5^+ stationary points shown above indicate that the somewhat arbitrary choice of geometry used in the calculations presented in Table 6.6 does not affect the picture it portrays, merely changing the exact relative energies somewhat.

Experimentally, two distinct isomers of both C_7^+ and C_9^+ have been observed [84,88] with differing mobilities or chemical reactivities. These have been referred to as "linear" (reactive) and "cyclic" (unreactive), but the basis for these structural assignments is not strong. Parent and McElvany [84] relied on very simple calculations such as those of Bernholc and Phillips [97] at the semiempirical MNDO level which considered a very restricted set of possible structures. Von Helden and coworkers [88] also measured the mobilities of linear and cyclic alkanes and found that their ratios matched those observed for the two isomers of the pure carbon species. In fact, since "linear" alkanes are not actually linear in the strict sense usually applied to pure carbon clusters, von Helden's experiments suggest that the difference between a truly linear cluster, and one that is distorted from linearity could not be resolved. Although this may be viewed as a matter of semantics, application of the term "linear" in this context is somewhat misleading; it is likely that the reactive "linear" isomer seen in experiments is, in fact, nonlinear due to the Renner-Teller effect. Spectroscopic or Coulomb explosion studies on these cations will be required, probably in conjunction with more detailed theoretical studies, to resolve this question.

6.8 Recapitulation

The ground state of C_5^+ has been found to be $^2\Sigma^+$, with $C_{\infty v}$ symmetry, with a $^2\Pi_g$ state 9 kcal mol^{-1} higher in energy. Harmonic stretching frequencies of the two structures have been computed and should help spectroscopists in identifying this molecule. With respect to bending motions, both surfaces are rather flat — especially the $^2\Pi_g$ state. At the FSCCSD level, the $^2\Sigma^+$ state is stable, but with other methods it is a transition state. However even if this state is found to be nonlinear with more reliable methods, the change in energy would be expected to be small, and would not change the important conclusions.

Although they were not deemed the most reliable results for judging relative energies, etc., FSCC methods proved invaluable in this study. They provided the first insight into the nature of the problem that had plagued other calculations, and were used to explore several PES at once for interesting features. The third-order triples approximations, FSCCSD+T(3) and FSCCSD+T*(3), appear suffer from an interaction between the level of approximation and the electronic structure of linear molecules that uniformly favors Π states by a substantial amount. It is expected that better treatment of the triples contribution will produce more reasonable results.

FSCC methods have also been applied to other clusters in the C_n^+ (n odd) series, and it appears that C_5^+ is the worst possible case with respect to proximity of the states. As the size of the cluster increases, the $^2\Pi$ state drops in energy with respect to the $^2\Sigma$, so that for largely molecules, the ground state almost certainly derives from the $^2\Pi$. Of course since it is a degenerate state, Renner-Teller effects may result in the actual ground state nonlinear, but this will require a significant computational effort to establish.

CHAPTER 7
SUMMARY

The Fock-space coupled cluster theory has been derived and its relationship with the more familiar single reference CC theory discussed. The full FSCCSDT equations for the (0,1) sector (one electron ionizations) have been presented in the form of spin orbital equations along with the necessary elements of the coupled cluster effective Hamiltonian, $\bar{H}_N$, also in spin orbital form. Several perturbative and iterative approximations to the full FSCCSDT model are proposed as a compromise between the cost of the complete inclusion of triple excitation effects and the improved accuracy they should afford. The approximations, as presented, do not have certain invariance properties which might be desirable. In SRCC methods, experience has shown that the incorporation of the terms required to obtain the desired invariance generally leads to improved performance of the approximate triple excitation method. The modifications to the proposed FSCC triples approximations to meet these requirements were discussed. It was also observed that approximating the triple excitation contribution causes the method to lose the invariance with respect the choice of active space which would apply to either the FSCCSD or FSCCSDT methods. The proof of this invariance relies on satisfaction of the Fock-space Bloch equation, so it is not clear that any approximate method can be formulated with the property, and the severity of the problem in practice will have to be determined by computational experiments.

As a first step in understanding triple excitation effects in FSCC methods, two of the simplest approximations have been implemented for use with both closed- and open-shell reference functions. The FSCCSD+T(3) method includes only third-order contributions of triples to the energy, and the FSCCSD+T*(3) method incorporates some higher-order effects by replacing raw H_N elements used in the evaluation of the T(3) contribution with $\bar{H}_N$. The spin integrated equations from which the computer program was written are given in the Appendix. These methods were then applied to a variety of molecules in order to get a general feeling for how the FSCC third-order triples approximation perform compared to FSCCSD and single reference methods.

Computational experiments with different active spaces show that in most cases, the uncertainty introduced is small. There are, however, a few molecules for which the effect is more pronounced. Ideally, it would be useful to be able to *predict* which systems will have the largest uncertainty, but no common thread could be found among the cases studied; more experience with FSCC triples approximations will be required to reach that level. It is, however, a fairly simple matter to test the effect on any given molecule of interest. Calculations of ionization potentials, mostly using DZP-quality basis sets show that FSCCSD and FSCCSD+T*(3) both perform about as well as QRHF-CCSD[T] in comparison with experiment, with an average absolute error of about 0.2 eV. The higher-order effects included in the T*(3) model appear to have a moderating effect on the pure third-order correction, and thus compare better with experimental results. Fock-space methods should also be well-suited to the study of systems exhibiting symmetry breaking or other vibronic interaction effects, and several such systems are examined. Although

there is no *conclusive* experimental or theoretical data to compare with, it appears that FSCC methods are quite capable of obtaining good geometries, and in most cases good vibrational frequencies. For relative energies, however, the results are not so satisfying, either with the basic FSCCSD method, or when it is augmented with triples — while SRCC methods tend to show a "convergence" in the relative energy with increasingly sophisticated treatment of triples excitations, FSCCSD relative energies begin several kcal mol^{-1} away from the SRCC results and are not obviously improved by third-order triples. In fact throughout these calculations, there were signs of the basic differences between the SRCC excitation operator hierarchy and the FSCC hierarchy, which were described from a theoretical standpoint earlier.

A combination of SRCC and FSCC methods was applied to the problem of locating the ground state structure of C_5^+, attempting to use the advantages of each method. The FSCC methods proved invaluable for "exploring" the potential energy surface and focusing on regions of interest or uncovering potential problems such as strong vibronic interactions. In many electronic structure problems, regions of degeneracy or near-degeneracy are known *a priori* not to provide the sought-after property (i.e. local minimum), and by recognizing them, computational headaches can often be avoided.

During the course of the C_5^+ calculations, it became apparent that the FSCCSD+T(3) and FSCCSD+T*(3) methods show a very strong pattern of triples positive corrections for Σ states and negative for Π states, thus energetically favoring the Π state. This pattern is not observed in general, nonlinear molecules. It is concluded that

these effects are probably due to some aspect of the electronic structure of linear molecules being exaggerated by the low-order approximation used for triple excitations.

Despite these problems, the ground state of C_5^+ was determined to be $^2\Sigma^+$, with $C_{\infty v}$ symmetry, with a $^2\Pi_g$ state roughly 9 kcal mol^{-1} higher in energy. Both of these states appear to be linear, but have relatively flat potential surfaces with respect to bending. Fock-space coupled cluster calculations have also been performed on the series of molecules C_n^+, (n=3,5,7,9) in order to examine the implications of the C_5^+ results for the rest of the series. While problems with pseudo-Jahn-Teller interaction between the $^2\Sigma_g^-$ and $^2\Sigma_u^+$ states grows worse as the cluster gets larger, the Π state becomes much more stable than the Σs in C_7^+ and C_9^+. Thus C_5^+ is perhaps the worst of these clusters with respect to the complexity of its electronic structure, and the lowest linear energy linear structures of C_7^+ and C_9^+ are predicted to be $^2\Pi$, with the possibility of distortion from strict linearity due to the Renner-Teller effect.

There is one further aspect of these calculations which was mentioned very little in the previous chapters — the cost of the FSCC calculations. In the most common application of FSCC (0,1) methods, the (0,0) sector reference is a well-behaved closed-shell molecule. Consequently, the entire (0,0) calculation can be done using an RHF reference. Single reference CC, on the other hand, would require an open-shell reference function, and therefore an open-shell CC calculation, which is about four times more expensive than for a closed-shell reference (the FSCC calculation itself is a small fraction

of the cost of the reference CC calculation). In addition, the SRCC calculation is much more susceptible to convergence problems, so the calculations may take more iterations of the CC equations than the FSCC (0,0) closed-shell calculation. Although FSCC methods applied to open-shell reference functions don't have this advantage over SRCC, they do retain the second advantage of the Fock-space approach — the ability to evaluate several states in a single calculation. Single reference CC calculations of vertical IPs or excitation energies require one calculation per state involved, while FSCC can provide them all in a single calculation.

The computational advantages of the FSCC approach mean that a much more thorough examination of some complex electronic structure problems is possible compared to exclusive use of single reference methods, and although currently available FSCC methods do not seem to perform as well as might be desired for some aspects of the problem, this will often be outweighed by being able to explore the system better. As a result, it is well worth putting additional effort into improving our understanding of FSCC methods and their computational performance. With respect to the triples approximations investigated, it is clear that the excitation operator hierarchy of SRCC and FSCC is different, both theoretically and computationally. While low-order triples approximations perform quite well in most cases for SRCC methods, they are not so successful for FSCC. The obvious next step is to move to higher-level approximations, and look for better performance. But from the development of single reference triples approximations, it would seem that the most useful tool is a large base of calculations which make it possible to identify characteristics of molecules that lead to particularly good or poor results from

approximate triples methods, thereby better understanding existing methods and allowing more refined approach to formulating better approximations. Hopefully, this work represents the beginning of such an effort for the Fock-space coupled cluster method.

APPENDIX
IMPLEMENTATION OF THE PERTURBATIVE TRIPLES MODELS

A.1 Introduction

The various approximate triple excitation models presented in this work have been implemented in the ACES II program system [98] by building upon the FSCCSD program written by John F. Stanton. Due to intrinsic differences of these methods from the majority of other which have been implemented within the ACES II framework, and also due to differences among the programmers, there are some aspects of the FS triples implementation which bear comment in order to assist anyone who may wish to build on this work in the future. In addition, the FSCC literature in particular tends to avoid giving explicit equations, preferring the more compact operator or diagrammatic expressions. This makes for less cumbersome papers, but can lead to ambiguity as to exactly which terms are present in a given method. Consequently, I will present both the spin orbital equations and the final spin-integrated (suitable for general reference functions) which have been coded.

A.2 Spin Orbital Equations for the T(3) and T*(3) Models

The second-order triple excitation amplitudes of the T(3) model consist of four terms, two from $I\bar{I}I_N$, the three-body part of $\bar{H}_N$, and two from the contraction of converged $T_2^{(0,1)}$ with $\bar{W}_N$. The restriction on order means that only the W_N component of $\bar{W}_N$

will actually contribute.

$$D_{kij}^{\ddot{l}ab}\tau_{kij}^{\ddot{l}ab} = -(-)^p P(ki/j)\left\langle \ddot{l}m||ki\right\rangle t_{mj}^{ab} \tag{A.1a}$$

$$+(-)^p P(k/ij)\left\langle \ddot{l}a||ke\right\rangle t_{ij}^{eb} \tag{A.1b}$$

$$-(-)^p P(k/ij,ab)\langle mb||ij\rangle \tau_{km}^{\ddot{l}a} \tag{A.1c}$$

$$+(-)^p P(ki/j)\langle ab||ej\rangle \tau_{ki}^{\ddot{l}e}. \tag{A.1d}$$

The notation used above is that amplitudes from $T^{(0,0)}$ are denoted with t, and those from $T^{(0,1)}$ with τ; the dots, $\ddot{l}$ are used to indicate that l is restricted to be an active orbital, by analogy with the double arrow used to indicate active lines in diagrams. $D_{kij}^{\ddot{l}ab}$ is the coupled cluster denominator,

$$D_{kij}^{\ddot{l}ab} = f_{kk} + f_{ii} + f_{jj} - f_{\ddot{l}\ddot{l}} - f_{aa} - f_{bb}. \tag{A.2}$$

Remember that throughout this appendix, the target amplitude $\tau_{kij}^{\ddot{l}ab}$ is only correct through second order. Additional notation to indicate this would be too cumbersome.

The triples amplitudes contribute to the energy via the effective Hamiltonian,

$$\left(H_{N,\text{eff}}\right)_{\ddot{l}\ddot{k}} = \frac{1}{4}\langle ij||ab\rangle \tau_{\ddot{k}ij}^{\ddot{l}ab}. \tag{A.3}$$

To obtain the T*(3) model proposed by Pal, Rittby, and Bartlett [56], two modifications to the above equations are required. First, all H_N integrals appearing in Eqs. A.1,

A.2, and A.3 are replaced by the corresponding $\bar{H}_N$ elements:

$$f_{pq} \longrightarrow \bar{f}_{pq}$$

$$\langle pq||rs\rangle \longrightarrow \langle pq\bar{||}rs\rangle \tag{A.4}$$

Second, the denominator is modified to incorporate some effects from the renormalization term, $T_3^{(0,1)} \leftarrow H_{N,\mathrm{eff}} T_3^{(0,1)}$, by replacing the $\ddot{l}$ term with the corresponding diagonal of $H_{N,\mathrm{eff}}$. The resulting equations are:

$$\begin{aligned} D_{kij}^{*\ddot{l}ab}\tau_{kij}^{*\ddot{l}ab} = &-(-)^p P(ki/j)\left\langle \ddot{l}m\bar{||}ki\right\rangle t_{mj}^{ab} \\ &+(-)^p P(k/ij)\left\langle \ddot{l}a\bar{||}ke\right\rangle t_{ij}^{eb} \\ &-(-)^p P(k/ij,ab)\left\langle mb\bar{||}ij\right\rangle \tau_{km}^{\ddot{l}a} \\ &+(-)^p P(ki/j)\left\langle ab\bar{||}ej\right\rangle \tau_{ki}^{\ddot{l}e}, \end{aligned} \tag{A.5}$$

$$D_{kij}^{*\ddot{l}ab} = \bar{f}_{kk} + \bar{f}_{ii} + \bar{f}_{jj} - \left(H_{N,\mathrm{eff}}\right)_{\ddot{l}\ddot{l}} - \bar{f}_{aa} - \bar{f}_{bb}, \tag{A.6}$$

and

$$\left(H_{N,\mathrm{eff}}\right)_{\ddot{l}\ddot{k}} = \frac{1}{4}\langle ij\bar{||}ab\rangle \tau_{\ddot{k}ij}^{*\ddot{l}ab}. \tag{A.7}$$

It is worth observing, however, that in $H_{N,\mathrm{eff}}$, the integral $\langle ij||ab\rangle$ and the $\bar{H}_N$ element $\langle ij\bar{||}ab\rangle$ are identical, so that Eqs. A.1 and A.5 are in fact the same except for the $T_3^{(0,1)}$ amplitude.

A.3 Details of the Implementation

Implementation of the T(3) and T*(3) model in the ACES II program system was done both with an eye to the special features of the third-order models, and

at the same time providing a base for higher-level perturbative and iterative models up to full FSCCSDT. Also, as this is the first implementation of these methods within the ACES II system, performance concerns were subordinated to clarity and generality of the code. As a result, it may be possible to improve the performance of the third-order methods by specializing the code to them, however I think it is worth waiting on this until there is a larger body of experience with FS triples methods.

In order to avoid storing the complete set of $T_3^{(0,1)}$ amplitudes, their calculation is organized as a loop over the required $\left(k,\ddot{l}\right)$ pairs, and at each iteration evaluating contribution of a subset of $T_3^{(0,1)}$ having the same size as $T_2^{(0,0)}$ to $H_{N,\text{eff}}$. This approach should work for all methods not requiring a $T_3^{(0,1)} \leftarrow T_3^{(0,1)}$ contribution. Fixing $\left(k,\ddot{l}\right)$ also requires the ability to read integral and amplitude lists with these indices fixed. The original FSCCSD implementation includes a set of routines which has come to be known as the "Fock space I/O" (FSIO) package, which allows the use of subsets with indices restricted to active or inactive via scatter and gather operations using precomputed index vectors for each subset. This package was extended to allow for "temporary I/O" (TIO) vectors which can be easily changed to correspond to each $\left(k,\ddot{l}\right)$ in the loop. This avoids having to store precomputed scatter/gather vectors for *all* of the $\left(k,\ddot{l}\right)$ at a very small cost in CPU time. For methods that require storage of the full $T_3^{(0,1)}$ from one iteration to the next, some changes will have to be made. Since the current code is structured around the ability to store objects the size of $T_2^{(0,0)}$ in memory, it should be fairly easy to store the $T_3^{(0,1)}$ amplitudes so that each record ("distribution" in ACES II

terminology) holds an entire $T_2^{(0,0)}$–sized quantity corresponding to a given $\left(k,\ddot{l}\right)$, in the same fashion as is presently done in the SRCC triples codes which require storage of the amplitudes.

Probably the most distinctive aspect of this implementation is the treatment of the spin cases of $T_3^{(0,1)}$ in deriving the final form of the equations. Normally, using the permutational symmetry of the amplitudes, one would consider four unique spin cases. In order to simplify evaluation of approximations which don't need the full $H_{N,\text{eff}}$ matrix (spectator and active-active subsets, for example), the indices $\left(k,\ddot{l}\right)$ are treated as distinct from the remaining indices, (i,j,a,b). This leads to six distinct spin cases — two from the $\left(k,\ddot{l}\right)$ part times three from the other four indices — but keeps the code very simple with respect to the use of RHF vs. UHF references and the contribution of the amplitudes to $H_{N,\text{eff}}$. If the complete $T_3^{(0,1)}$ tensor must be evaluated, as for higher-level methods, it would make sense to treat the minimal set of spin cases and make full use of permutational symmetry. This will primarily involve reorganization of the contraction of the amplitudes into $H_{N,\text{eff}}$, and of course avoiding of the redundant terms in generating the amplitudes.

Because of the obvious similarity of the T(3) and T*(3) models, they have been implemented using a single set of routines capable of either method rather than two sets of routines distinguished only by accessing slightly different integral lists. This is done by writing the code for the T*(3) method and using an array to change the list numbers from those for $\bar{H}_N$ to those for H_N. (T*(3) is chosen as the "lead" method because the $\bar{H}_N$ integrals it requires lack the bra-ket transposition symmetry of the H_N integrals, so a code that is correct for T*(3) will be correct for T(3) when the integrals are changed, but

generally not for the reverse.) The same mapping of list numbers is used to handle the fact the for closed shell reference functions, many lists become redundant and are not stored. In most other ACES II code, different cases are used within the code for UHF vs. RHF references; in the FS triples, the approach is to use the same code with the list numbers properly mapped, and limit, at a higher level in the code, which spin cases are evaluated. It must also be noted that the evaluation of $\bar{H}_N$ in the program LAMBDA overwrites some of the pure H_N integrals, so it is necessary to preserve them in order to run an FSCCSD+T(3) calculation later. This is done with a very short program, SAVEINTS, which must be run before LAMBDA, and simply copies the relevant integrals to other (unused) list numbers. The list mapping mechanism then simply redirects references to the integrals lists to their new location rather than copying the integrals back into their original locations. By mapping the lists instead of copying them, it is possible to do both T(3) and T*(3) calculations after a FSCCSD in a single invocation of the program.

A.4 Final Equations for the T(3) and T*(3) Models

In Tables A.1—A.4 the final spin integrated form of the equations used in the third-order methods, suitable for a general open shell reference, is displayed. Six spin cases are shown, and the resulting terms are grouped according to the natural pairing of indices for the loop over irreducible representations of the $T_2^{(0,0)}$—like part of the amplitude. Only the T(3) equations are shown, but as discussed above, the T*(3) equations are identical except that $\bar{H}_N$ integrals are substituted for H_N.

Table A.1. Final spin integrated equations for Eq. A.1a (also shown at the top of the table). Uppercase indices denote alpha spin orbitals, lowercase beta spin. The symbol P in the equations denotes the permutation operator $(-)^p P(ij)$.

$-(-)^p P(ki/j)\langle lm\|\|ki\rangle t^{ab}_{mj}$			
Spin Case	Loop over Γ_{ij}		
AB IJ KL	$+P\langle LM\|\|KI\rangle t^{AB}_{JM}$		$+\langle LM\|\|IJ\rangle t^{AB}_{KM}$
ab ij KL	$+P\langle Lm\|Ki\rangle t^{ab}_{jm}$		
Ab Ij KL	$-\langle LM\|\|KI\rangle t^{Ab}_{Mj}$	$-\langle Lm\|Kj\rangle t^{Ab}_{Im}$	$+\langle Lm\|Ij\rangle t^{Ab}_{Km}$
AB IJ kl	$+P\langle Ml\|Ik\rangle t^{AB}_{JM}$		
ab ij kl	$+P\langle lm\|\|ki\rangle t^{ab}_{jm}$		$+\langle lm\|\|ij\rangle t^{ab}_{km}$
Ab Ij kl	$-\langle Ml\|Ik\rangle t^{Ab}_{Mj}$	$-\langle lm\|\|kj\rangle t^{Ab}_{Im}$	$+\langle Ml\|Ij\rangle t^{Ab}_{Mk}$

Table A.2. Final spin integrated equations for Eq. A.1b (also shown at the top of the table). Uppercase indices denote alpha spin orbitals, lowercase beta spin. The symbol P in the equations denotes the permutation operator $(-)^p P(ab)$.

$-(-)^p P(k/ij,ab)\langle la\|\|ke\rangle t^{be}_{ij}$			
Spin Case	Loop over Γ_{ij}	Loop over Γ_{ia}	Loop over Γ_{ib}
AB IJ KL	$-P\langle LA\|\|KE\rangle t^{BE}_{IJ}$	$+P\langle LA\|\|IE\rangle t^{EB}_{JK}$	$-P\langle LA\|\|JE\rangle t^{EB}_{IK}$
ab ij KL	$-P\langle La\|Ke\rangle t^{be}_{ij}$	$+P\langle La\|Ei\rangle t^{Eb}_{Kj}$	$-P\langle La\|Ej\rangle t^{Eb}_{Ki}$
Ab Ij KL	$+\langle LA\|\|KE\rangle t^{Eb}_{Ij}$ $+\langle Lb\|Ke\rangle t^{Ae}_{Ij}$	$-\langle LA\|\|IE\rangle t^{Eb}_{Kj}$ $-\langle Lb\|Ej\rangle t^{EA}_{IK}$	$-\langle Lb\|Ie\rangle t^{Ae}_{Kj}$
AB IJ kl	$-P\langle lA\|kE\rangle t^{BE}_{IJ}$	$+P\langle lA\|eI\rangle t^{Be}_{Jk}$	$-P\langle lA\|eJ\rangle t^{Be}_{Ik}$
ab ij kl	$-P\langle la\|\|ke\rangle t^{be}_{ij}$	$+P\langle la\|\|ie\rangle t^{eb}_{kj}$	$-P\langle la\|\|je\rangle t^{eb}_{ik}$
Ab Ij kl	$+\langle lA\|kE\rangle t^{Eb}_{Ij}$ $+\langle lb\|\|ke\rangle t^{Ae}_{Ij}$	$-\langle lA\|eI\rangle t^{eb}_{kj}$ $-\langle lb\|\|je\rangle t^{Ae}_{Ik}$	$-\langle lA\|jE\rangle t^{Eb}_{Ik}$

A.5 Testing

Of course programs are rarely exactly correct when they are first written, and they must be tested to verify their correctness and point up bugs. This section lists some of

Table A.3. Final spin integrated equations for Eq. A.1c (also shown at the top of the table). Uppercase indices denote alpha spin orbitals, lowercase beta spin. The symbol P in the equations denotes the permutation operator $(-)^p P(ab)$.

$-(-)^p P(k/ij,ab)\langle mb\|\|ij\rangle \tau_{km}^{la}$			
Spin Case	Loop over Γ_{ij}	Loop over Γ_{ia}	Loop over Γ_{ib}
AB IJ KL	$-P\langle MB\|\|IJ\rangle \tau_{KM}^{LA}$	$-P\langle MB\|\|KJ\rangle \tau_{MI}^{LA}$	$+P\langle MB\|\|KI\rangle \tau_{MJ}^{LA}$
ab ij KL	$-P\langle mb\|\|ij\rangle \tau_{Km}^{La}$	$-P\langle Mb\|Kj\rangle \tau_{Mi}^{La}$	$+P\langle Mb\|Ki\rangle \tau_{Mj}^{La}$
Ab Ij KL	$-\langle Mb\|Ij\rangle \tau_{KM}^{LA}$ $-\langle Am\|Ij\rangle \tau_{Km}^{Lb}$	$-\langle Mb\|Kj\rangle \tau_{MI}^{LA}$ $-\langle MA\|\|KI\rangle \tau_{Mj}^{Lb}$	$+\langle Am\|Kj\rangle \tau_{Im}^{Lb}$
AB IJ kl	$-P\langle MB\|\|IJ\rangle \tau_{Mk}^{Al}$	$-P\langle Bm\|Jk\rangle \tau_{Im}^{Al}$	$+P\langle Bm\|Ik\rangle \tau_{Jm}^{Al}$
ab ij kl	$-P\langle mb\|\|ij\rangle \tau_{km}^{la}$	$-P\langle mb\|\|kj\rangle \tau_{mi}^{la}$	$+P\langle mb\|\|ki\rangle \tau_{mj}^{la}$
Ab Ij kl	$-\langle Mb\|Ij\rangle \tau_{Mk}^{Al}$ $-\langle Am\|Ij\rangle \tau_{km}^{lb}$	$-\langle mb\|\|kj\rangle \tau_{Im}^{Al}$ $-\langle Am\|Ik\rangle \tau_{mj}^{lb}$	$+\langle Mb\|Ik\rangle \tau_{Mj}^{Al}$

Table A.4. Final spin integrated equations for Eq. A.1d (also shown at the top of the table). Uppercase indices denote alpha spin orbitals, lowercase beta spin. The symbol P in the equations denotes the permutation operator $(-)^p P(ij)$.

$(-)^p P(ki/j)\langle ab\|\|ej\rangle \tau_{ki}^{le}$			
Spin Case	Loop over Γ_{ij}		
AB IJ KL	$+P\langle AB\|\|EJ\rangle \tau_{KI}^{LE}$		$+\langle AB\|\|EK\rangle \tau_{IJ}^{LE}$
ab ij KL	$+P\langle ab\|\|ej\rangle \tau_{Ki}^{Le}$		
Ab Ij KL	$+\langle Ab\|Ej\rangle \tau_{KI}^{LE}$	$+\langle Ab\|Ie\rangle \tau_{Kj}^{Le}$	$-\langle Ab\|Ke\rangle \tau_{Ij}^{Le}$
AB IJ kl	$+P\langle AB\|\|EJ\rangle \tau_{Ik}^{El}$		
ab ij kl	$+P\langle ab\|\|ej\rangle \tau_{ki}^{le}$		$+\langle ab\|\|ek\rangle \tau_{ij}^{le}$
Ab Ij kl	$+\langle Ab\|Ej\rangle \tau_{Ik}^{lE}$	$+\langle Ab\|Ie\rangle \tau_{kj}^{le}$	$-\langle Ab\|Ek\rangle \tau_{Ij}^{El}$

the tests that have been applied to the FS triples code in the course of its development. While they are probably obvious to most people, all have proven useful and none should be forgotten.

1. Symmetry. Given a molecule with point group symmetry, the code should give the same result when run in C_1 or in full symmetry.
2. UHF vs. RHF. For a closed shell molecule, using UHF and RHF reference functions should give the same result.
3. Spin inversion. For an open shell molecule, the code should give the same results with the spins of all electrons flipped. For example, a triplet state should give the same result whether the two unpaired electrons are alpha or beta spin.
4. Size extensivity. For size extensive methods, the same results should obtain from a single molecule and from two, widely separated identical molecules. When used with very tight convergence criteria and other tolerances, this can be an extremely accurate test.
5. Separate implementation. After all other tests are satisfied, it may be useful to make a very simple, straightforward implementation of the equations as an independent check. For example, the basic equations can be followed literally by forming a large tensor of antisymmetrized integrals from a number of integral lists, and likewise for the amplitudes, and comparing the results element-by-element with the primary implementation. As this approach tends to be memory intensive and slow, small simple test cases are usually the best.

There are also a number of tests which are not applicable to the current third-order triples models, but should be kept in mind for situations in which they are appropriate.

1. Active space invariance. Fully iterative FSCC methods should give the same result for any choice of active space.

2. Invariance to orbital rotations. For methods which (theoretically) have this property, it can be tested by, for example, using an ROHF reference function with and without semicanonical orbitals, or by other methods which modify the occupied-occupied or virtual-virtual parts of the Fock matrix.

REFERENCES

1. R. J. Bartlett, editor, *Comparison of Ab Initio Quantum Chemistry with Experiment for Small Molecules*, D. Reidel, Dordrecht, Holland, 1985.

2. R. J. Bartlett and G. D. Purvis, Int. J. Quantum Chem. **14**, 561 (1978).

3. R. J. Bartlett and G. D. Purvis III, Physica Scripta **21**, 255 (1980).

4. M. Born and R. Oppenheimer, Ann. Phys. **84**, 457 (1927).

5. M. Born and K. Huang, *Dynamical Theory of Crystal Lattices*, Clarendon Press, Oxford, 1951.

6. H. A. Jahn and E. Teller, Proc. R. Soc. London, Ser. A **161**, 220 (1937).

7. I. B. Bersuker, *The Jahn-Teller Effect and Vibronic Interactions in Modern Chemistry*, Plenum Press, New York, 1984.

8. R. Renner, Z. Phys. **92**, 172 (1934).

9. H. Sponer and E. Teller, Rev. Mod. Phys. **13**, 75 (1941).

10. I. B. Bersuker, *The Jahn-Teller Effect. A Bibliographic Review*, IFI/Plenum, New York, 1984.

11. T. J. Lee, D. J. Fox, H. F. Schaefer III, and R. M. Pitzer, J. Chem. Phys. **81**, 356 (1984).

12. A. Szabo and N. S. Ostlund, *Modern Quantum Chemistry: Introduction to Advanced Electronic Structure Theory*, Macmillan, New York, first edition, 1982.

13. P. A. M. Dirac, *The Principles of Quantum Mechanics*, Number 27 in The International Series of Monographics on Physics, Oxford University Press, Oxford, fourth edition, 1958.

14. P. Jørgensen and J. Simons, *Second Quantization-Based Methods in Quantum Chemistry*, Academic Press, New York, 1981.

15. G. C. Wick, Phys. Rev. **80**, 268 (1950).

16. R. J. Bartlett and G. D. Purvis III, Annals of the New York Academy of Sciences **367**, 62 (1981).

17. R. Ahlrichs, Theor. Chim. Acta **35**, 59 (1974).

18. F. Keil and R. Ahlrichs, J. Am. Chem. Soc. **98**, 4787 (1976).

19. K. A. Brueckner, Phys. Rev. **97**, 1353 (1955).

20. K. A. Brueckner and C. A. Levinson, Phys. Rev. **97**, 1344 (1955).

21. K. A. Brueckner, R. J. Eden, and N. C. Francis, Phys. Rev. **98**, 1445 (1955).

22. K. A. Brueckner, Phys. Rev. **100**, 36 (1955).

23. J. Goldstone, Proc. R. Soc. London Series A **239**, 267 (1957).

24. F. Coester, Nucl. Phys. **7**, 421 (1958).

25. F. E. Harris, B. Jeziorski, and H. J. Monkhorst, Phys. Rev. A **23**, 1632 (1981).

26. S. A. Kucharski and R. J. Bartlett, Adv. Quantum Chem. **18**, 281 (1986).

27. S. A. Kucharski and R. J. Bartlett, Theor. Chim. Acta **80**, 387 (1991).

28. M. R. Hestenes, *Conjugate Direction Methods in Optimization*, Springer-Verlag, New York, 1980.

29. P. E. S. Wormer, F. Visser, and J. Paldus, J. Comput. Phys. **48**, 23 (1982).

30. G. D. Purvis III and R. J. Bartlett, J. Chem. Phys. **75**, 1284 (1981).

31. P. Pulay, Chem. Phys. Lett. **73**, 393 (1980).

32. P. Pulay, J. Computat. Chem. **3**, 556 (1982).

33. Y. S. Lee, S. A. Kucharski, and R. J. Bartlett, J. Chem. Phys. **81**, 5906 (1984).

34. R. J. Bartlett, J. Phys. Chem. **93**, 1697 (1989).

35. I. Lindgren, Physica Scripta **32**, 291 (1985).

36. I. Lindgren, Physica Scripta **32**, 611 (1985).

37. C. M. L. Rittby and R. J. Bartlett, Theor. Chim. Acta **80**, 469 (1991).

38. D. Mukherjee, Pramāna **12**, 203 (1979).

39. D. Mukherjee, Chem. Phys. Lett. **125**, 207 (1986).

40. D. Sinha, S. K. Mukhopadhyay, M. D. Prasad, and D. Mukherjee, Chem. Phys. Lett. **125**, 213 (1986).

41. D. Sinha, S. Mukhopadhyay, and D. Mukherjee, Chem. Phys. Lett. **129**, 369 (1986).

42. I. Lindgren and D. Mukherjee, Physics Reports **151**, 93 (1987).

43. S. Pal, M. Rittby, R. J. Bartlett, D. Sinha, and D. Mukherjee, J. Chem. Phys. **88**, 4357 (1988).

44. R. Chaudhuri, D. Sinha, and D. Mukherjee, Chem. Phys. Lett. **163**, 165 (1989).

45. M. A. Haque and D. Mukherjee, J. Chem. Phys. **80**, 5058 (1984).

46. A. Mukhopadhyay, R. K. Moitra, and D. Mukherjee, J. Phys. B: Atom. Molec. Phys. **12**, 1 (1979).

47. Y. S. Lee, S. A. Kucharski, and R. J. Bartlett, J. Chem. Phys. **82**, 5761 (1985).

48. M. Urban, J. Noga, S. J. Cole, and R. J. Bartlett, J. Chem. Phys. **83**, 4041 (1985).

49. S. J. Cole and R. J. Bartlett, J. Chem. Phys. **86**, 873 (1987).

50. J. Noga, R. J. Bartlett, and M. Urban, Chem. Phys. Lett. **134**, 126 (1987).

51. J. Noga and R. J. Bartlett, J. Chem. Phys. **86**, 7041 (1987).

52. J. Noga and R. J. Bartlett, J. Chem. Phys. **89**, 3401 (1988).

53. S. Pal, M. Rittby, R. J. Bartlett, D. Sinha, and D. Mukherjee, Chem. Phys. Lett. **137**, 273 (1987).

54. U. Kaldor, J. Computat. Chem. **8**, 448 (1987).

55. M. Rittby, S. Pal, and R. J. Bartlett, J. Chem. Phys. **90**, 3214 (1989).

56. S. Pal, M. Rittby, and R. J. Bartlett, Chem. Phys. Lett. **160**, 212 (1989).

57. A. Haque and U. Kaldor, Chem. Phys. Lett. **120**, 261 (1985).

58. J. D. Watts, J. Gauss, and R. J. Bartlett, J. Chem. Phys. (1993), *to appear.*

59. N. C. Handy, J. A. Pople, M. Head-Gordon, K. Raghavachari, and G. W. Trucks, Chem. Phys. Lett. **164**, 185 (1989).

60. R. P. Mattie, *Theory and Implementation of Coupled Cluster Methods for Direct Calculations of Ionization Energies*, PhD thesis, University of Florida, 1993.

61. T. H. Dunning, Jr., J. Chem. Phys. **90**, 1007 (1989).

62. C. W. Bauschlicher, Jr. and P. R. Taylor, J. Chem. Phys. **86**, 2844 (1987).

63. J. B. Peel and G. D. Willett, J. Chem. Soc., Faraday Trans. 2 **71**, 1799 (1975).

64. H. Bock, R. Dammel, and L. Horner, Chem. Ber. **114**, 220 (1981).

65. R. Schulz and A. Schweig, J. Electron Spectrosc. Relat. Phenom. **28**, 33 (1982).

66. J. D. Watts, M. Rittby, and R. J. Bartlett, J. Am. Chem. Soc. **111**, 4155 (1989).

67. S. Lacombe, D. Gonbeau, J.-L. Cabioch, B. Pellerin, J.-M. Denis, and G. Pfister-Giollouzo, J. Am. Chem. Soc. **110**, 6964 (1988).

68. G. Herzberg, *Electronic Spectra and Electronic Structure of Polyatomic Molecules*, volume III of *Molecular Spectra and Molecular Structure*, D. Van Nostrand, Princeton, New Jersey, 1966.

69. J. F. Stanton, R. J. Bartlett, and C. M. L. Rittby, J. Chem. Phys. **97**, 5560 (1992).

70. C. Baker and D. W. Turner, J. Chem. Soc. D: Chem. Comm. , 480 (1969).

71. T. H. Dunning, Jr., J. Chem. Phys. **53**, 2823 (1970).

72. L. T. Redmon, G. D. Purvis III, and R. J. Bartlett, J. Am. Chem. Soc. **101**, 2856 (1979).

73. M. Rittby and R. J. Bartlett, J. Phys. Chem. **92**, 3033 (1988).

74. L. Engelbrecht and B. Liu, J. Chem. Phys. **78**, 3097 (1983).

75. K. Kawaguchi, E. Hirota, T. Ishiwata, and I. Tanaka, J. Chem. Phys. **93**, 951 (1990).

76. J. F. Stanton, J. Gauss, and R. J. Bartlett, J. Chem. Phys. **94**, 4084 (1991).

77. J. F. Stanton, J. Gauss, and R. J. Bartlett, J. Chem. Phys. **97**, 5554 (1992).

78. A. Faibis, E. P. Kanter, L. M. Tack, E. Bakke, and B. J. Zabransky, J. Phys. Chem. **91**, 6445 (1987).

79. Z. Vager and E. P. Kanter, J. Phys. Chem. **93**, 7745 (1989).

80. J. D. Watts, J. F. Stanton, J. Gauss, and R. J. Bartlett, J. Chem. Phys. **94**, 4320 (1991).

81. R. S. Grev, I. L. Alberts, and H. F. Schaefer III, J. Phys. Chem. **94**, 3379 (1990).

82. R. S. Grev, I. L. Alberts, and H. F. Schaefer III, J. Phys. Chem. **94**, 8744 (1990).

83. P. R. Taylor, J. M. L. Martin, J. P. François, and R. Gijbels, J. Phys. Chem. **95**, 6530 (1991).

84. D. C. Parent, J. Am. Chem. Soc. **111**, 2392 (1989).

85. M. E. Geusic, M. F. Jarrold, T. J. McIlrath, L. A. Bloomfield, R. R. Freeman, and W. L. Brown, Z. Phys. D **3**, 309 (1986).

86. P. P. Radi, M. E. Rincon, M. T. Hsu, J. Brodbelt-Lustig, P. Kemper, and M. T. Bowers, J. Phys. Chem. **93**, 6187 (1989).

87. P. P. Radi, M. E. Rincon, M. T. Hsu, J. Brodbelt-Lustig, M. Rincon, and M. T. Bowers, J. Chem. Phys. **92**, 4817 (1990).

88. G. von Helden, M.-T. Hsu, P. R. Kemper, and M. T. Bowers, J. Chem. Phys. **95**, 3835 (1991).

89. M. Vala, T. M. Chandrasekhar, J. Szczepanski, and R. Pellow, J. Mol. Struct. **222**, 209 (1990).

90. W. Weltner, Jr. and R. J. van Zee, Chem. Rev. **89**, 1713 (1989).

91. J. D. Watts, J. Gauss, J. F. Stanton, and R. J. Bartlett, J. Chem. Phys. **97**, 8372 (1992).

92. D. E. Bernholdt, J. D. Watts, I. Cernusak, R. J. Bartlett, and G. F. Adams, Theoretical studies of carbon clusters, Contributed Poster, 30^{th} Sanibel Symposia, St. Augustine, Florida, 1990.

93. B. J. Ortman, R. H. Hauge, J. L. Margrave, and Z. H. Kafafi, J. Phys. Chem. **94**, 7973 (1990).

94. P. Botschwina and P. Sebald, Chem. Phys. Lett. **160**, 485 (1989).

95. P. Botschwina, J. Chem. Phys. **95**, 4360 (1991).

96. K. Raghavachari and J. S. Binkley, J. Chem. Phys. **87**, 2192 (1987).

97. J. Bernholc and J. C. Phillips, J. Chem. Phys. **85**, 3258 (1986).

98. J. F. Stanton, J. Gauss, J. D. Watts, and R. J. Bartlett, ACES II, an *ab initio* program system.

BIOGRAPHICAL SKETCH

David Edward Bernholdt was born in 1964 in Clearfield, Pennsylvania and grew up in the suburbs of Chicago, Illinois. After earning a B. S. in chemistry from the University of Illinois at Urbana-Champaign in 1986, he moved to the University of Florida for his graduate work.

At Florida, in addition to the usual course of study and research for a Ph. D. in chemistry, David also experienced the joys of a well-tuned bureaucracy in the University administration, and of a state that provides no visible support for education. Nevertheless, David feels that his time at Florida was, on the whole, profitably spent.

In his free time, David pursues numerous other interests, but since he hasn't had much free time lately, he is at a loss to remember what they are. After graduation, David is hoping to regain some of those memories and, with his wife, the former and current Janice Lynn Musfeldt, is looking forward to finding a solution to the "two-body problem" in the rapidly changing world of science.

I certify that I have read this study and that in my opinion it conforms to acceptable standards of scholarly presentation and is fully adequate, in scope and quality, as a dissertation for the degree of Doctor of Philosophy.

Rodney J. Bartlett, Chairman
Graduate Research Professor of Chemistry

I certify that I have read this study and that in my opinion it conforms to acceptable standards of scholarly presentation and is fully adequate, in scope and quality, as a dissertation for the degree of Doctor of Philosophy.

William H. Hager
Professor of Mathematics

I certify that I have read this study and that in my opinion it conforms to acceptable standards of scholarly presentation and is fully adequate, in scope and quality, as a dissertation for the degree of Doctor of Philosophy.

N. Yngve Öhrn
Professor of Chemistry and Physics

I certify that I have read this study and that in my opinion it conforms to acceptable standards of scholarly presentation and is fully adequate, in scope and quality, as a dissertation for the degree of Doctor of Philosophy.

Samuel B. Trickey
Professor of Physics

I certify that I have read this study and that in my opinion it conforms to acceptable standards of scholarly presentation and is fully adequate, in scope and quality, as a dissertation for the degree of Doctor of Philosophy.

William Weltner, Jr.
Professor of Chemistry

This dissertation was submitted to the Graduate Faculty of the Department of Chemistry in the College of Liberal Arts and Sciences and to the Graduate School and was accepted as partial fulfillment of the requirements for the degree of Doctor of Philosophy.

May 1993

Dean, Graduate School

UNIVERSITY OF FLORIDA
3 1262 08553 9210